Sonic properties of silks

Thesis Abstract

Beth Mortimer

New College Oxford Silk Group
Hilary, 2014 Department of Zoology

A Thesis submitted for the degree of Doctor of Philosophy in Zoology.

Supervised by Dr Chris Holland, Prof. Clive R. Siviour and Prof. Fritz Vollrath

Silks are biomaterials made by spiders and silkworms, evolved for natural functions ranging from protection to predation. The research presented in this Thesis combines principles and methods from engineering, physics and biology to study the material properties of single silk fibres from a biological perspective. In particular, the factors that contribute to the variation in properties of single silk fibres are investigated. The first part of the Thesis focuses on silks made by silkworms. Whether naturally spun or forced reeled, the mechanical properties of these silks are sensitive to a range of environmental and processing conditions, such as humidity, stretching and reeling speed. The research presented in this section contributes to the understanding of how these applied conditions affect silk mechanical properties, which can be understood in terms of silk's protein structure and biological context. The second section compares both silkworm and spider silk single fibres to other materials in terms of their sonic properties – how the materials propagate sound waves, whether following impact, or propagating vibrations. The results are discussed in the context of the silk's natural function for impact resistance (silkworm cocoon or spider web) and vibrational signalling (spider silks). The Thesis ends with a discussion of how the presented techniques can be applied to help further our understanding of orb web function through studying spider silks. Overall, this interdisciplinary Thesis contributes to our understanding of the structure-property-function links of these fascinating biomaterials.

For David Porter –
a greatly valued colleague, mentor and teacher,
whose talent and dedication to science was
unmatched.

Acknowledgements

I've had help and support from a range of people that have made this Thesis possible.

Firstly, a really big thank you to all my supervisors who have provided so much help and support. I'm sorry for nagging them incessantly, and really appreciate their patience. Chris especially has gone above and beyond in all aspects of my academic development, and for that I'm extremely grateful. Clive was always available for thoughtful advice and I really appreciate his time and kind words for me. Lastly, Fritz is full of so many creative ideas that are really inspiring, and has been a real help in my progression forward. Given where I started, it is thanks to them that I've got to the end, with research to be proud of.

A big thanks to my collaborators at the University of Strathclyde, without them I would not have made the jump into the vibrational properties of silks and it has saved my Thesis as well as being the basis of my future research. So James and Shira, thanks for hosting me in your lab and your support with the research.

There are so many people who have been a help in the Oxford Silk Group and Engineering, so a really big thank you to them for their part. A special thank you to David Porter, who practically supervised me for half of the time! I really appreciate his time and sound advice and it really helped me in the last few months to have someone to talk things through with in the lab. Also to Alex Woods, for sharing his research on the paralysis of silkworms before his patent was finalised, and Sophie Scott and John Sherwin for their help reeling silkworms. For their help and data: Nick Hawkins, Juan Guan, and Alex Greenhalgh, all of whom it has been a pleasure to work and be friends with. For their support and advice when needed, thanks go to: Gwilym Davies, Maxime Boulet-Audet, Fujia Chen, Darshil Shah, Tom Gheysens, Imke Greving and Bjoern Greving. For the help I really needed in the Engineering Science Department, thanks go to Richard Duffin, Kalin Dragnevski and Daniel Drodge.

For funding, I thank the Leverhulme Trust, who kindly agreed to an extension on the three-year grant, as well as Polytec for the loan of the vibrometer equipment. I have also been lucky enough to work as part of Jesus College for the last two years, who have partially funded some of the research. The lectureship has brought me a welcome break from academic work, confidence, development of my teaching skills, as well as rewarding relationships across all levels of the College. Special thanks to Graham Taylor for his trust and support.

I'd also like to thank the spiders and silkworms.

Lastly, I thank my friends and support network for their patience and kindness: many thanks to past and current members of the Animal Flight Group, Cicely and William, and Mum and Dad. Last, but by no means least, Blakey – couldn't have done it without you!

Publications

Drodge, D. R., Mortimer, B., Holland, C. and Siviour, C. R. 2012. Ballistic impact to access the high-rate behavior of individual silk fibres, *J. Mech. Phys. Solids*, **60** (10), pp. 1710-1721.

Mortimer, B., Drodge, D. R., Dragnevski, K., Siviour, C. R. and Holland, C. 2013. *In situ* tensile tests of single silk fibres in an Environmental Scanning Electron Microscope (ESEM), *J. Mater. Sci*., **48**, pp. 5055-5062.

Mortimer, B., Holland, C. and Vollrath F. 2013. Forced reeling of *Bombyx mori* silk: separating behavior and processing conditions, *Biomacromolecules*, **14** (10), pp. 3653-3659.

Mortimer, B. and Holland, C. The use of spider silk as a biomaterial. Chapter 15 in *Advances in Silk Science and Technology*: Woodhead publishing. In press.

Mortimer, B., Gordon, S., Siviour, C. R., Holland, C., Vollrath, F. and Windmill, J., The speed of sound in silk: linking material performance to biological function. Open Access online at *Advanced Materials,* DOI: 10.1002/adma.201401027

Mortimer, B., Guan, J., Holland, C., Porter, D. and Vollrath, F., *Bombyx mori* silks: A structural basis for processing, properties and potential. Submitted to *Acta Biomaterialia.*

Mortimer, B., Siviour, C. R., Holland, C. and Vollrath F., Spider silks as structural and signalling components in the web of *Nephila edulis*. In prep.

Mortimer, B., Holland, C. and Vollrath, F., Vibrational properties of the signal thread in the web of *Zygiella x-notata*. In prep.

Drodge, D. R., Mortimer, B., Holland, C. and Siviour, C. R., Mechanical properties and drag effects on spider silks during high-rate impact. In prep.

Porter, D., Drodge, D. R., Mortimer, B., Holland, C. and Siviour, C. R., Accounting for plastic flow during the high-rate impact of polymers. In prep.

Table of Contents

List of Tables and Figures

Chapter 1 Introduction

1.1 Synopsis

Biological structures made by organisms for use outside the body can be termed 'extended phenotypes'[1]. Spider webs and silkworm cocoons are excellent examples, as silks have evolved for use outside the body through the process of controlled protein denaturation. Several aspects of silk have been shaped by evolution: the silk primary protein sequence, processing into a dry fibre, and behaviour during construction[2-4]. However, evolution acts on the functionality of the end product: how the structure increases the individual's fitness.

The functionality of a structure stems from its properties – in the case of silks, its material characteristics: including mechanical, thermal and sonic (sound propagation) properties. Understanding the characteristics of the whole silk structure is complex due to the combinations of multiple types of silks that behave and interact non-linearly.

My approach, as presented in this Thesis, is to study the properties of individual silk fibres to help understand whole biological structures. There is a wealth of variability of properties in dry silk fibres; variability that stems from environmental, processing and physical factors. Linking these properties to their structural basis and biological function is useful not only for answering biological questions about the evolution of silk, but enables us better to understand and harness the diversity of silk for engineering applications.

This introduction starts with a brief discussion on the defining features of silk. An overview of the amazing diversity of silk types is then laid out: between taxa and even within an individual, in the case of orb weaving spiders. This Thesis concentrates on only three of these silks – orbweaver major and minor ampullate silks and the silk of the domesticated silkworm *Bombyx mori*, which are then introduced along with their natural silk structure context. One particular

factor affecting silk variability is then discussed – rate-dependence, where mechanical properties change due to the speed of deformation. The introduction finishes with an overview of the research scope and an outline of the Thesis chapters.

1.2 What is silk?

Silks are defined as hierarchically structured biopolymers that are spun – they are proteins that are defined by their processing from a gel-like dope to a dry fibre[2]. Importantly, silks are not grown, unlike other biopolymer proteins such as collagen and keratin, and are used exclusively outside the body[5]. Silk proteins are stored as gel-like dopes in silk glands, where the primary protein chains are around 250 kDa long[6]. When silk is pulled, the dope flows through a tapering duct[2, 7-8]. Water is removed during this process, which is controlled by pH changes along the duct. Water removal enables hydrogen bonds to form between amide-amide groups, rather than amide-water hydrogen bonds[7, 9]. The loss of water, a kind of controlled protein denaturation, as well as the shear stresses in the duct cause protein secondary and tertiary structures to form, such as ordered beta sheets[10-12].

Due to their impressive mechanical properties (see Figure 1.1), there have been a number of attempts to produce silk synthetically to obtain large yields of silk protein. For example, silk genes have been expressed in organisms such as *Escherichia coli* and even goats, who express the 'silk' in their milk[13-14]. These proteins are not spun in a duct, so according to the definition are not silks and do not contain similar protein structures or mechanical properties[15]. There is therefore a need to be able not only to make the silk dope protein in large quantities, but to mimic the duct and spinning process as well. This is not so easy – there appears to be order in the packing of silk proteins within the gland that predispose the silk to form the fibre in the duct[16]. Furthermore, terminal domains at the end of these silk proteins may enable controlled assembly of the proteins during spinning[17-18]. These small details of the structure and chemical

make-up of the natural silk dope and spinning apparatus are needed to successfully artificially produce silks[15, 19].

Silks have evolved many times independently within the Arthropods, including at least 23 times within the insects, once within the spiders and at least once within the crustaceans[20-22]. Whereas insects will produce one type of silk at one particular life stage, spiders produce multiple types of silk throughout their life. These silks have independently evolved similar protein sequences and processing conditions, but they differ in the origin of the silk-storing gland(s)[3, 12, 21]. These convergences reveal remarkable constraints on the protein composition and processing of silk, indicating that there are a limited number of ways to make a silk fibre. As is shown below, this creates a paradox with the astonishing diversity seen in silks in terms of functional uses and material properties. Due to the non-linear viscoelasticity of silk and its dependence on hydrogen bonding[5], a limited number of sequences and possible protein structures can lead to many different materials.

1.3 Silk fibre diversity

1.3.1 Spider silks

All 40 000 known species of spider produce silk from spinnerets located on their abdomen[4, 23]. Basal spiders, the Mesothelae and Mygalomorphae, contain a small proportion of spider diversity, whereas the more derived Araneomorphae contain 38 000 species[23] and differ in their silk production and use. Basal spiders produce silks from three glands that are used indiscriminately to make egg cocoons, line burrows and make webs whose support is substrate-dependent, such as funnel-webs[24-26].

The low diversity of basal spiders and their silk-use can be explained by the relatively poor mechanical properties of their silks compared to the more derived Araneomorphae: basal silks are ten times less strong, with an associated reduction in toughness (energy-absorption

ability)[27]. In fact, these silks cannot hold the spider's own weight, so niches are restricted to ground-dwelling habitats. Despite the comparatively poor strength, basal spider silks are used for their sensory properties to propagate vibrations[28-30], rather than as mechanical or adhesive snares. Therefore, the sonic properties of silks were important for the silk's natural function early on in spider evolution.

Basal and more derived spiders differ in their silk gene sequences, which lead to different protein secondary structures that in turn explain mechanical property differences (Table 1). The basal silks contain some unique repetitive sequences in their silk genes involving amino acids such as serine and threonine[31-32]. However, all spider silk genes share repeats of alanine (polyA), suggesting that these sequences have been maintained over 240 million years[31].

Table 1. Protein sequence and suggested secondary structure for a range of orbweaver and non-orbweaver spider silks. Amino acids: A = alanine, S = serine, G = glycine, X = varied/unknown, V = valine, Q = glutamine, P = proline and a lower case n means repeated a number of times.

Silk type	**Repetitive sequence**	**Suggested secondary structure**	**Reference(s)**
Basal spider fibroins	A_n, S_n, GX and AQ_n	Varied/unknown	31-32
Non-orbweaver MaSp	A_n, GA_n, GV_n, GS_n	Orientated beta sheet	31, 33
Major Ampullate: MaSp1	A_n, GA_n, GGX	Orientated beta sheet	31, 34
Major Ampullate: MaSp2	$GPGX_n$	Beta spiral	35
Minor ampullate: MiSp1 and 2	GGX, GA_n + serine rich spacers	Orientated beta sheet	36
Flagelliform	GPGGX (GGX and spacer)	Beta spiral, no preferential orientation	37
Cylindriform/Tubuliform: TuSp1	Long repetitive sequence	Orientated beta sheet	38-39
Aciniform: AcSp1	Long repetitive sequence	Less orientated beta sheet, alpha helix	39-40

The radiation of the Araneomorphae coincided with the evolution of ampullate silk, around 150 million years ago[26-27, 41]. This group contains wandering spiders with an active hunting predatory

niche, such as jumping and wolf spiders, and sit-and-wait web spinners, such as the orb web and cobweb spinners. Across the Araneomorphae, ampullate silks show consistent high toughness and high strength, with variability controlled by external processing conditions[42]. Major ampullate, or dragline silk, has similar gene sequences across the Araneomorphae, including glycine-alanine (GA) and polyA repeats (Table 1)[31, 33]. The orb web spinning families Araneidae and Nephilidae in the Araneomorphae make the major and minor ampullate silks (genes named MaSp and MiSp respectively) that are studied in this Thesis. However, they make many more silks than just ampullate silks, which are outlined in the next section.

1.3.1.1 Orbweaver silks

Orbweavers produce up to seven different types of silk, with different protein primary sequences (Table 1). Spiders use gland-specific expression of these silks, and the silk fibres leave the body through different spigots on the spinnerets[43]. The seven different types of silks made by orbweavers show an impressive range of mechanical performance (Figure 1.1)[44-45].

Aciniform silks (gene AcSp) form the wrapping silk for prey, as well as the inner part of the egg sac[40]. These silks are very thin and are relatively understudied due to the difficulty in forced reeling the silks under controlled conditions[45]. However, they show impressive toughness, often quoted as having the best toughness out of all spider silks[45]. Capture spiral silk is formed of a core flagelliform silk, with a coating of hygroscopic aggregate silk glue[46]. Capture spiral silks show impressive extensibility and poor strength, with contradictory evidence on their relative toughness (resulting from difficulties in consistent testing conditions and cross-sectional area measurements, see Chapter 7)[45, 47-48]. The role of flagelliform and aggregate silks in the orb web is further discussed in Section 1.4.1.1. Cylindriform, or tubuliform silk (gene TuSp) is used in the outer coating of egg sacs. It has been relatively understudied and shows intermediate mechanical performance[49]. Piriform silks form adhesive disks to enable the spider to stick its silks to the substrate in the spider's environment[50]. Lastly, major and minor ampullate tough

silks are used in the orb web and contain proteins that are expressed from two genes[31, 34-36]. These silks are further discussed in Section 1.4.1.

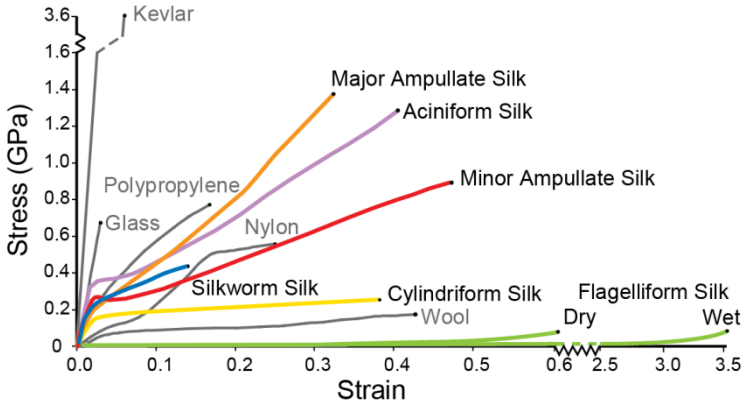

Figure 1.1. Stress-strain curves comparing silkworm silk (blue) to spider silks: major ampullate (orange), aciniform silk (purple), minor ampullate silk (red), cylindriform silk (yellow) and wet and dry flagelliform silk (green, where the latter contains an aggregate silk coating). Reference curves for synthetic and other biopolymers are also given. Data taken from [45-46, 51-52].

The diverse properties of orbweaver spider silks are explained by their differences in material structure. The tougher silks (ampullates, aciniform) show orientated beta sheet structures, the less tough cylindriform silks show less oriented beta sheet and alpha helix structures, whereas flagelliform silks have no preferential orientation and are thought to contain beta spiral structures (Table 1)[39, 53-54]. These structures, in turn, are explained by amino acid composition and sequence, where a higher glycine and alanine content leads to more ordered structures, whereas the presence of proline leads to more disordered structures, due to its non-linear ('kinked') backbone that prevents close packing[55]. Major ampullate silk combines both types of structures at the nanometer scale, which is thought to lead to dragline silk's exceptional toughness[56].

The spider silk gene sequences give information on the evolution of orbweaver spider silks. Ampullate and flagelliform silks have very repetitive sequences, which are conserved across the orbweavers, suggesting that selection has maintained these sequences over 150 million years[31, 36, 57]. The cylindriform silk gene also has a single origin in the orbweavers, and often cylindriform glands will also express major ampullate silk proteins[38]. By examining the terminal sequences of

these genes, the relatedness between the different silk genes can be determined: aciniform genes are most closely related to ampullate genes, suggesting that they are a very divergent member of the ampullate silk 'family'[40].

As well as shaping the silk composition, natural selection has also acted on other traits within the spider, which have coevolved with the silk sequences. The silk gland and duct shapes are particularly important for the processing of the silk dopes into the dry protein fibre, as well as their associated biochemistry[7, 9, 58-59]. Spider silk-use has also coevolved with the prey insect species, resulting in an arms race and leading to varied behaviours to construct effective web architectures out of the silks for catching prey[4].

1.3.2 Insect silks

The ability to spin silk in the insects has evolved at least 23 times independently, with evidence from different glandular origins of silk expression[20-21]. Unlike spiders, insects will typically make only one type of silk at one particular life stage. Across the insects, functional uses for insect silks match those of spiders, from prey capture (glow worm silks[60]), to reproductive uses (bristletails[61]), egg protection (book lice[62]), lining burrows (webspinner[63]), structural functions (wasps[64]), lifelines (midges[65]) and protection from predators (thrips[66]).

Compared to spiders, there is relatively little research quantifying the diversity of insect silk mechanical properties[21, 67-71] (with the exception of lepidopteran cocoon silks, which are discussed below). This has been attributed to the difficulty in obtaining sufficiently large specimens for mechanical testing, although dimensions and sufficiently sensitive testing equipment may be another factor[72]. There has, however, been a focus on the diversity of the structures of insect silks and four main types of secondary structures have been identified, including: alpha helix, beta strand, 3_2 helix and 3_1 helix[21]. Whereas the alpha helices lead to coiled-coil structures, which show extensible properties with low strength (up to 200 % strain

and 200 MPa)[70-71], beta strands lead to beta sheet structures, with strong and tough properties, like lepidopteran silks (see silkworm silk in Figure 1.1)[10]. Therefore, there are not only analogous functional uses of silk between insects and spiders, but also analogous protein structures and mechanical properties.

Lepidopteran silks are used to make protective cocoons during pupal metamorphosis and are studied in this Thesis. Butterfly and moth cocoons show diversity in the material properties of silk fibres, binding between fibres and layers, porosity of layers and chemical composition[73-74]. These properties in turn affect cocoon morphology and physical properties, including impact behaviour[73-75]. Some chemicals act as deterrents to potential predators, for example calcium oxalate is a toxic chemical present on several cocoons, and is deposited when the caterpillar urinates during cocoon construction[73, 76]. Studies on the chemical composition of cocoons reveal a fascinating diversity – where differences are so common that a lepidopteran phylogeny can be reconstructed based on the chemical fingerprint of their silks[77]. As well as silk and other introduced chemicals, cocoons will often use surrounding vegetation such as leaves or twigs to help camouflage their cocoon, and may even incorporate predator-deterrent spines from their caterpillar body[78].

1.3.3 Harnessing silk diversity

Silks are incredibly diverse in properties and functional uses, and it is likely that there is more diversity that is yet to be discovered. This diversity is an incredible resource from which novel biopolymers can be developed[31]. Nature has developed these materials through over 300 million years of research and development, providing bioinspiration for the next generation of materials[79]. The biological approach is critical to understanding the links between structure, property and function, as shaped by natural selection given evolutionary constraints. Hence, to harness the diversity of silk for bioinspired devices or materials, researchers must understand silk as a biological material, which is the approach taken in this Thesis.

1.4 Silks and their natural structures

This Thesis studies major and minor ampullate silks from three species of orbweaver spider: *Nephila*, *Araneus* and *Zygiella*, as well as some capture spiral silks from *Nephila*. These silks are compared to *Bombyx mori* cocoon silk for a comparison across independently evolved silks, and are further compared to synthetic materials. Further details on ampullate and naturally spun *B. mori* silks are given below in the context of the natural structures in which they are used, with a focus on the more heavily researched spider silks.

1.4.1 Orbweaver ampullate silks and the orb web

Out of all the spider silks made by the natural world, the material that has received the most research interest is orbweaver major ampullate, or dragline silk[19, 27]. This is undoubtedly due to its impressive mechanical performance, particularly its toughness. This is illustrated in Figure 1.1, where spider dragline silk combines high strength and extensibility, resulting in high energy absorption to break (area under the curve)[5, 47]. The superior mechanical properties of dragline silk were shaped by over 150 million years of evolution, involving selection pressures to absorb the energy of a falling spider, or prey kinetic energy in the web[31, 80-81]. The toughest-known spider dragline silk belongs to a large orbweaver, Darwin's bark spider, which makes the largest webs recorded[82]. These mechanical properties make spider dragline silk a gold standard for bioinspired material design, which opens up a range of potential applications[15, 79].

An important and often overlooked contributor to these tough properties is simply the small diameters of these silks (typically 1-3 μm in diameter), where a small size allows for higher fibre strength[83]. This has negative implications for the attempt to create dragline silk-like properties from genetic engineering of silkworms to include spider silk genes, as silks produced via silkworm spinning ducts are larger (10 – 20 μm)[15, 84]. Major ampullate silk ducts have evolved to optimise the processing of these silks into thin fibres, even as the spider grows[7]. Thinness

additionally has advantages in terms of material conservation, saving energy for the spider, and reducing visibility to aerial prey[85-86].

Despite their credentials, spider dragline silk is inherently variable when compared to man-made polymers. The variation in dragline silks from an individual spider can be explained partially by differences in spider behaviour that alter specific processing conditions on the silks, such as spinning speed or silk stretching[42, 87-88]. This variability is useful to the spider, as processing conditions can rapidly alter silk fibre properties, making them suitable for a wide range of conditions[89].

Environmental conditions have an effect on mechanical property variability, particularly important for dragline silks, which contract in response to water, in a process known as supercontraction. Dragline silks are made up of two proteins: MaSp1 and MaSp2[35]. It is the latter that causes supercontraction due to the high proportion of proline in its protein sequence[90]. Different species contain different proportions of proline, which directly alters the extent to which their dragline silks can supercontract[91]. Importantly, the silks can be stretched following supercontraction to alter mechanical properties predictably, allowing spiders to tailor their dragline silk mechanical properties[90]. The link between supercontraction and protein structure has been quantifiably modelled to explain the range of mechanical profiles possible for a given proline content[91].

Minor ampullate silk shows impressive toughness, but without the ability to supercontract[92]. These silks have been relatively understudied[92-93], and there are unanswered questions on the evolutionary pressures leading to two ampullate silks. Interestingly, the glands of major and minor ampullate silks are remarkably similar in shape, where the minor ampullate is smaller (hence the name)[44]. Evidence suggests that both ampullate silks evolved at similar times with the emergence of the Araneomorphae[26].

Combined, processing and environmental conditions alter fibre hydration, hydrogen bonding and proportion of order within the fibre structure. These parameters can be quantified to model the range of mechanical properties of not only dragline silk, but the whole range of other spider and insect silks[5].

1.4.1.1 Orb webs

An orb web is a two-dimensional composite silk structure made of four different types of silks (Figure 1.2)[86].

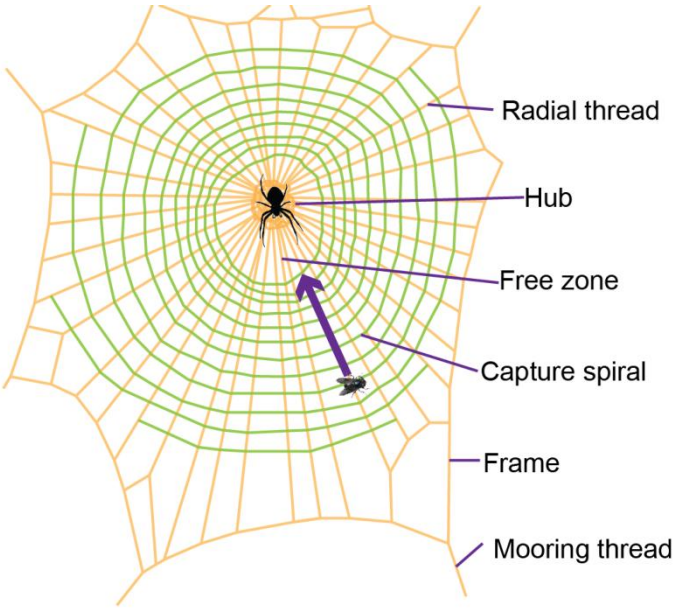

Figure 1.2. A schematic drawing of the structure of an orb web. The spider sits in the hub of the web, which is formed of converging radial threads, made from major ampullate silks (orange) that propagate vibrations to the spider from prey (purple arrow). Encircling capture spiral threads are made from flagelliform and aggregate silk (green). There is often a free zone around the hub where no capture spiral is laid to allow the spider to move to the opposite side of the web. The web is fixed to the environment using frame and mooring threads, attached via piriform silk disks. Minor ampullate silks sometimes form an additional non-sticky spiral[93].

There is evidence of a single origin of the orb web, as there are ampullate and flagelliform silk gene analogues in both the basal cribellate orb weaving spiders, as well as the more recent and diverse ecribellate orbweavers[94-95]. Spider behaviour is vital for using these silk types appropriately to engineer functional structures[4]. In fact, orb webs are multifunctional structures as they are used both as prey capture devices and as platforms to transmit vibrations[96-97].

1.4.1.1.1 Orb webs for prey capture

As 'sit-and-wait' predators, all orbweavers rely on their web to intercept, stop and retain flying prey. The spider requires a certain level of prey mass, rather than number of prey, to sustain itself, leading to selection for webs that are able to catch large, but rare prey[98]. This is experimentally supported across orbweavers, where large prey make up 17 % of catches, but 85 % of prey 'biomass'[99].

Prey interception is related to choice of web location and aspects of web architecture[100]. Cross-species trends have shown that, in general, the bigger the web, the larger the prey that they can catch, and generally these webs are made by larger and older spiders[101-102]. Spiders adjust the mesh size and prey area of their webs to allow interception of prey of the appropriate size[103-104]. Also, under space constraints, web geometry will be adjusted to allow sufficient web capture area for prey interception[105].

Large webs are also prone to intercepting flying animals that are rarely considered edible prey by spiders, such as birds or bats[106]. Web decorations, or stabilimenta, may provide a signal to warn these large prey that the web is there – seen in some species including *Argiope* sp.[107]. It is hypothesised that these stabilimenta are not seen in all species as they are costly to produce, and in some cases lead to reduced success of prey capture[107]. It is also argued that stabilimenta function for prey attraction, which is not supported in all cases[108].

Prey capture is achieved by the absorption of prey kinetic energy, which may be internal, using the silk's viscoelasticity to dissipate energy, or external, using air drag[109]. Experimental studies suggest that radial threads absorb most of the energy during high-energy prey impact (fast speed or big 'prey')[81, 110]. Across orbweavers, the proportion of energy damped by radial threads internally is conserved[111], meaning that only silk volume (diameter and use) affects total internal energy absorption. This is supported by the ability of large webs to absorb more energy than smaller ones[101].

One unresolved factor is the relative importance of air drag on orb web energy dissipation, argued to be very important[109], or not involved[81]. Two factors may contribute to this disagreement. Firstly the experiments differ in the amount of energy being applied to the webs, the former being small and the latter often breaking through the webs. When small energies are applied, internal damping is less likely to have an effect if silks do not yield, which may increase the importance of air drag. Secondly, the diameter of the silks interacts with the speed of impact to determine the air drag factor – these studies make different assumptions about the relative role of inertial and viscous forces on the silks, which have direct effects on their quantified effect of drag. Further studies are needed in this area to determine the role of air drag on silks of different diameters moving at different speeds.

The flagelliform/aggregate capture spiral has been shown to have little effect on energy absorption, but increases web area, leading to higher air drag[81, 109]. In fact, under high wind conditions, spiders will lay down less capture spiral to avoid high air drag[112]. The capture spirals are believed to function primarily for prey retention, illustrated by experimentally increasing mesh size, which decreases prey retention time[113]. In addition, as the capture spiral is electrically conductive, it can attract and retain pollen, a potentially vital energy source for small or young spiders, who are less likely to catch flying prey successfully[114].

Humidity is vital for the function of the web. The aqueous aggregate glue in the capture spiral provides extensibility by both plasticizing the flagelliform silk and creating droplets with surface tension[46]. Drying the water coating results in stiffer and less extensible mechanical properties, as well as reduced stickiness[46]. The aqueous coating allows the silk to remove water from the atmosphere[115], as it is in equilibrium with the air humidity, and when eaten, the capture spiral makes up a significant proportion of the daily water intake for the spider[116]. Wet webs have also been suggested to have better prey catching ability compared to dry webs, but with variability

between species[117]. This is possibly explained by the interaction between capture spiral function, supercontraction ability of the major ampullate silk, and web geometry.

1.4.1.1.2 Orb webs as multifunctional structures

The orb web is an ideal model for light-weight composite functional structures. Whereas high energy absorption and the use of webs for aerial prey capture is a relatively recent spider innovation[118], spider silk has been used for its vibrational signalling function since the basal spiders, for example as 'trip wires' radiating out of burrows[4, 23]. In the orb web, vibration signalling plays a vital role following prey retention, as a rapid signal to the spider that prey has been caught. The radial threads are best positioned for this function, transmitting vibrations from the capture area to the spider in the web centre, or hub (Figure 1.2). Spiders will orientate towards the vibrating radii within milliseconds[96, 119].

The vibrational properties of spider silks have been measured using non-contact laser vibrometry, allowing the signalling functions of webs to be explored[96, 120]. Silk fibres in the radii can transmit longitudinal, transverse and lateral vibrations, where the former has the lowest attenuation over distance, explained by the damping action of the silk junctions on transverse and lateral waves[121]. This also correlates with behavioural data, showing that spiders preferentially respond to longitudinal waves when their webs are vibrated[119]. However, the vibrational properties of webs are complex, making the role of the individual silk types on the vibrational function hard to ascertain. This is further explored in Chapter 6.

1.4.2 *Bombyx mori* silk and the cocoon

Silks are made by all lepidopteran species to form cocoons to protect the pupa from predators, parasitoids and the environment during metamorphosis into an adult[21, 74-75]. *Bombyx mori* is a common model organism for scientific research and its silk has been used for over 5000 years in the textile industry. These moths have been through extensive artificial selection, primarily

selecting for white cocoons that can be easily unravelled[122]. This domestication complicates the relationship between natural selection and cocoon function (and silk properties), but comparison to other types of wild cocoons support that the strength of *Bombyx* silk is not a particular outlier in the Lepidoptera[73-74, 123].

The caterpillar of *Bombyx mori*, known as a silkworm, uses silk to form a protective non-woven composite cocoon around itself before metamorphosis[124]. The unwound fibres of these cocoons consist of two core fibres ('brins') of fibroin bound together by sericin, a bonding protein, forming a composite fibre[74]. Using minimal specimen preparation, cocoon silk fibres can be unravelled from cocoons by softening them with water[122]. The fibres can be further processed by removing the sericin and separating the brins in a process called degumming, which affects fibre mechanical properties[125].

The silks are produced from two labial silk glands, making up around 20 % of the dry caterpillar body mass prior to spinning[126]. The silks are pulled from the silkworm spinnerets by a figure-of-eight head movement from the silkworm[127]. The rheology of these silks in comparison to spider silks and even synthetic polymer processing has been shown to be remarkably similar[12]. By the time the ducts from the silk glands converge, a dry fibre is formed and sericin is added as a coating[128]. The behavioural influence of the silkworm on silk processing following this point is further outlined in Chapter 4.

Silkworms use their figure-of-eight movement to construct a cocoon of several layers[124]. Sericin forms the bonds between the fibres and layers to form the composite structure[124]. These bonds can be modelled to explain and quantitatively predict the mechanical response of the cocoons and other composites[129]. Furthermore, the layered structure and relatively weak sericin binder increases the toughness and damage limitation of cocoons, as layers can delaminate from each other during compression[75]. If cocoon layers are separated experimentally, the inner layers

show stronger mechanical properties than the outer layers, contributing to the protective function of the cocoon[124].

Cocoons also act as barriers to the environment for the pupa, which influences their structure and properties. The interaction between the *Bombyx mori* cocoon and humidity is further outlined in the introduction of Chapter 3.

1.5 Silk rate-dependence

One particular focus of this Thesis is the variation in properties caused by the strain-rate (Chapter 5), which is relevant for both the spider and silkworm silks. Silks have functional uses by silkworms or spiders for a range of mechanical events, from impact protection to supporting the weight of a fallen spider. These events have different time components – some apply stress or strain very quickly, whereas others apply the stress or strain sustained over a long period of time. To date, most studies quantifying silk mechanical properties have been at low strain-rates (e.g. 0.0025 s^{-1} in Chapter 3), which have advantages of obtaining high resolution data. However, the response of silks to faster events, such as impact, is vitally important for understanding their natural function. At high speeds of impact, stress and strain are often dissipated using propagating sound waves; hence studying silk rate-dependence can be a complementary method for studying the sonic properties of silk.

Most polymers exhibit increasing stiffness and yield strength with increasing strain-rate, with higher strength accompanied by lower extensibility. This is due to the strain-rate dependence of the viscous flow of polymer chains relative to each other after yield – less time for this flow results in an apparent increase in stiffness[130]. In order to test these predictions experimentally, a range of different techniques are used to access strain-rates from 10^{-4} s^{-1} to high-rates of 10^{5} s^{-1}, [131]. The high-rate techniques are particularly difficult for silks given their thin diameters and low

axial stiffness[132]. Results of stress-strain properties for spider dragline silks gathered using different methods employing different strain-rates are given in Table 2.

Methods to probe silk's low-rate mechanical properties are the most common and are typically used to generate the stress-strain curves seen in Figure 1.1. At these rates, fibres can be mechanically pulled apart using a tensile tester. One of the first studies of rate-dependence of dragline silk used this technique across the strain-rate range of 0.0005 to 0.024 s^{-1}, [97]. Spider silk stiffness and strength almost doubled over this range (Table 2).

To access higher strain-rates, objects may be dropped onto the silk, normal to the fibre axis. When dropping objects at the speed of 1 m s^{-1}, strain-rates of up to 30 s^{-1} can be accessed resulting in an increase in stiffness, strength, and toughness of dragline silk[47]. However, as stresses up to 4 GPa are reached, the validity of this method is called into question, due to the theoretical limit of strength, given silk's protein structure[5].

Table 2. Mechanical properties of spider dragline silk over different rates.

Technique	**Strain-rate (s^{-1})**	**Maximum stress (GPa)**	**Maximum strain (%)**	**Initial modulus (GPa)**	**Energy absorbed (MJ m^{-3})**	**Reference**
Tensile tester	0.0005	0.65	24	9.8	91	[97]
Tensile tester	0.001	0.83	12	12.1	63	[133]
Tensile tester	0.002	0.72	24	8.9	106	[97]
Tensile tester	0.024	1.12	27	20.5	158	[97]
Object dropping	20-50	2-4	20-50	25-40	500-1000	[47]
Miniature Kolsky bar	1700	1.43	19	34.4	193	[133]
Ballistic impact	3000	-	10	20	-	[134]

More recently, an experimental approach has been developed to access high strain-rates around 1700 s^{-1} using a miniaturized Kolsky bar apparatus[133]. Using this technique, specimens are pulled apart at high rates using an air pressure-driven mechanism. At these speeds, measuring load and extension of a thin specimen of spider silk becomes particularly problematic as the mechanisms for high-speed loading also create mechanical noise. In this paper, a laser is used to measure displacement and the specimen is mounted in contact with a sensitive load cell, which replaces the transmission bar commonly found in Kolsky bar apparatus[133]. The results also indicate an increase in stiffness and strength, although not to the levels seen in the object-dropping experiments (Table 2). Minor ampullate silk was also tested using this technique, and showed similar trends in mechanical properties over increasing strain-rate.

Even higher strain-rates can be accessed using ballistic impact, to over 3000 s^{-1}, [131]. This technique involves high-speed imaging of the sonic transverse stress wave produced from transverse impact of a projectile fired from a gas gun, and is outlined in Chapter 5.

Studying the high-rate mechanical properties of silk is relevant for understanding the natural performance scope of these materials, both in the web or in cocoons. Furthermore, as propagating stress waves can be imaged at high-rate following impact, the sonic wavespeeds of fibres can be measured. This is useful for understanding spider dragline silks, as their sonic properties are vital for web function as they transmit vibrational sensory information[119-120].

1.6 Research scope

This Thesis aims to contribute to the understanding of variation in the mechanical (Chapter 3-5, 7) and sonic properties of single fibres of silks (Chapters 5-7). This variation stems from environmental factors (Chapter 3), applied processing conditions (Chapter 4), rate of deformation (Chapter 5) and even the tension and number of silk fibres (Chapter 6 and 7). Through studying single fibres, an understanding can be built up of the properties of complex

composite structures in terms of their constituent parts. Furthermore, I hope to shed more light on the evolution of silk, and how its properties can be harnessed for suitable engineering applications.

1.6.1 Chapter introductions

1.6.1.1 Chapter 2 Methods

Using a combination of physical science's techniques, including tensile testing, scanning electron microscopy, laser vibrometry and ballistic impact, the mechanical, morphological and sonic properties of silks were measured. This chapter outlines the various techniques used in the research presented, as well as the silk harvesting methods, including forced reeling of spiders and silkworms.

1.6.1.2 Chapter 3 Humidity sensitivity of naturally spun *Bombyx mori* silk

Dry silk fibres are inherently sensitive to changes in humidity, which affects their mechanical properties. This chapter investigates the humidity sensitivity of *B. mori* cocoon silk and applies the silk as a humidity sensor inside the Environmental Scanning Electron Microscope, to help inform best-practices for *in situ* fibre deformation, with the potential for high-zoom imaging.

1.6.1.3 Chapter 4 Forced reeled silks of *Bombyx mori*

The forced reeling of silkworms is a relatively new endeavour, but was required in order to generate samples for the varied experiments. This chapter explores the potential of silkworm forced reeling to prepare consistent silks with desired properties for engineering applications. In particular, methods to restrain the worms to allow sustained reeling and the effect of applied processing conditions are investigated, such as reeling speed and stretch. Importantly, these silks are also compared to naturally spun cocoon silks in terms of morphology, mechanical properties and structure.

1.6.1.4 Chapter 5 High-rate ballistic impact of silks

As outlined in this introduction, silks are rate-dependent, with implications for their mechanical properties during impact. This chapter proposes high-rate ballistic impact as a method for quantifying the change in mechanical properties at strain-rates approaching 5000 s^{-1}. The method images and quantifies the stress waves that propagate during impact, which are further investigated in Chapter 6.

1.6.1.5 Chapter 6 Sonic properties of silks

Spider silks are used in the orb web as both mechanical and vibration signalling materials. This chapter explores the structural basis of the sonic properties of silks, by quantifying the sonic wavespeeds using ballistic impact and laser vibrometry, and comparing to theoretical equations. The consistency of these properties is explored, as well as the potential trade-off between mechanical and vibrational functions.

1.6.1.6 Chapter 7 Future outlooks

The combinations of techniques given in this Thesis are then further applied to some difficult and unanswered questions on spider silks, relevant for whole web function. In particular, capture spiral silks are explored, as well as the properties of the signalling thread of the sector web spider *Zygiella*.

1.6.1.7 Chapter 8 General conclusions

The Thesis concludes with some general links between silk property variation and their protein structure and natural function.

Chapter 2 Methods

2.1 Introduction

In order to study the mechanical and sonic properties of single fibres of silks, a range of standard and novel experimental methods were used. Silkworm and spider silks were studied, collecting from the naturally spun structures and direct forced reeling from the animal's spinnerets. This gave a wide range of materials, natural and semi-natural, which were variable in structure, properties and morphology. These silks were also compared to synthetic viscoelastic polymers and metals to allow interpretation of silk properties in the wider context of man-made materials. This also provides an opportunity to infer the limitations of evolutionary specialization of silks.

A particular challenge for studying these materials is employing suitable and sensitive techniques to cope with the thin fibre diameters, which can be less than 1 µm in diameter (*Zygiella* minor ampullate 0.89 µm) and up to 30 µm (silkworm cocoon silk). High resolution and low force load cells were used for mechanical testing and fibre dimensions were accurately measured using a scanning electron microscope (SEM).

Furthermore, the silks are sensitive to humidity. For all silks, to a greater or lesser extent, water acts as a plasticizer, influencing hydrogen bonding structure by interacting with fibre tension[135]. For major ampullate silk, water causes supercontraction, which results in a significant reduction in modulus[87, 90, 136]. For these reasons, the humidity and tension history of the silks has to be carefully controlled during all stages of reeling, storage and specimen measurement.

In the case of silkworms, this Thesis presents techniques that are a major step forward in the controlled collection of silk; allowing hundreds of meters to be harvested from one worm using forced reeling[137]. Additionally, novel methods to accurately measure the irregular cross-sectional

area of silkworm silks are also presented. These techniques are vital for realistic calculations of the stress-linked mechanical property parameters, enabling fair comparison to other materials.

This chapter gives an overview of the methods common to all or many of the chapters in this Thesis. For chapter-specific methods, including the majority of the novel and specialised techniques developed for material property testing, please refer to the methods section of the chapter concerned.

2.2 Silkworm silks

Bombyx mori silkworm silk specimens were sourced both from cocoons (naturally spun; see 2.2.1) and directly from silkworm spinnerets through forced reeling (see 2.2.2 and 2.2.3).

2.2.1 Cocoons

Naturally spun cocoon silk specimens were taken from a single *Bombyx mori* cocoon. Over 800 metres were gathered from one cocoon, which was enough for all the experiments (for area variation see Chapter 4, Table 7). Variability between different cocoons has been shown to be low when reeling and storage conditions are consistent, so the results from this single cocoon are assumed to be representative[138]. The cocoons were sourced from China and were expected to be around seven years old at the time of unravelling. The unravelling technique is similar to that of the silk industry[139]. The cocoon was softened in Type II water and then unwound whilst still partially submerged onto a motorized spool and stored in lab conditions (c. 20 °C, 40 % relative humidity).

Cocoon specimens run in the dynamic mechanical thermal analysis (DMTA) in Chapter 4 were taken from a different cocoon, prepared in a similar way by Juan Guan, sourced from Jiangsu province, provided by Prof. Yaopeng Zhang from Donghua University, Shanghai.

2.2.2 Silkworms

Final instar *Bombyx mori* silkworms were reared on a mulberry diet in Pavona, Italy. In the lab, worms were stored in an incubator at 9 °C for up to two weeks (after which spinning was unlikely due to silk gland coagulation (C. Holland pers. commun.)). To encourage spinning, worms were taken from the incubator and stored in lab conditions (c. 20 °C, 40 % RH) in falcon tubes. After the worms had been out of the incubator for one hour, some of them were selected for reeling. Worms were selected if they had started the construction of their cocoon (so were often cut out of partially completed cocoons). Prior to reeling, the silkworms were weighed and pictures were taken against a background of graph paper (see Figure 2.1a).

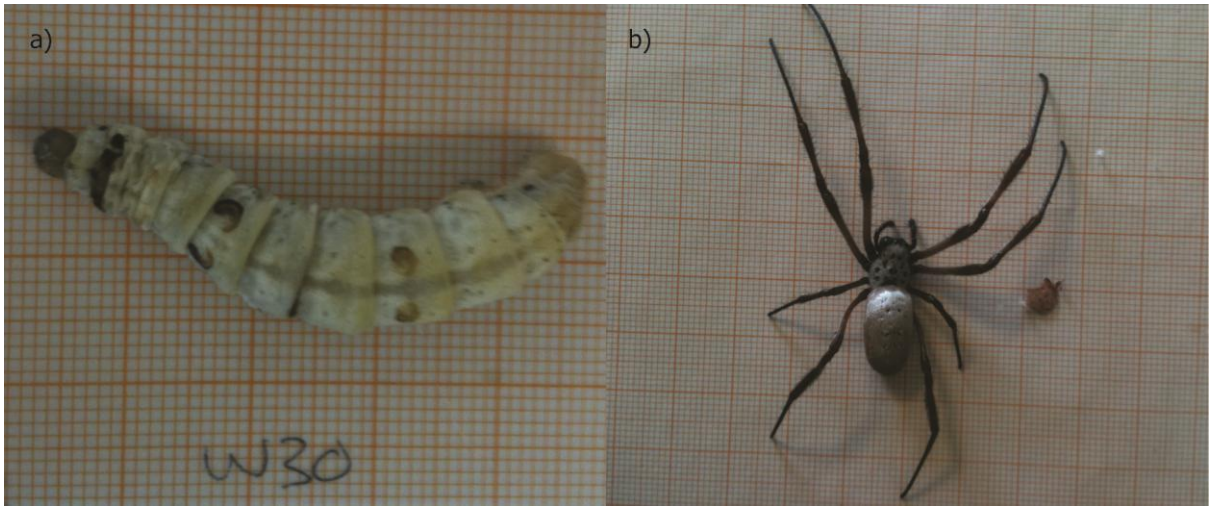

Figure 2.1. Example pictures of **a)** *Bombyx mori* silkworm and **b)** *Nephila edulis* spider (anaesthetized). One large orange square is 10 mm.

2.2.3 Forced reeling of silkworms

To permit forced reeling, the silkworms were immobilised after they started spinning. Native worms were restrained either by hand around the head or suspended from a pole using tape around their body (see Figure 2.2). Similar worm head movement was still possible with both methods. Other worms were immobilized using paralysis, details can be found in Chapter 4.

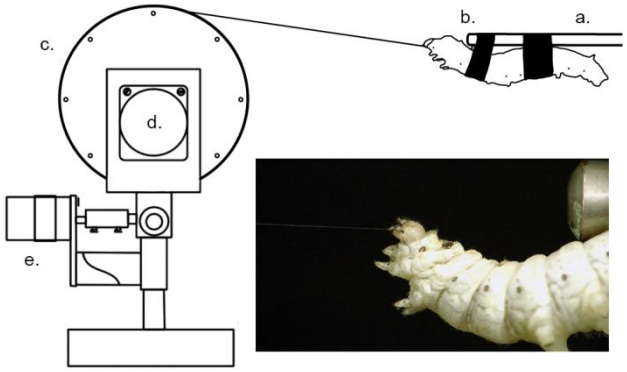

Figure 2.2 Experimental set-up for silkworm forced reeling a) post holding silkworm **b)** tape restraining worm, with one between the true legs and prolegs, and another on the prolegs. Reeling device viewed from the side with **c)** spool **d)** reeling motor and **e)** horizontal translation motor. Reprinted with permission from Mortimer, B., *et al.* Biomacromolecules 14 (10): 3653-3659. Copyright 2013 American Chemical Society

Silk was reeled onto a spool that was rotated by a calibrated motor (Figure 2.2). The spool was translated horizontally using another motor, or moving by hand. Both temperature and humidity were recorded per reeling. In this set-up, reeling speed was modified by controlling motor voltage. For silkworm forced reeling, speeds between 6 and 30 mm s^{-1} were chosen, spanning most of the natural range for spinning[127] (faster speeds were not practically possible). Specimens from the beginning and end of reeling at each speed were excluded.

2.2.3.1 Modifications of forced reeling of silkworms

In brief, the forced reeling of silkworms was further modified, allowing: dipping the silk into water during reeling, changing the temperature of the silkworm during reeling and stretching the silk during reeling. Please see Chapter 4 for details.

2.3 Spider silks

Spider silks were obtained either through the forced reeling of immobilised spiders[88, 140] (see 2.3.1) or using naturally spun web silks[93] (see 2.3.2).

2.3.1 Forced reeled

Nephila edulis spiders were housed in a greenhouse (12 – 35 °C, depending on season) and reared on *Drosophila* and *Calliphora* sp. diet. Spiders selected for reeling were anaesthetized in

carbon dioxide for 5-10 minutes, and then caged dorsal-side-down using pins. The number of fibres and the type of silk required (major and/or minor ampullate silk) were determined by observing spider spinnerets under a dissection microscope (Olympus SZ40, Tokyo, Japan). The spiders were then reeled using the basic forced reeling set-up of silkworms (see Figure 2.2) where a constant reeling speed of 20 mm s^{-1} was used, similar to the average natural spinning speed[88]. Some long specimens (over 25 mm) were reeled directly onto cardboard frames (see Chapter 6). Per reeling, pictures were taken of the spider (see Figure 2.1b), spider weight was taken, and temperature and humidity were recorded.

Large *Araneus diadematus* and *Zygiella x-notata* were also forced reeled for their silks. These were sourced from the urban areas in Oxford and housed in 30x30x5 cm Perspex frames. The immobilisation techniques and reeling techniques are similar to those mentioned above, except a shorter time was used in the carbon dioxide.

2.3.2 Web silks

Where web silks were required, spiders were moved into Perspex frames (*Nephila* in 40x40x10 cm frames)[93]. The spiders were kept in lab conditions (c. 20 °C, 40 % RH and a 16h:8h light–dark cycle). Every day the spiders that had built a web were given a fly (*Drosophila* and adult *Calliphora* for *Zygiella* and *Nephila* respectively), taken from the spider greenhouse, and their web was collapsed for the spider to re-ingest. Spiders had to make at least two webs in the frame for a web to be used. Methods to mount *Nephila* capture spiral web silks or *Zygiella* signal threads are outlined in Chapter 7.

2.4 Non-silk materials

For comparison, a synthetic polymer was also studied – medium tenacity nylon (Goodfellow Cambridge Ltd). Nylon in particular was selected as it represents a synthetic analogue to natural silks: both are semicrystalline polyamides, but nylon has much coarser order-disorder domains

of larger size (micrometres)[141]. The nylon was supplied as a three-filament twine, from which a single strand was unwound for mounting, applying minimal tension during unravelling.

As a control, a rate-independent linear elastic material was also selected - Copper beryllium alloy (CuBe; Cu98:Be2, Goodfellow Cambridge Ltd.).

Cross-sectional area, density and a reference stress-strain plot of these materials can be found in Appendix A.

2.5 Specimen preparation

2.5.1 Specimen storage

Most silk was stored under tension on a spool in lab conditions (c. 20 °C, 40 % RH) to minimise variation due to extrinsic factors, such as storage humidity[138]. To fix the silk onto the spool under tension, nail varnish was used. Some forced-reeled silkworm silks were stored under tension in sealed dry conditions to infer the effect of such storage conditions (see Chapter 4). Spools with a large amount of silk were stored loose, where blue-tack was used to secure the loose end of the silk (used only in Chapter 4 (labelled) and Chapter 5). Nylon was kept in a sealed box to minimise humidity variation and CuBe was stored in lab conditions.

2.5.2 Specimen mounting

For reeling, two types of spools were used, which affected the specimen mounting method (Figure 2.3).

- Some spools were fixed (Figure 2.3), where specimens had to be removed from the spool one at a time using dividers. Using a micromanipulator, the silk was glued to the dividers. Specimens were then either glued into frames for tensile testing (sandwiched between cardboard, see Figure 2.7) or glued directly onto carbon-tape-coated SEM

stubs for imaging (not silkworm silks, see 2.6.1). Care was taken at both stages not to apply additional tension to the fibre.

- Other custom-made spools allowed each inter-rung section to be removed (Figure 2.3). This allowed many specimens to be mounted simultaneously directly onto cardboard frames (see Figure 2.7) or SEM stubs.

- Slack specimens (including nylon and CuBe wire) were unravelled from a spool and mounted using superglue into frames or onto SEM stubs, applying minimal tension.

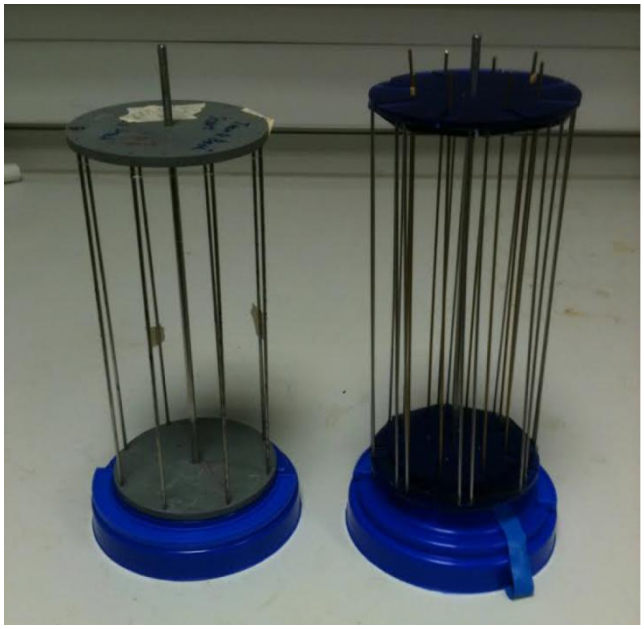

Figure 2.3. Different types of spools used in the Thesis. Fixed (left) and custom made spool where inter-rung segments can be removed (right).

All spools had an inter-rung distance of c. 30 mm, limiting the length of forced-reeled silks under tension. Therefore, specialised methods were developed to allow specimens up to 180 mm to be mounted under tension, by mounting the specimens during reeling (see Chapter 6). For the most part, frames for tensile testing were made of cardboard and had a gauge length of 10 mm, which was chosen for consistency with previous studies from the group and within the field (see Figure 2.7)[91, 93, 142]. Other frame sizes were used also for the vibrometry tests (see Chapter 6), and the effect on mechanical property measurements may be an area for further study, as gauge length is likely to play a small (albeit minor) effect. For the experiments at high humidity, frames were

made of acetate (Chapter 3). All frames were custom designed and then cut using a laser cutter (LS-3040, HPC Laser Ltd., UK).

2.6 Cross-sectional area

All silk areas were measured in an SEM (Neoscope 2000, Nikon Instruments UK), at high vacuum, 10 kV and often at c. x2200 magnification. Pictures were analysed using ImageJ software (NIH). With the exception of silkworm silk, diameters were measured to calculate a circular cross-sectional area (e.g. spider silk in Figure 2.4). Nylon and copper beryllium specimens were checked for their diameter in the SEM, which matched the manufacturers' diameter. Prior to imaging, specimens were sputter coated, most for 150 seconds, 18 mA, giving a 12.5 nm coating of gold/palladium (Quorum Technologies SC7620).

2.6.1 Silkworm silks

Cross-sections of silkworm silks tend to be highly irregular and variable in dimensions (Figure 2.4), meaning that they cannot simply be assumed to be a circle for which the area could be calculated from a diameter measurement. For accurate cross-sectional measurement, silk was carefully transferred from the spool onto dividers[140]. Whilst maintained under tension, the silk fibres were glued with cyanoacrylate along their length onto a section of solder wire, as straight as possible. The solder wire was then either glued into rigid plastic tubing and transversely sectioned into discs, or sectioned directly using razor blades. The thin discs were then treated with 200 mg l^{-1} protease solution in a 38 °C water bath for around 24 hours. The protease digests some of the silk fibre, leaving an outline in the glue equal to the silk's original cross-section. The outer section of the silk fibre was digested more than the inner, suggesting that sericin is easier to break down due to its less ordered structure[129]. The time in the water bath was found to be sufficient to partially digest the silks, creating a dark hole during imaging that makes the silks more visible and easier to find. The discs were mounted onto SEM stubs and sputter coated and

imaged as above, where area (and sometimes additionally Feret's diameter) was measured in ImageJ.

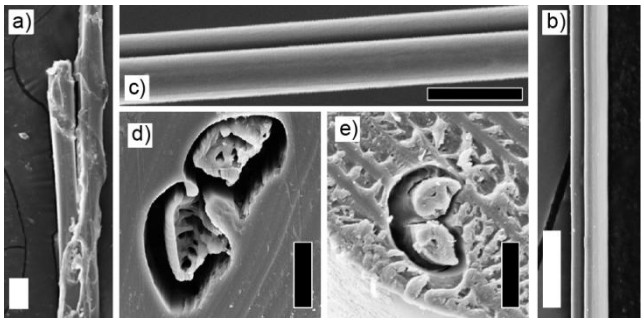

Figure 2.4 SEM images of silks. a) Naturally spun *B. mori* silkworm silk, **b)** forced reeled *B. mori* silkworm silk and **c)** *Nephila* major ampullate silk, where white bars denote 20 μm and black bars denote 10 μm. **d-e)** show the protease-digested cross-sections for naturally spun and forced reeled silkworm silks respectively. NB the dark hole in the glue represents the shape and area of the fibre in the cross-sections, rather than the white brins which have been digested in a protease before imaging. Forced reeled silks were reeled at 6 mm s^{-1}. Reprinted with permission from Mortimer, B., *et al.* Biomacromolecules 14 (10): 3653-3659. Copyright 2013 American Chemical Society

2.6.2 Area allocation

For spider silks, the mean diameter from at least five spider silk specimens (where each specimen area is an average of 3-10 measured disks) was used to calculate the cross-sectional area per spider reeling (only one speed was used). Diameter variation was low (see Appendix A) and specimens were taken from throughout the reeled length, excluding the beginning and end specimens.

Unlike spider silks, the variability in cross-sectional area of silkworm silks was large, even within one individual and one reeling speed (see Chapter 3). Data in Figure 2.5 give the difference in stress-strain curves spread for forced reeled silks with different area allocation. As tensile testing and cross-sectional area measurement are destructive, separate silk samples are used for both measurements. Two approaches are used: either assigning the area measured from the nearest specimen to the tensile tested specimen, or assigning the mean area. For the latter, the spread between samples is identical to the load-extension curves, as the same area is assigned to all curves. Therefore, assuming that silks are likely to be consistent in their mechanical properties

during spinning at a consistent rate, as the mean area gives less spread for the curves, the mean area for each speed of a worm is used for area allocation. Furthermore, by using only one area, a source of experimental variation is excluded, minimizing the variation in the stress-linked mechanical property parameters. This is further supported with data in Chapter 4.

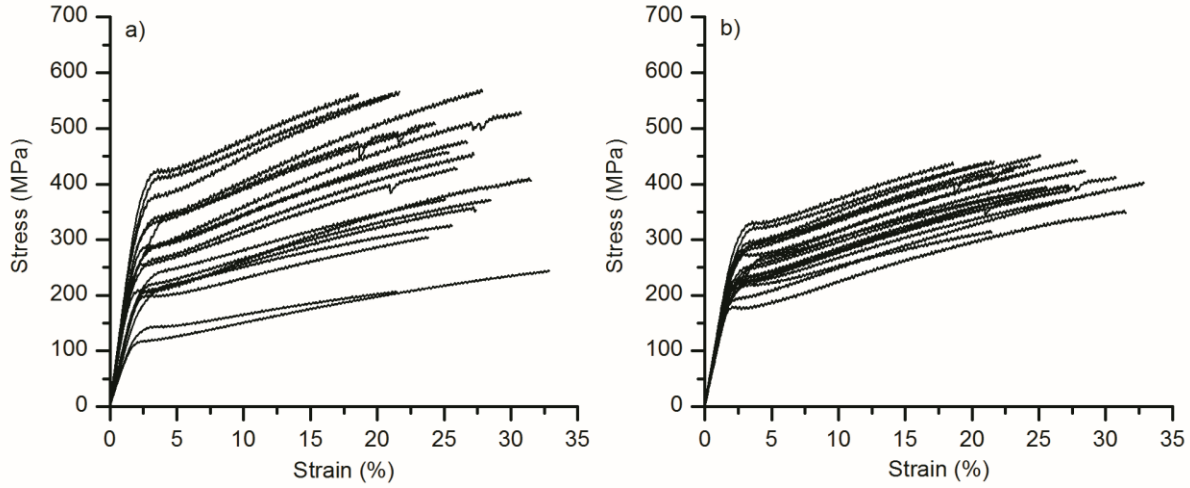

Figure 2.5. Stress-strain curves of an unparalysed worm reeled at 10 mm s^{-1} using **a)** area of specimen nearest tensile tested specimen, **b)** mean area, which is identical to the spread in load-extension raw curves. Reprinted with permission from Mortimer, B., *et al.* Biomacromolecules 14 (10): 3653-3659. Copyright 2013 American Chemical Society

Further analysis of these data revealed the number of specimens required to give an area with good chance of being representative (compared to the mean from over 100 specimens). For cocoon silk, a mean of at least 4 specimens is required to achieve a comparable area and suitable error (quantified by repeating the method 10 times). For forced reeled silk, the minimum was slightly higher, at 5 specimens. Due to the random fluctuation in area for both silks (i.e. position on the silk length does not predict area; see Chapter 4), the benefit of averaging more specimens only gradually decreases the chance of deviating from a mean taken with over 100 specimens. The specimens should be collected randomly across the entire reeled/spooled specimen length, to keep it representative.

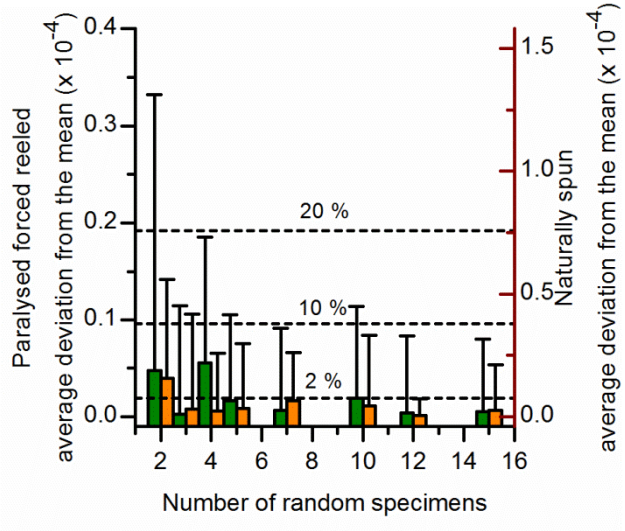

Figure 2.6. Average deviation from the mean (bars) for 10 repeats using a different number of specimens per average (x axis). Error bars give the standard deviation, where there is around 70 % chance that an average using a different N lays within this value. Black axis and green bars give data for paralysed forced reeled silks, whereas the red axis and orange bars give naturally spun data. The dashed lines correspond to 2 %, 10 % and 20 % change in calculated stress when the different area is used.

2.7 Low-rate tensile testing

Three tensile testers were used, one for standard experiments (5 N load cell, model 5512, Instron, UK), one for specialised experiments (5 N, Z0.5, Zwick GMBH, Germany), and another one for portable experiments (2 N, Deben Microtest tensile stage, UK).

Common to all tensile tests, specimens were mounted into clamps and cardboard frames were cut prior to experimenting (see Figure 2.7). Specimens were pulled apart until broken, where load and extension were measured throughout the experiment. Only specimens that broke in the middle were used as data. For spider silks, this was difficult to assess given their small diameter, so specimens were only excluded if they did not fit with the general pattern of five other specimens. For most cases, these experiments were performed in lab conditions (c. 20 °C, 40 % RH). In other experiments (see Chapter 3), humidity was controlled during experimenting using a Wetsys system (Wetsys, Setaram). The most common controlled strain-rate was 40 % min^{-1}, but the Deben stage had a limit of 1.5 mm min^{-1}. For Instron experiments, load-extension data were analysed using a Microsoft Excel macro. For Deben and Zwick experiments, the data

were analysed in Microsoft Excel. Figures were drawn using Origin Software (OriginPro8). Any editing of figures was performed in Adobe Illustrator or Photoshop CS6.

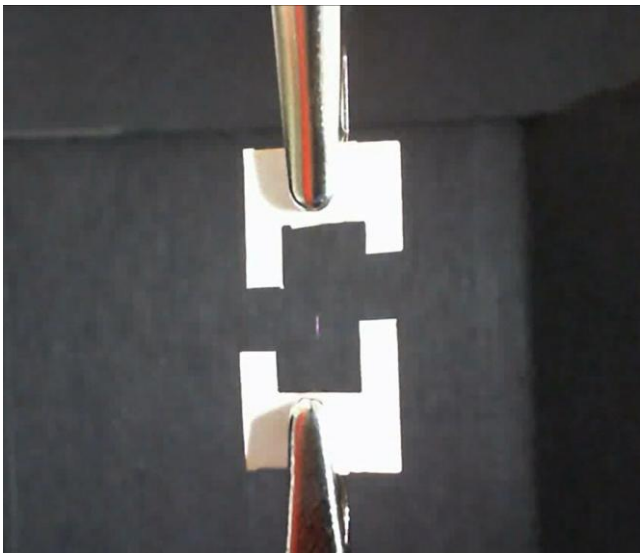

Figure 2.7. Spider silk specimen in 10 mm laser cut cardboard frame, cut and placed in the crocodile clip clamps of the Zwick tensile tester. Where possible, gaps between the clamp and the sample were minimised.

2.7.1 Modifications of set-up

Tensile testing equipment was used extensively in the Thesis in a variety of experimental set-ups, set out below:

- The Deben tensile stage is designed to fit into an environmental scanning electron microscope (ESEM; Carl Zeiss Evo LS 15 VP-SEM), where specimens can be pulled apart *in situ* during imaging (Chapter 3).

- Additionally, the Deben stage was used during laser vibrometry experiments to control the load and extension whilst the sonic properties of the materials were characterized (see Chapter 6, 7).

- The Zwick was also modified to measure the load and extension of silk being reeled directly from silkworms. Although not generating data on the mechanical properties of

the forced reeled silks, these data give information on the behavioural control of the silkworms under different immobilisation techniques (see Chapter 4).

- Specimens were also measured for their high-rate mechanical properties, to allow comparison to the low-rate properties (Chapter 5).

2.8 Statistics

Statistical analysis was performed using Minitab (v. 13) software. Non-parametric tests were used with a 95 % confidence interval[143]. Paired (one-tailed) Mann-Whitney and Moods sign statistical tests were performed, and Kruskal-Wallis tests were performed when more than two groups were compared. For the Mann-Whitney tests, assumptions are made that the treatments only differ in their medians and not in their variation. When this is not the case, the Moods sign test was used, which is less powerful but does not assume equal variance. In some cases, p values were not calculated to minimise the number of tests performed and so decrease the likelihood of a Type II error. In these cases, significance can be inferred by tests already performed and greater differences in medians.

Chapter 3 Humidity sensitivity of naturally spun *Bombyx mori* silk

3.1 Synopsis

This chapter applies the techniques described in Chapter 2 to investigate the sensitivity of the mechanical properties of single fibres of naturally spun *B. mori* cocoon silk to humidity. Humidity is an important factor for the natural function of silkworm silk, as cocoons are mechanical and environmental barriers between the pupa and the outside world during the vulnerable stage of metamorphosis. Furthermore, the humidity sensitivity of silk fibres makes them useful as a humidity detector, and here silk is employed for this function inside an Environmental Scanning Electron Microscope (ESEM), which allows mechanical testing within a humid environment combined with imaging of fibre deformation.

This chapter is adapted from a published article (Mortimer *et al.* 2013[144]) and my contribution involved preparing all specimens, testing them, analysing the data and writing the manuscript. C. Holland, C. R. Siviour, D. R. Drodge and K. I. Dragnevski helped in experimental method and design, as well as data interpretation and edits to the manuscript.

3.2 Introduction

Silk cocoons are composite structures of fibroin fibres and sericin glue[78]. Sericin is hygroscopic, absorbing water from its environment[145], which has direct influences on its action as a binder in the composite cocoon structure. Therefore, humidity is an important environmental factor affecting the mechanical properties of the cocoon, important for its protective function. Cocoons spun in high humidity are less stiff, but with a higher extensibility, resulting in no change in toughness[145]. High relative humidities also result in less distinct cocoon layers that are easier to separate, due to the

spreading of the softer sericin. Indeed, softening of the sericin to allow cocoon unravelling has been selected for during silkworm breeding[122].

The cocoon structure also interacts with humidity to influence silkmoth development during metamorphosis[145-146]. Silkworm cocoons from a range of species have cocoon porosities to appropriately match silkworm ecology and environment[74]. For *Bombyx* cocoons, one study has shown how the layering structure of the cocoon controls water permeability[146]. The outside layers provide a barrier to liquid water, keeping the cocoon from being saturated, whereas the inner layers create a humidity trap within the cocoon to prevent pupal desiccation. Other studies contradict this and conclude that cocoons present no barrier to oxygen or water diffusion[147].

Few studies have assessed the humidity sensitivity of unravelled *Bombyx mori* silk fibres[142]. In agreement with silks from other animals, drier fibres tend to be stiffer and break earlier, whereas wetter fibres are less stiff and more extensible[87, 142, 148]. These trends can be explained by the action of water as a plasticizer within the disordered regions of the silk fibre, increasing the mobility of protein chains and decreasing the attractive forces between chains[46, 149-150]. This effect has been modelled in terms of a shift in glass transition temperature, where drier fibres are more brittle and wetter fibres are more rubbery[135, 148].

On top of the influence of humidity on silkworm silk's stress-strain response, information is missing on the failure mechanisms involved at different humidities. Due to the small size of the silk fibres, imaging of specimen deformation has to be performed within a high-resolution microscope, for example electron-imaging microscopes. The Environmental Scanning Electron Microscope (ESEM) allows high magnification imaging of fibre deformation during *in situ* mechanical testing within a gas environment (Figure 3.1)[151-152]. This potentially allows the matching of stress-strain properties at different humidities to fibre imaging. Additionally, silk properties can be used as a calibrant to assess ESEM humidity levels, as well as assess the effect of specimen preparation techniques on specimen humidity.

The ESEM allows imaging in a gas environment by allowing higher pressures in the imaging chamber compared to the electron column, which must be under a high vacuum. This is achieved through a process called differential pumping[153]. Unlike the traditional SEM, this means that imaging gasses, such as water vapour or nitrogen, can be present in the specimen chamber. It also removes the necessity for coating of non-conducting specimens, which is required in a traditional SEM to prevent charging[154].

Using water vapour as imaging gas ('wet-mode'), specimen hydration can be controlled along water's vapour pressure curve, by setting chamber pressure and specimen temperature (see next section). In theory, the capability should minimise drying effects, whilst simultaneously preventing free water from covering and obscuring the specimen[155-159]. This makes this technique popular for imaging the deformation of humid-sensitive biological specimens, from cells to fibres (see Figure 3.1)[160-171].

An ideal *in situ* experiment would allow the collection of both valid mechanical properties and informative ESEM images. Pictures of the mechanical deformation of silk can provide information on failure mechanisms[151, 163] and crack propagation[162, 172]. Due to the fine diameters of silk (e.g. the fibres used in this chapter were 25-35 µm across), a high magnification is required to obtain sufficient surface detail to be useful. However, increasing the magnification increases the electron beam intensity and thus the risk of beam damage, which will accumulate when a region is imaged continuously or repeatedly[173]. Metallic coating can mitigate beam damage both by preventing charge accumulation, and reducing image noise, in turn reducing acquisition times, thus allowing for higher-magnification images[151, 174]. However, the beneficial effect of coating is reduced when it cracks (Figure 3.1). Additionally, the effect of metallic coating on the mechanical properties of silk is not well understood.

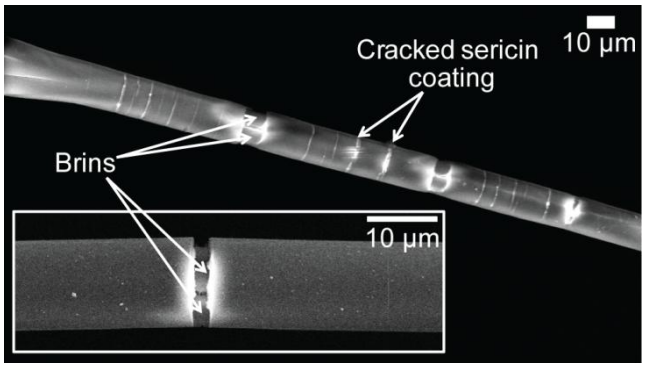

Figure 3.1. Gold/palladium coated forced reeled *B. mori* silkworm silk fibre imaged in an ESEM at 100 Pa (1.3 nm coating) at low zoom and higher zoom (inlaid). White bar denotes 10 µm. Two inner brins can be seen in the centre through cracks in the sericin and metal coating. The cracks have formed due to the *in situ* application of load. The magnification is high, proving good detail, but are poor conditions for specimen charging unless coating is used. The white regions show charging of the fibre is limited to within the crack, due to the lack of coating within the damaged fibre.

This chapter investigates the mechanical properties of *Bombyx mori* silk in experimental environments of different humidities. The interaction between specimen humidity and specimen preparation techniques are also investigated, including the effects of metallic coating, specimen tension and pump-down procedure in wet-mode. These data give insights into the mitigation techniques that can be used to finely control specimen humidity inside the ESEM, applicable to a range of humid-sensitive biological specimens. The humidity sensitivity of these silks is also interpreted in the natural context of the cocoon.

3.3 Methods

3.3.1 Tensile testing

All tensile tests were performed in a Deben Microtest tensile stage with a 2 N load cell at a deformation rate of 1.5 mm min^{-1}. The stage is designed to fit into the ESEM (Carl Zeiss Evo LS 15 VP-SEM) for *in situ* microscopy experiments, with 10 mm gauge length specimens. As described in Chapter 2, silk fibres were mounted in frames, which were cut just prior to tensile testing and ESEM pump-down. For some specimens, jaws were closed by 0.5 mm after the frames were cut, introducing a 5 % slack on the fibre prior to the pump-down procedure (labelled Low Vacuum Slack, Table 3).

Further *ex situ* tensile tests were conducted at controlled humidities (10 - 80 % RH). The data for the 40 % RH specimens use room humidity, which was measured using a humidity sensor (labelled Ambient). Humidities for the other fibres were controlled using a Wetsys system (Wetsys, Setaram). Fibres were left in the humid environment for 10 minutes before experimenting. The time was picked due to the quick rate of hydration/dehydration in silks, of which the latter is slowed following high humidities, only reached here in Humid Cycle (see cocoon specimens in Appendix Figure A.2, single fibres are expected to react quicker). Other details on the tensile testing and analysis are given in Chapter 2.

3.3.2 ESEM conditions

For all specimens measured in the ESEM, specimens were left at the experimental conditions outlined in Table 3 for around ten minutes before tensile testing. All specimens within the treatments outlined in Table 3 had the same waiting time. The electron gun was switched off for all tensile tests to prevent charging effects and damage[173].

For Low Vacuum and Humid specimens, the imaging gas was dry Nitrogen and water vapour, respectively. Humidity in the ESEM was controlled by varying the pressure and temperature inside the vacuum chamber to achieve the target humidity, as calculated using a vapour pressure curve (Figure 3.2)[175]. A calculated relative humidity of 40 % was assumed to be equivalent to lab conditions.

Temperature was controlled using a commercial coolstage (Deben UK) fitted 2 mm below the length of the specimen and between the jaws of the tensile tester. This ensures that the specimen is held as close to the desired temperature as possible throughout the experiment, important for the specimen humidity (Figure 3.2)[163]. Prolonged and repeated use of the ESEM wet-mode leads to an increase in humidity inside the ESEM chamber, making the actual humidity difficult to quantify, adding to the error of humidity estimates shown in Table 3. This effect led to the formation of ice crystals at -1 °C after continued wet-mode usage. As this effect was particularly pronounced for

Humid Cycle, pressure and temperature were increased to 1 °C to produce an equivalent humidity. Experiments resulting in ice crystals were rejected. Due to the low free water content in silk (~ 5 %, see Chapter 4) temperatures below 0 °C are not expected to affect stress-strain response as silk's storage modulus does not change much over this temperature range[176-177].

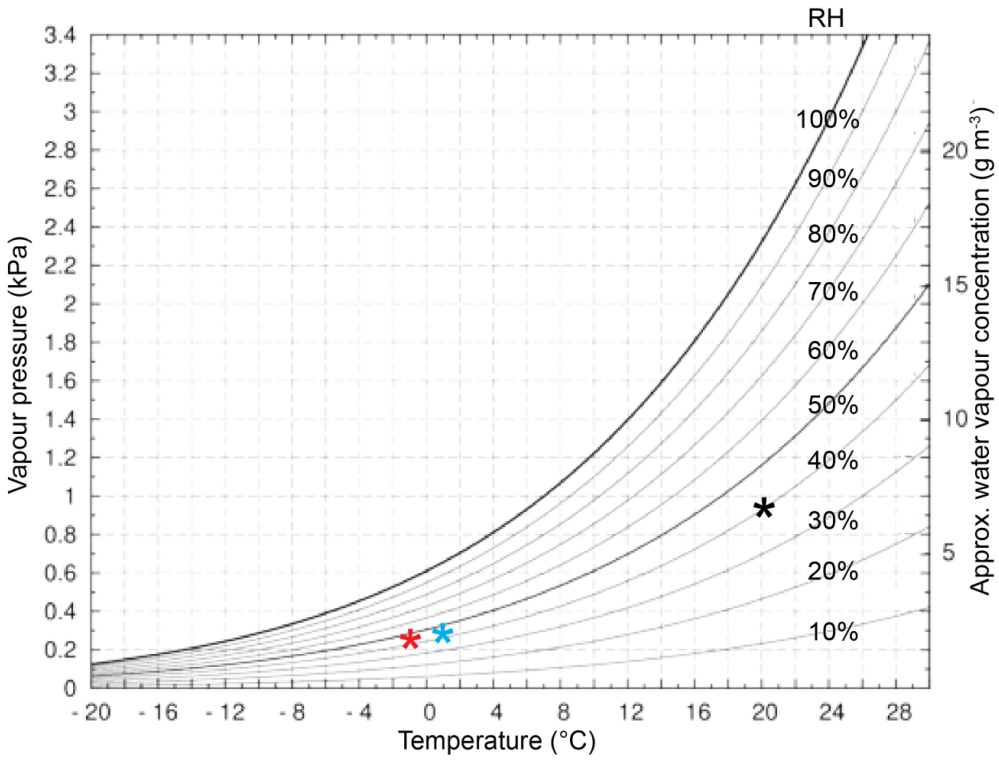

Figure 3.2. Vapour pressure curve for water. At a certain pressure and temperature, water vapour will have a specific value of relative humidity (RH). Black star gives the coordinate for lab conditions (c. 40 %, 20 °C), blue star gives the conditions in the ESEM for Humid Cycle specimens and red star gives the conditions in the ESEM for other Humid specimens. All are equivalent to c. 40 % RH. Adapted from www.conservationphysics.org/vapap/vapap.

With the exception of Humid Cycle, the experimental pressure was reached by a ramp pump-down from ambient pressure to experimental pressure, which often overshot the intended pressure. This means the machine control often reached pressures below the intended experimental pressure (see lowest pressure for pump-down conditions in Table 3). The Humid Cycle experiments involved a pump-down cycle between high and low pressures multiple times, to ensure gas in the chamber is replaced with water vapour[178], followed by a ramp-down to experimental pressure. Both temperature and vacuum range were recorded during different treatments, to track humidity variability through the duration of the experiments (see Table 3).

Table 3. Treatment design. Experimental conditions and pump-down conditions are given. For ramp-down pumping method, the pressure often overshoots the selected experimental pressure, so lowest pressures will be lower than experimental pressure. These are included to give a range of humidities encountered during pump-down for humid specimens. For Humid Cycle specimens, the pressure is cycled 6 times before ramping down to the experimental pressure. Higher pressures were chosen for the cycles to replace the gas in the chamber with water vapour. Pressure was then pumped down to the lower humid experimental pressure. All fibres were held at the final experimental conditions for 10 minutes before measurement.

	Experimental conditions				Pump down conditions				
Treatment	Pressure (Pa)	Temp (°C)	RH (%)	Atmosphere	Pumping method	Lowest pressure (Pa)	Cyclic pressure range (Pa)	Lowest RH (%)	Specimen preparation
Ambient	~ 100 000	~ 22	~ 40	Air	Ambient				
Ambient Coated	~ 100 000	~ 22	~ 40	Air	Ambient				1.3nm of Au/Pd coating
Low Vacuum	100	vacuum	0	Nitrogen	Ramp down	98			
Low Vacuum Coated	100	vacuum	0	Nitrogen	Ramp down	98			1.3nm of Au/Pd coating
Low Vacuum Slack	100	vacuum	0	Nitrogen	Ramp down	98			5% slack
Humid	250	-1 ± 0.2	30-40	Water vapour	Ramp down	198		30	
Humid Coated	250	-1 ± 0.2	30-40	Water vapour	Ramp down	198		30	1.3nm of Au/Pd coating
Humid Cycle	285	1 ± 0.2	35-40	Water vapour	Cyclic - 6 cycles, then ramp to testing pressure	282	412-811	35	

Some specimens were coated on each side for 15 seconds at 18 mA with an Au/Pd target in a sputter coater (Quorum Technologies SC7620), giving a 1.3 nm coating (labelled Coated in Table 3). The metallic coating on the fibre represents only a minor increase in fibre area (0.02 %), so is not expected to offer any mechanical reinforcement. The plasma of metal ions used in the sputtering process may cause damage to the fibre, but this effect cannot be separated from the effect of the coating itself.

3.4 Results & Discussion

3.4.1 Measuring humidity sensitivity

Silk mechanical properties are sensitive to environmental humidity, shown by *in situ* tensile tests in an ESEM (Figure 3.3a), and experiments under controlled humidity conditions (Figure 3.3b). By reference to the latter, it is possible to infer the relative humidity conditions inside the ESEM. For the Low Vacuum nitrogen experimental atmosphere, relative humidity is just under 10 %, and for the Humid Cycle water vapour atmosphere, relative humidity is around 60 %.

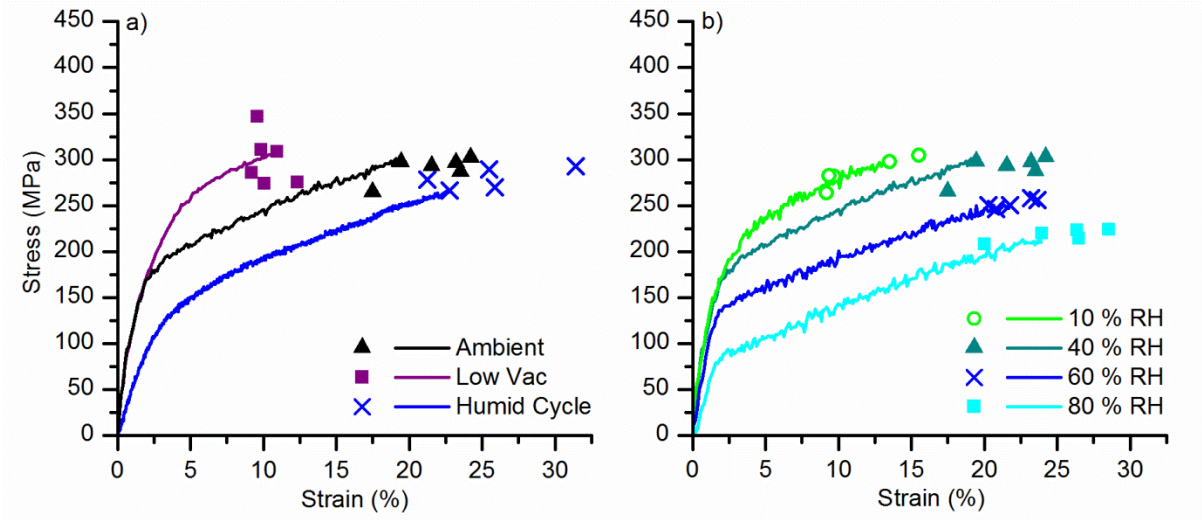

Figure 3.3 a) Stress-strain curves of silk fibres, comparing ambient conditions versus the ESEM low vacuum and wet-mode set to ambient humidity. Scatter points give the break points of other fibres measured under the same conditions with lines showing a representative specimen from the treatment. Kruskal-Wallis showed significantly different break strains between the three ($p < 0.01$). **b)** Effect of relative humidity during experiments on the stress-strain curves of silk fibres measured outside the ESEM. The data of 40 % RH are taken from the Ambient data set.

Silk break strain is significantly different between experimental environments (Kruskal-Wallis statistical test, $p < 0.01$). With reference to both panels in Figure 3.3, at humidities under 60 % RH, silk failure occurs at a constant stress, and above, silk failure occurs at a constant strain. This trend fits in with previous research on the humidity sensitivity of naturally spun silks[142]. Reduced strength and initial modulus at high humidities is explained by the onset of a moisture-induced glass transition in the disordered fraction, beginning at about 50 % RH at room temperature[142]. Either side of this transition, the type and combination of hydrogen bonded structures in the amorphous region set the limits of the maximum stress and strain[179].

Vacuum would be expected to affect mechanical properties by removing free water from the silk structure, resulting in a loss of plasticizer. This increases the attractive forces between the protein chains in the amorphous regions of the silk[46, 150], leading to a higher yield stress, stiffer material post-yield and failure at lower strains. Indeed, the post-yield modulus is significantly higher for Low Vac compared to Ambient fibres (Mann-Whitney test, $p < 0.01$; post-yield data given in Table 4). The effect of dehydration is rapid, as silk properties changed within a few minutes of being in the vacuum. Unlike other fibres measured, the failure points of repeated specimens measured under vacuum show high variability, and do not fail on stress-strain contours. This suggests that drying the silks increases structural variability, whether macro-structure, such as cracking or brin separation, nano-structure, such as distribution and proportion of disorder, or molecular structure, with the number and type of hydrogen bonds. The vacuum will dry the silks in proportion to the time spent in the vacuum, which was the same for all Low Vac specimens.

To further investigate the importance of hydration history of these silk fibres, the specimens were put into vacuum and then removed for tensile testing in ambient conditions. These specimens were compared to specimens that had not been through a vacuum, which were not

significantly different (Figure 3.4). This suggests that silk dehydration is reversible and rehydration happens at similarly quick rates. This is supported by data in Appendix Figure A.2.

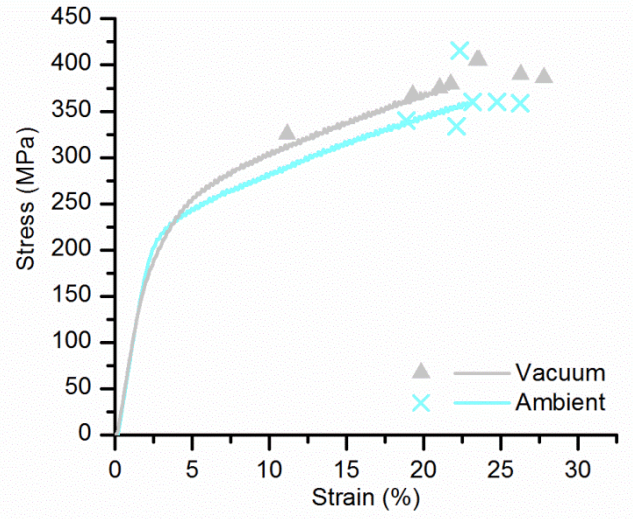

Figure 3.4. Stress-strain profiles of ambient and vacuum-treated cocoon silks. Vacuum treatment involves non-coated silks which have been through a vacuum (identical to that used in the sputter coater for the coated silks), but measured in identical conditions to the Ambient treatment. These tensile tests were carried out using an Instron 5512 tester (model 5512, Instron, UK) with a 5 N load cell at 40 % min^{-1} and analysed in an Excel macro. Ambient and Vacuum are not significantly different in their breaking strain and stress (Mann-Whitney two-tailed test, $p = 0.95$ and $p = 0.18$ respectively). Vacuum effect is therefore reversible, where fibres are hypothesised to rehydrate before measurement under ambient conditions.

Humid Cycle used a temperature and pressure that predicted a humidity equivalent to that of Ambient fibres (c. 40 % RH). However, the silk mechanical properties suggest that the humidity was higher than intended (c. 60 % RH). This could be explained by the saturating humidities (100 % RH) during cyclic pump-down at the higher pressures, from which the silk has not completely dried. This is also seen in Appendix Figure A.2, where dehydration is slower than rehydration, following relative humidities of 80 %. This means dehydration time is dependent on the humidity level reached, and is slower following saturation. A longer period at the environmental conditions may ameliorate this (i.e. longer than 10 minutes between pump-down and measuring), to make sure equilibrium in humidity between the silk and the experimental environment is reached.

However, despite measurement after consistent times, this trend is not seen in all fibres within this treatment, as the variation is large (Table 4). This suggests that there is variation in humidity inside the ESEM chamber between subsequent experiments, and highlights potential weaknesses in using vapour pressure curves to control humidity.

3.4.2 Specimen preparation and humidity

Details of stress-strain characteristics of silks measured in different ESEM environments using varied specimen preparation techniques are given in Table 4. Specimen preparation technique therefore influences fibre performance. Variation in the break strain was seen to be the largest between treatments, which mirror the post-yield modulus trends. Therefore, break strain can be proposed as a single property indicator of the effect of specimen preparation technique on fibre mechanical properties. Figure 3.5 compares the break strain values for all the experiments. Lines between bars denote a paired statistical test, where the star denotes a significant difference.

Table 4. Stress-strain results for all treatments, giving mean value, number of experiments (*N)*. Coloured conditioning of cells indicate specimens that exhibit mechanical properties lower (red) or higher (green) than those of the Ambient control (yellow).

Treatment	N	Break Strain (%)	Breaking Stress (MPa)	Breaking Energy (J cm^{-3})	Initial modulus (GPa)	Post-yield modulus (MPa)
Ambient	7	21.50	302	25.2	7.05	559
Ambient Coated	9	16.70	313	20.5	8.44	669
Low Vacuum	6	10.30	300	11.6	7.74	794
Low Vacuum Coated	9	9.20	292	9.9	8.05	852
Low Vacuum Slack	8	13.40	306	15	6.71	697
Humid	7	13.50	284	15.2	9.36	671
Humid Coated	7	14.80	284	16.9	10.7	607
Humid Cycle	5	25.40	279	25.6	5.83	539

Lower Ambient Higher

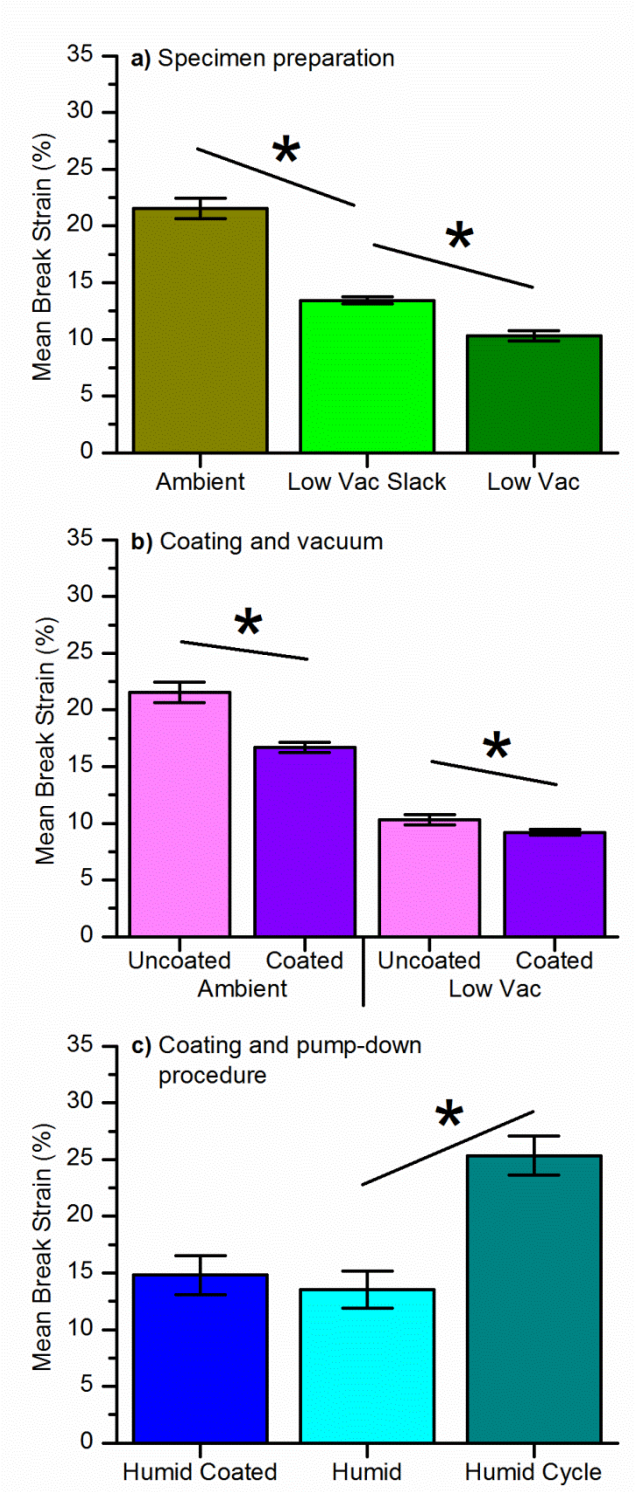

Figure 3.5. Effect of different specimen preparation techniques on break strain of silk under different experimental humidities, where error bars give the standard error of the mean. Asterisk denotes statistically significant difference between pairs. **a)** Effect of introducing slack (5 %) onto the silk fibre prior to pump-down on the break strain compared to no slack, low vacuum and ambient conditions; **b)** effect of vacuum and coating on the break strain of silk fibres; **c)** effect of pump-down procedure and coating on the break strain of silk fibres measured in the ESEM wet-mode.

3.4.2.1 Tension under low vacuum

Adding slack to a silk fibre prior to pump-down significantly increases break strain compared to Low Vacuum ($p < 0.01$), but did not restore break strain to ambient levels, which is still significantly higher ($p < 0.01$; Figure 3.5a). During specimen deformation, Low Vacuum Slack and Low Vacuum specimens are essentially the same, as slack is removed as the specimens are pulled apart. Therefore, it is the tension during pump-down that causes this significant effect, possibly due to fibre contraction when dehydrated (fibre length contraction can be seen in Appendix Figure A.2). Tension can therefore be considered to affect the loss of water from a fibre, or otherwise influence the breaking mechanism, such as proportion of surface flaws.

Adding slack is hypothesised to make the sericin less likely to crack due to specimen contraction during evacuation. Figure 3.6 shows longitudinal cracking in a silk fibre due to brin separation under low vacuum conditions when the fibre was under tension. Unlike the transverse cracking in Figure 3.1, due to applied load and metallic coating, the longitudinal cracking shown here is due to brin separation following fibre contraction, which is likely to affect a greater proportion of the fibre. This type of cracking is also seen in cocoons spun under low-humidity conditions[145]. Sericin cracks could lead to stress concentration that might hasten failure, although the modulus of sericin is comparably low[129]. However it is more likely that the sericin coating prevents water loss from the main structural components of the fibre – the brins, and that cracks weaken the fibre by allowing additional water loss under vacuum.

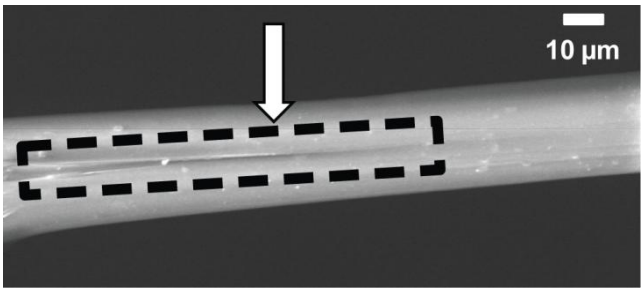

Figure 3.6. Uncoated silk fibre imaged in an ESEM at 15 Pa (under a nitrogen atmosphere). The fibre was pumped down under tension, so is analogous to the Low Vacuum specimens. The white bar denotes 10 µm. White arrow points to the start of a longitudinal crack in the sericin coating, running to the left from the arrow inside the highlighted box. To the right the sericin is uncracked, and the surface structure is smooth. The imaging pressure is used for better quality imaging and is not expected to differ in humidity from 100 Pa, which was used as the experimental pressure for mechanical measurements (effectively 0 % RH).

3.4.2.2 Coating

When measured in ambient and low vacuum conditions, coated specimens also showed significantly lower break strains (ambient, $p < 0.01$; and low vacuum, $p = 0.03$; Figure 3.5b), but with little effect on breaking stress or initial modulus. Water diffusion can also explain the mechanical properties of fibres subjected to sputter coating, as diffusion rates into/out of the fibre will be impeded by the metallic layer. This layer may prevent rehydration of the fibre following sputter coating, which occurs under vacuum. The low humidity of the plasma coating chamber is then effectively 'locked in', thus decreasing break strain at ambient conditions. As break strain is also lower for coated specimens under vacuum, it is also likely that the metallic coating exacerbates sericin cracking under tension, further decreasing break strain.

Despite the effect of coating on mechanical properties, there are advantages to applying coating as it helps to reduce specimen charging and is conventionally used in SEM. The use of some degree of fibre coating for imaging in low vacuum mode may therefore be preferable to no coating in order to obtain images at sufficient magnification to resolve features of interest. However, the coating only protects the surface of the fibre, and may not maintain this benefit after sericin cracking has occurred and the uncoated fibroin is exposed to the beam (Figure 3.1 and Figure 3.6)[172].

3.4.2.3 Pump-down procedure in wet-mode

However, for humid experiments, coating did not decrease break strain and is not significantly different from the non-coated humid specimens ($p = 0.7$). This is explained by the cracking of the metallic coating during pump-down in tension (Figure 3.5a), which would then allow the humidity of the experimental conditions to increase fibre hydration, and so break strain.

Cyclic pumping also significantly increases break strain compared to a ramp-down ($p < 0.01$), up to levels similar to those seen in ambient specimens. Previous studies have also shown that a ramp-down procedure leads to a higher degree of specimen dehydration[178]. This is because a non-cyclic pump-down leads to a higher proportion of dry air present, as air is not replaced by water vapour to the same extent[178]. The degree of specimen dehydration caused by the pump-down procedure will inevitably effect the time to equilibrate at a specified humidity prior to measurement, affected by the pressure, target humidity and machine capabilities. Overall, the data support the use of cyclic pump-down as the optimal procedure for humid specimen observation.

These data also highlight the need for improvement in the application of this procedure and machine control. In particular, all fibres measured in wet-mode showed increased mechanical property variability, which is assumed to be due to changes in humidity between repeat experiments of the same treatment. The theoretical lowest humidity for Humid and Humid Coated based on lowest recorded values of both pressure and temperature in the chamber gave 30 % RH. Inferring from Figure 3.3b, the silk break strains from Humid and Humid Coated suggest that the humidity may in fact be as low as 10 % RH. This may be explained partially by the specimen being at a higher temperature than the Peltier chip, leading to a lower humidity at that pressure due to the vapour pressure curve[178]. However, this is unlikely as specimens were consistently placed a close as possible to avoid such a temperature gradient and there is no evidence of a similar effect for the Humid Cycle specimens.

3.4.3 Humidity sensitivity of silk

What are the implications of the sensitivity of mechanical properties of the individual fibres for the natural context of the cocoon? A simple scaling up of the properties suggests that toughness of the individual fibres will only be negatively affected at very high or very low humidities, as shown by the areas under the curves in Figure 3.3. However, due to the non-woven composite structure of the cocoon, the effect of humidity on toughness is more complex.

Compared to single fibres, cocoons have a greater capacity to store water as they have a higher proportion of sericin. As the relative humidity increases, the water mass in cocoon sections increases, up to 47 % for 100 % RH specimens[145], more than the maximum for single fibres (5 %; see Chapter 4). The 3D structure of the cocoon and the unravelling process may also contribute to the difference in water mass between cocoons and fibres. At high humidities, this leads to sericin expanding due to its higher volume. This has two implications. Firstly, the porosity of cocoons could change as a function of their humidity, becoming less porous as humidity increases, creating a passive permeability control. Secondly, very high humidity can lead to composite collapse, as the binding sericin will become too soft, explaining the easy separation of cocoon layers in cocoons spun in humid conditions[145]. This may also explain the selection for oxidative phenolic tanning, which requires water to become active and creates cross-linking bonds within the cocoon structure[145, 180] – it provides a control mechanism to increase cross-linking in the cocoon structure to increase stiffness when the integrity of sericin may be lost. However, in terms of the artificial selection of *Bombyx*, this sericin softening is exactly what was selected for to allow easy reeling, and correlates with white cocoons with low proportion of tanning and so cross-linking[122]. Overall, although the humidity sensitivity of the fibres will play a role in cocoon function, the interaction between sericin and humidity in the composite structure is likely to have a larger effect.

The humidity sensitivity of silk also has useful applications in engineering as a calibrant material for certain techniques. In particular, specific material behaviour can be matched to observable structure in the ESEM. In order to achieve this, the next step will be to measure which ESEM environments and specimen preparation techniques minimise beam damage of the specimen during imaging[173].

3.5 Conclusions

Naturally spun *Bombyx mori* silk has different mechanical properties depending on its environmental humidity. At lower humidities, break strain reduces and fibres fail at a constant stress. Whereas at higher humidities, fibres soften, showing reduced strength and breaking at constant failure strains. This transition is explained by a moisture-induced glass transition in the silk structure, causing increased molecular chain mobility at the higher relative humidities[149].

Storage humidity, however, has been shown to be relatively unimportant, as silk can dehydrate and hydrate rapidly and reversibly. Silk saturation with water, however, leads to longer dehydration times needed to equilibrate with the experimental environment.

Due to the fact that silk's mechanical properties are sensitive to environmental humidity, the effect of preparation techniques on specimen humidity during experimentation can be investigated. For example, tension exacerbates water loss, proposed to be due to promotion of fibre cracking. A metallic coating can prevent water diffusion in and out of the fibre, but if cracked, may promote sericin cracking and further water loss. Lastly, cyclic pump-down during ESEM wet-mode ensures chamber hydration, but leads to specimen saturation.

In the context of the cocoon, the humidity sensitivity of the individual fibres is unlikely to play a role in cocoon function compared to the interaction between sericin binder and humidity, which expands and softens significantly at high humidities. This may explain the need for cross-linking

enzyme activity at high humidities that lead to cocoon tanning, particularly seen in wild silkmoth cocoons in order to maintain mechanical integrity.

This chapter has also shown how the humidity sensitivity of silk fibres can be used as a calibrant to assess how experimental environments and techniques affect specimen humidity. This is useful beyond understanding silk properties to a range of humid-sensitive specimens that can be measured *in situ* in the ESEM. The next step is to assess how these specimen preparation techniques affect specimen imaging *in situ*, to allow useful matching between mechanical properties and specimen deformation.

The manipulation of stress-strain properties of silkworm silks is explored in the next chapter, using forced reeling of silkworms. Naturally spun silks are compared to forced reeled silks in terms of their fibre morphology, mechanical properties and protein structure.

Chapter 4 Forced reeled silks of *Bombyx mori*

4.1 Synopsis

This chapter continues research into mechanical property variation in *Bombyx* silks, comparing naturally spun cocoon silks used in Chapter 3 to forced reeled *Bombyx* silks. Forced reeling allows processing conditions to be manipulated, enabling specific factors that affect mechanical property variability to be investigated. Here, ways to immobilise silkworms for reeling, as well as the effect of reeling speed, applied postdraw, and storage conditions on the mechanical properties are investigated. Data provided from J. Guan complements this research by investigating the different structures formed by these processing conditions. This chapter provides insights into the importance of natural spinning conditions for silk structure and properties. Furthermore, it allows the performance scope of *Bombyx* silks to be investigated, beyond the natural processing conditions, useful for the use of these silks in engineering and medicine.

This chapter is adapted from two papers: data in Sections 4.4.1-4.4.3 is published (Mortimer *et al.* 2013[137]) and data from 4.4.2-4.4.5 is submitted (Mortimer *et al.* to *Acta Biomaterialia*). My contributions were preparation of all the silk specimens, mechanical testing and SEM imaging, as well as analysis of the data, interpretation and writing the papers. C. Holland and F. Vollrath helped with experimental design, data interpretation and manuscript editing for both papers. J. Guan and D. Porter provided the DMTA data and interpretation, as well as editing for the second paper. TGA data was provided by N. Hawkins, with interpretation from C. Holland and D. Porter.

4.2 Introduction

As well as collecting silk from the cocoon, where the silk is naturally spun, silks can be forced reeled directly from the silkworm. Forced reeling uses the natural silk dope spun *in vivo*, but the

processing conditions are somewhat 'unnatural' since the silk fibre is pulled directly from the spinnerets[127, 137, 181]. As these silks do not go through the cocoon layering and unravelling process, forced reeling provides the potential to produce silk fibres with more consistent fibre morphology. Also, unlike industrial processing, forced reeling avoids fibre unravelling from a cocoon under wet heat in a chemical environment[122], which will be expected to affect the inherent properties of the thread due to the viscoelasticity of silks[135, 177]. Importantly, forced reeling allows the control of processing and environmental conditions under which the silk is spun, allowing greater control of fibre variability than is possible with naturally spun silk.

This leads to the potential to tailor the mechanical properties of a thread[127] by reeling under controlled experimental conditions[182]. The potential for detailed hypothesis testing is significant because this technique allows the investigation of a wide range of variables (that have been previously investigated with spider silks[80, 87-88, 140, 183-185]), such as spinning speed, body temperature, postdraw medium, animal physiology (e.g. anaesthesia, blood pH) and air humidity.

Whereas naturally spun and forced reeled silks are spun *in vivo* using natural protein dope feedstock, 'silk' fibres can also be spun artificially from reconstituted silk fibroin (RSF) protein molecules that have been obtained from native silks after dissolving in strong chaotropic agents[186-187]. Importantly for industrial uses, RSF can be processed in a number of ways to produce films, fibres, and a variety of 3D structures, with a wide range of potential applications, principally for use in biomedical research[188-191]. Studying forced reeled silks bridges the gap between the naturally spun and artificially produced *Bombyx*-derived proteins. For example, the influence of processing conditions on the structure-property links of forced-reeled silks gives an indication of the performance range and limitations of materials derived from this protein sequence, which can inform RSF research.

4.2.1 Forced reeled silk variability

However, forced reeled silks still have high inter-fibre variability. This complicates the quantification of the exact effect of processing conditions on the properties of silks. Additionally, alert and resisting silkworms are able to break the thread or otherwise interfere with the reeling process through other physiological or behavioural means, which explains the relatively little research on the forced reeling of silkworms[192]. This is additionally a problem for the industrial use of forced reeled silkworm silks, as long consistent fibres (with high strength) would be most desirable. The key to addressing these issues is the separation of behavioural influence from the effect of processing conditions. In spiders, the behavioural control of load during reeling has been shown to influence predictably variability and properties of drawn fibres[185, 193]. However, until now, reeling force in silkworms has not been controlled or quantified.

A silkworm can apply load on to the nascent thread through internal and/or external means. External loading could occur using either or both of two pairs of facial palps (maxilla and labial) or the 'true' (thoracic) legs positioned below the spinneret. From observation and scanning electron microscope (SEM) images, the first pair of legs is proposed to be best positioned to hook onto the silk. In support of this assertion, the claw on the leg has a nook of a size comparable to a naturally spun silk fibre (Figure 4.1a). Although the legs do not interfere with silk during cocoon construction, non-Bombycoidea caterpillars use their thoracic legs to climb back up the silk thread, which is used as a lifeline (but how the silkworms slow down during the fall is untested)[194-195]. The exact method of load application is presently unknown, but is not important for the interpretation of the experiments. Moreover, it might well be possible that total loading history on a thread is likely to differ between individual worms and between multiple reeling events due to the speed and angle of reeling and the status/experience of the worm. This multiplicity of contributing factors may explain the high variation in forced reeled silks between different silkworms[196].

Internally, silkworms possess a silk press which, when activated, increases the diameter of the silk fibres[128]. Although it has been a long observed feature of silkworm anatomy[197], so far the mechanics of the press have only been inferred from superficial structural analysis. Using data from silkworm dissection, as well as recent histological and micro-CT observations[128, 197-198], Figure 4.1b aims to summarise the known anatomy of the silk press. Both the dorsal and ventral muscles act to increase the silk duct lumen when contracted (Figure 4.1b inset). Lumen size narrows when the muscles are relaxed due to elastic recoil of the cuticle-lined wall. Detail of the musculature may be found elsewhere[128, 198].

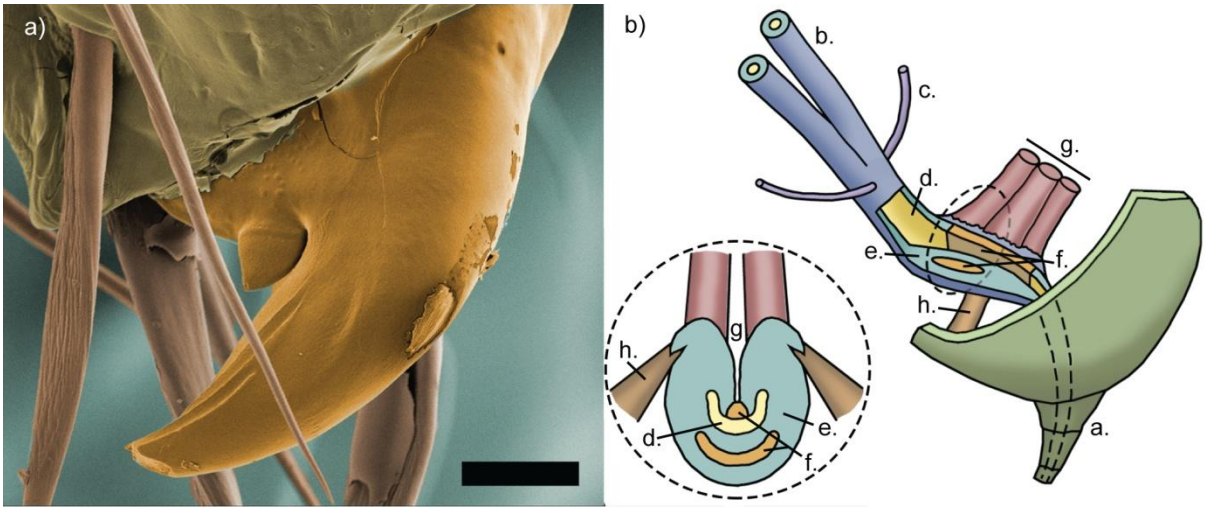

Figure 4.1. **a)** SEM false colour image of the claw at the end of the first thoracic leg of a silkworm. Black scale bar denotes 50 µm. Note the notch on the inner side of the claw that corresponds to c. 20 µm, the diameter of a naturally spun silk fibre. **b)** Drawing of the silk press inside a silkworm before the spinneret (green, a). The two ducts (blue, b) run from the two silk glands and then merge. Ducts from the Filippi's gland (purple, c) join before the silk press. At the press, there is a smaller lumen (yellow, d) and a thickening of the tube wall (turquoise, e). There is a long ventral plate that meets the lumen and a smaller plate imbedded in the wall (orange, f). Ventral (red, g) and dorsal (brown, h) muscles control the press to increase lumen size when they are contracted. Elastic recoil of the cuticle-lined wall enables lumen contraction. The inset image gives the transverse section through the press.

This chapter presents a novel method that induces natural silkworm paralysis by using the animals' own 'play-dead' anti-predator defence, which is induced hormonally by a specific paralytic peptide[199]. The paralytic peptide is naturally produced by silkworms in their haemolymph[200]. The peptide was first isolated and purified by Ha *et al.* (1999), who confirmed its ability to cause rapid and rigid paralysis when injected back into the haemolymph[200]. The

peptide is naturally produced immediately following bleeding[201]. The paralysis serves to prevent silkworm movement and 'bleeding out' following cuticle puncture, but also triggers an immune response[202].

4.2.2 Effect of processing conditions

Using these techniques for silkworm immobilisation, the effect of processing conditions on the forced reeled silks can then be investigated. For example, reeling speed affects the mechanical properties of forced reeled spider and silkworm silks[88, 127, 181, 203]. It is assumed that the reeling speed affects the shearing of the silk dope whilst in the duct[88], thus a faster reeling speed would result in an increase in beta sheet content while at the same time leading to a decrease in fibre diameter[88, 203]. In spiders, it has been shown that there is an optimum speed for breaking energy and stress, which matches the average natural spinning rate[88]. However with silkworms, increasing reeling rate does not affect breaking energy, and maximum stress increases to an impressive one Giga Pascal (GPa)[127, 203].

Like reeling speed, processing conditions such as postdraw (stretching the fibres during reeling) or wet-reeling (dipping the silk through water during reeling) would also be expected to create additional order[183]. Adding tension to the fibre before it is fully 'set' creates stress-induced molecular alignment[204], allowing hydrogen bonding during drying to 'lock' the order into place[183]. Indeed in spider spinning, such post-processing additions affect mechanical properties by increasing order within the fibre[87, 183]; something also seen in synthetic polymer spinning[205-208]. To further increase the degree of molecular order in a finished silk fibre, processing conditions of parameters like temperature, stress and solvation would need to exceed the yield point or glass transition temperature to allow macromolecular mobility[177].

Understanding the relationship between protein structure and mechanical properties is a vital step towards using silk or silk-derived proteins for specific applications. One of the most useful

analytical tools allowing the matching of properties and structure is dynamic mechanical thermal analysis (DMTA), with detailed research to date helping to elucidate the protein structure of RSF[190, 209-213], native silk fibres[135, 176-177, 179], and artificially spun fibres from natural silk dope[214-216]. This research has revealed differences in thermal behaviour between the different silk-derived proteins; most importantly, differences in glass transition temperatures (Tg) that can be linked to the degree of order in the protein, which in turn is a key component of protein structure determining mechanical performance[177].

Processing conditions such as chemical or isothermal treatment, or applying postdraw, have been shown in RSF to influence the structures present[150, 209-210, 217-221]. Other studies make the important link between the treatment, the mechanical properties and the protein structure[176, 190, 222-224]. To date, artificially spun silks (unless treated considerably post-spinning) are unable to match their natural counterparts[15]. This is most likely because the processing conditions used lead to dissimilar supra-molecular structures[15].

4.2.3 Overview

This chapter aims firstly to measure the effectiveness of the naturally-produced paralytic peptide as a way to control silkworm behaviour during forced reeling, and so control forced reeled silk variability. Then, using appropriate worm immobilisation techniques, the effect of a range of processing conditions on the mechanical properties of silkworm silks will be investigated, to explore the extent to which silk properties can be tailored for specific applications. To provide insights into the effect of processing conditions on structure-property links, the thermal properties of a diverse range of forced reeled silks will also be studied. These results should provide insights into the potential and limitations of *Bombyx*-derived silks, bridging the gap between naturally spun and artificially produced RSFs.

4.3 Methods

Methods for the preparation of forced reeled silkworm silks (basic set-up), silk storage and mounting, tensile testing and cross-sectional area are given in Chapter 2. Presented here, novel methods were developed in silkworm immobilisation using paralysis, as well as modified forced reeling techniques. The forced reeled silks were also probed for their thermal properties by N. Hawkins and J. Guan to infer the structures present using standard thermogravimetric analysis (TGA) and dynamic mechanical thermal analysis (DMTA).

4.3.1 Silkworm paralysis

This Thesis develops the use of silkworm paralysis as a method of immobilising silkworms. Worms were injected with 0.1 ml of 10 mg l^{-1} paralytic peptide in water solution into the first pseudopod base into the haemolymph. A shallow injection is used to help ensure the silk gland is not pierced. The paralytic peptide was custom synthesised by Activotec, Cambridge. The peptide sequence is ENFVGGCATGFKRTADGRCKPTF, modified so that the two Cys amino acids at positions 7 and 19 have an intra-disulfide bond[199]. This is to increase the stability of the peptide.

Following injection, all silkworms ceased movement, becoming rigidly straight and stopping spinning even if silk was protruding from their spinnerets (see Figure 4.2, Figure 4.6). After approximately 30 minutes of complete paralysis, they would recover their ability to spin silk, which agrees with observations of anaesthetized spiders[140]. Therefore worms were left for 30 minutes after injection in lab conditions (c. 20 °C, 40 % RH) until they started spinning again.

Paralysed worms were then reeled in a semi-paralysed state by suspending them, as described in Chapter 2. Silkworm movement appears normal, but they were less likely to break the silk thread and can be reeled for long periods of time (up to 6 hours). During reeling, the appearance of unparalysed and paralysed silkworms was identical, where only the head and body movement differs.

Figure 4.2. Pictures of silkworms: unparalysed (left) and a few minutes after paralysis injection (right). Arrow gives the site of injection, at the base of the first pseudopod. The paralysed worm was rigid and immobile.

4.3.2 Load during reeling

Paralysed and unparalysed worms' reeling behaviour was compared by measuring the load exerted during reeling. To quantify this, a silk thread from a stationary silkworm was fixed to a load cell that was then moved, similar to other published research (set-up in Figure 4.3)[185, 225]. A tensile tester (500 N, Z0.5, Zwick GMBH, Germany) was used to record load and displacement over the reeling period. The silk was attached to the load cell by covering the silk end in tape, which was then placed into a crocodile clip attached to the load cell. The position of the tape and silk within the crocodile clip was kept consistent between trials. Spinning silkworms were held carefully around their head during reeling using thumb and forefinger, rather than the bull-clip shown in Figure 4.3 (where the worm was more likely to move and wriggle out). The silk was reeled at a constant speed of 10 mm s^{-1} for up to 70 cm.

All data were processed in Microsoft Excel by removing slack from the initial stages of reeling then zeroing the initial load. Background levels of load over displacement without silk attachment were also measured to provide a control.

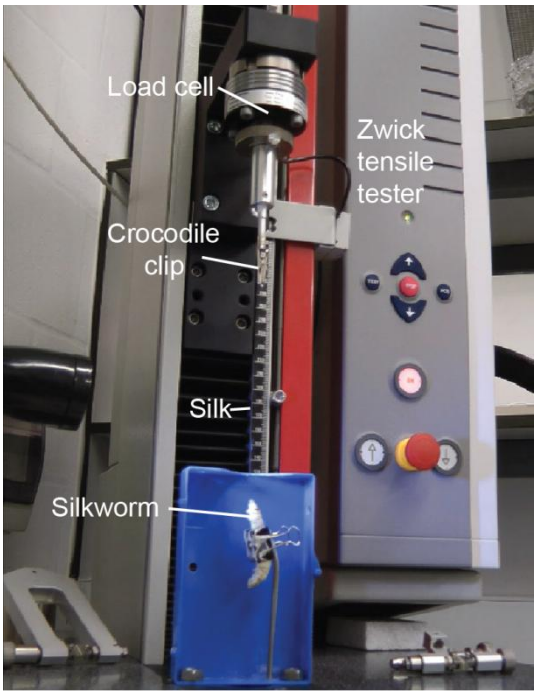

Figure 4.3. Measurement of load versus displacement during silkworm forced reeling. Worms were immobilised at the bottom and their silk was attached to the load cell via a crocodile clip by taping the end of the silk. The load cell then moved up at a constant speed, reeling the silk from the worm. In the experiments, worms were held by hand rather than using the bull-clip shown here.

4.3.3 Modifications of forced reeling of silkworms

Forced reeling allows processing conditions to be manipulated, which have direct influences on the structures, and so the thermal and mechanical properties of the silks. Here, applied postdraw and the effect of worm temperature were investigated during forced reeling.

4.3.3.1 Postdraw reeling

Instead of reeling the silk straight onto the spool, silks can be stretched during reeling to influence the mechanical properties before the silk has fully formed all its hydrogen bonds[183]. These postdrawn silks were run through a water bath (at 19 °C) via a Teflon-coated guide before winding through motorised wheels, which applied a controlled postdraw (Figure 4.4). Cold water was necessary to minimise sticking to the underwater guide, assumed to be due to sericin.

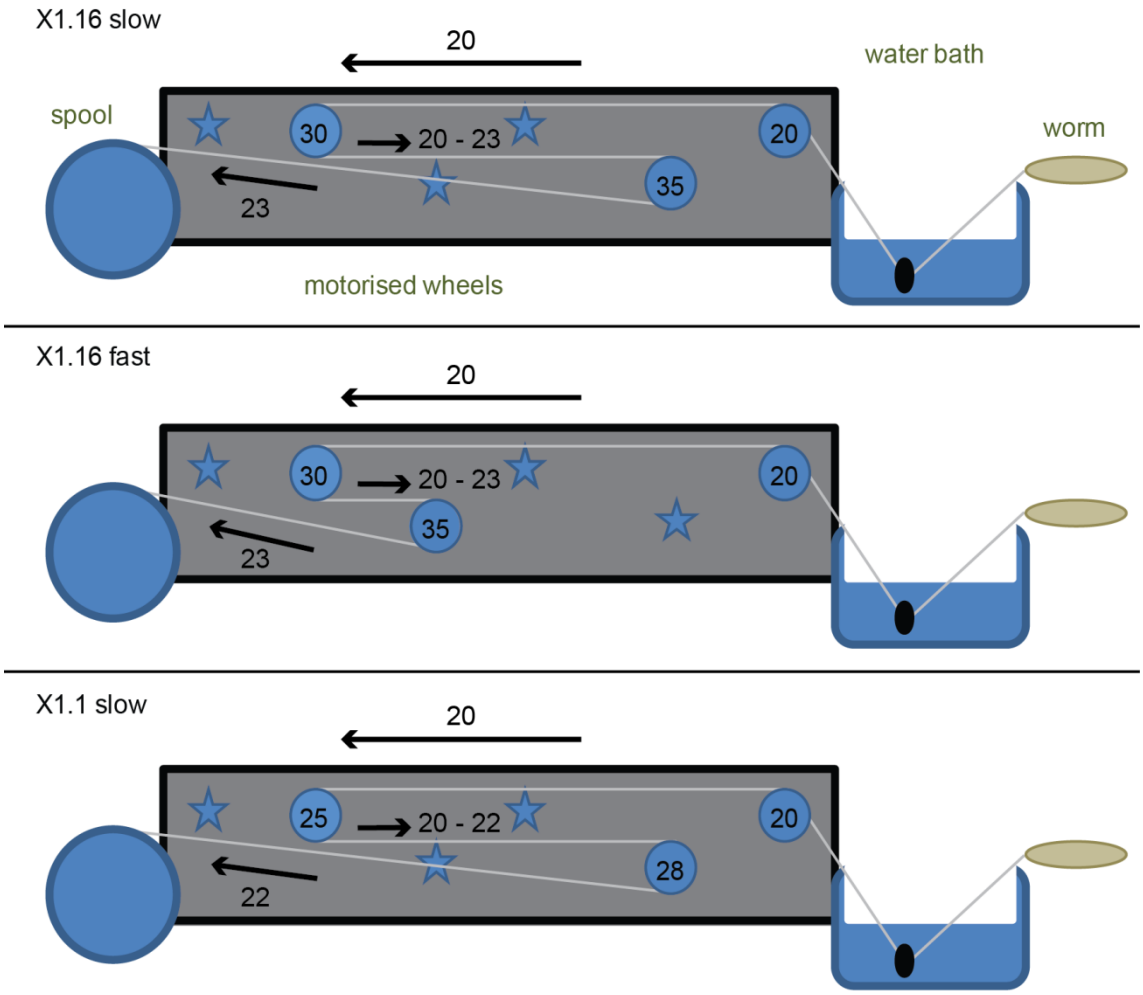

Figure 4.4. Experimental set-up for wet postdraw experiments. Worms were suspended from a pole and silk was reeled at a speed of 20 mm s^{-1} through a water bath under a Teflon coated guide. The silk then ran on three motorised wheels before collection onto a rotating spool. Speeds and direction of silk at different positions in the apparatus are given (in mm s^{-1}). The number on the wheels gives the diameter of the wheel in mm (turns per second is the same for all wheels). Stars give the comparable positions of rotating axels not occupied by wheels. Upper row of wheels rotated anti-clockwise, bottom row rotated clockwise.

The second wheel during reeling was found to control the reeling speed from the worm, which was set to 20 mm s^{-1}. This was expected to be due to the 180° contact with the silk and was inferred using nail varnish on the silk as a marker and measuring its speed through the apparatus. This method also showed that wheels should be covered in tape, to allow better grip on the silk. The purpose of the first wheel was therefore not to control the speed of the silk, but the angle through the apparatus, so was not covered in tape. The third wheel was placed at different distances away from the second wheel, giving fast (close) or slow (far) postdrawn silks

(see Table 5). Following the third wheel, the silk was collected onto a motorised spool, travelling at the same speed as the third wheel.

Table 5. Reeling conditions for the postdrawn forced reeled silks. Error on the postdraw applied comes from the error in measured wheel diameter covered in tape, which was used to work out the circumference and speed of the rotating wheel.

Silkworm	Initial reeling speed (mm s^{-1})	Postdraw applied	Distance between postdraw wheels (mm)	Postdraw applied per second (s^{-1})
x1.16 slow	20	0.16 (±0.04)	226	0.014
x1.16 fast	20	0.16 (±0.04)	99	0.032
x1.1 slow	20	0.10 (±0.04)	226	0.009

4.3.3.2 Temperature reeling

As outlined in Chapter 2, the worms were immobilised by taping them to a pole. If a copper pole is used, the high thermal conductivity can be exploited to influence the temperature of the worm during reeling, as silkworms are poikilothermic. Worms were attached along the length of their body to a copper pipe through which either cold or warm water was running. For the cold reeling, a water bath with a cooler was used, where water flows through the copper pipe by use of a water pump. During reeling, water temperature remained constant within ±0.2°C. For the warm reeling, a water bath was used, including an inbuilt pump and thermostat.

The copper pole temperature was measured using a thermometer against its surface, labelled 'cold' and 'warm' respectively. To further increase temperatures, insulation is added around the worm to increase the expected worm temperature ('hot' reeling). Worm temperature was measured using a thermometer; however, gradients of temperature are expected, so the readings are approximate. For 'hot' reeling, temperature measurement of the pipe was not possible due to the practical difficulties of measuring through the insulation. Table 6 gives the temperatures and reeling speeds used for each treatment. The properties of the silks are

compared to worms reeled in the basic set-up at ambient conditions, where worm temperature is c. 20 °C.

Table 6. Temperatures and reeling speeds of different temperature treatments. Worm temperature is given as a range as temperature measurements using a thermometer were not exact.

Label	Water temperature (°C)	Pipe temperature (°C)	Worm temperature (°C)	Reeling speeds (mm s^{-1})
Cold	8	10	11-14	10, 20
Warm	59	45	32-36	10, 20
Hot	59	-	c. 40	20

4.3.4 Thermogravimetric analysis (TGA)

These experiments were performed by Nick Hawkins, using a methodology developed in the Oxford Silk Group. TGA allows the thermal properties of the silks to be investigated, by measuring the weight change over temperature – giving information on bound water and thermal decomposition. Aluminium pans and 100 µl crucibles were pre-tared on the TGA balance prior to adding the specimen (TA Instruments Q500 TGA). Approximately 0.3 mg (3 m) of silk (naturally spun and forced reeled) was unravelled from a spool and carefully transferred into the aluminium pan. The specimen was then heated at a rate of 3 °C min^{-1} from ambient temperature to 300 °C in Nitrogen gas flowing through the TGA furnace at a rate of 100 cc min^{-1}.

TGA also measured degummed naturally spun silk as a comparison. The degumming process is described in detail elsewhere[226]. Juan Guan prepared the degummed silk specimens.

4.3.5 Dynamic mechanical thermal analysis (DMTA)

These experiments were performed by Juan Guan, using a methodology developed in Guan *et al.*[142]. DMTA explores the dynamic mechanical properties of silks by applying a deformation frequency over a temperature range. This gives information on the structures present in the

silks, particularly the amount of order or disorder. All the dynamic mechanical thermal experiments were performed on TA Q800 under DMTA multi-frequency strain mode. The parameters kept as constants were (i) temperature ramp rate at 3 °C min^{-1}, (ii) frequency at 1 Hz and (iii) dynamic strain at 0.1 %. The selection of these constant parameters was based on the most common polymer testing procedure as well as a compromise between experiment duration and data quality[135, 177, 179]. A preload force equivalent to 50 MPa stress was applied in order to keep the fibre in tension throughout the dynamic oscillation.

Two types of temperature scans were conducted for forced reeled silks. Firstly, a full-range temperature scan from -100 °C to +270 °C, and secondly cyclical temperature scans with the first ramp up to +120 °C or +180 °C, which are abbreviated as 120 °C annealing and 180 °C annealing, respectively.

RSF fibres were also used for DMTA experiments. They were supplied by Wang Qin at Fudan University. The RSF solution was obtained using the same method as Wang *et al.*[227] and the fibres were obtained through wet-spinning similar to the methods used in Yan *et al.*[228].

4.4 Results & Discussion

The results from this research fall into five sections. First, the effect of paralysis peptide on silkworm reeling behaviour is investigated. Then, by comparing paralysed and unparalysed worms, the effect of reeling speed on forced reeled silks is presented. These results suggest inherent differences between naturally and forced spun silks, which are further explored in terms of fibre morphology and area, and thermal properties. To explore the full range of mechanical properties open to forced reeled silks, the effect of a range of processing conditions is then presented. Lastly, the structural differences between naturally spun silks and varied forced reeled silks are explored through the use of DMTA in collaboration with J. Guan.

4.4.1 Paralysis

The results indicate that silkworms are able to effect load during forced reeling (Figure 4.5). The likelihood of a worm applying load was unaffected by reeling repeats. Paralytic peptide injection causes this force to be smaller and more consistent (Figure 4.5a and b). Both paralysed and unparalysed silkworms showed a maximum load that was significantly higher than the background (Mann Whitney two-tailed test, $p=0.0197$ and Moods sign test $p<0.01$ respectively).

Importantly, unparalysed worms are able to apply a breaking load during spinning (Figure 4.5a). These instances were rare during the load reeling experiments (mean is c. 0.01N), but in the basic set-up every unparalysed silkworm broke the silk thread during reeling at least once, with rare exceptions and regardless, the animals interfered with reeling in almost every instance. Force measurements of this maximum load curve give loads of around 0.08 N, equivalent to over 700 MPa based on an average area for a forced reeled silkworm fibre at 10 mm s^{-1} (the speed of reeling for these experiments: 1.05×10^{-4} mm^2, n= 23). Such a load would exceed the breaking stress for these silks, which is up to 550 MPa (Figure 4.10). In contrast, the maximum force that spiders have been observed to apply during forced reeling (using their internal friction breaking mechanism[225]) has not exceeded 60 % of the breaking load[185, 193, 225]. This may be explained by the more natural context of forced reeling for spiders – the sensory inputs of forced reeling are likely to be similar to falling[225]. Therefore spiders may not apply high loads as breaking should be prevented during falling. Silkworms, however, may be less likely to fall due to their arboreal locomotion[229], so may not recognise the sensory inputs of reeling and respond by breaking the fibre to conserve their silk.

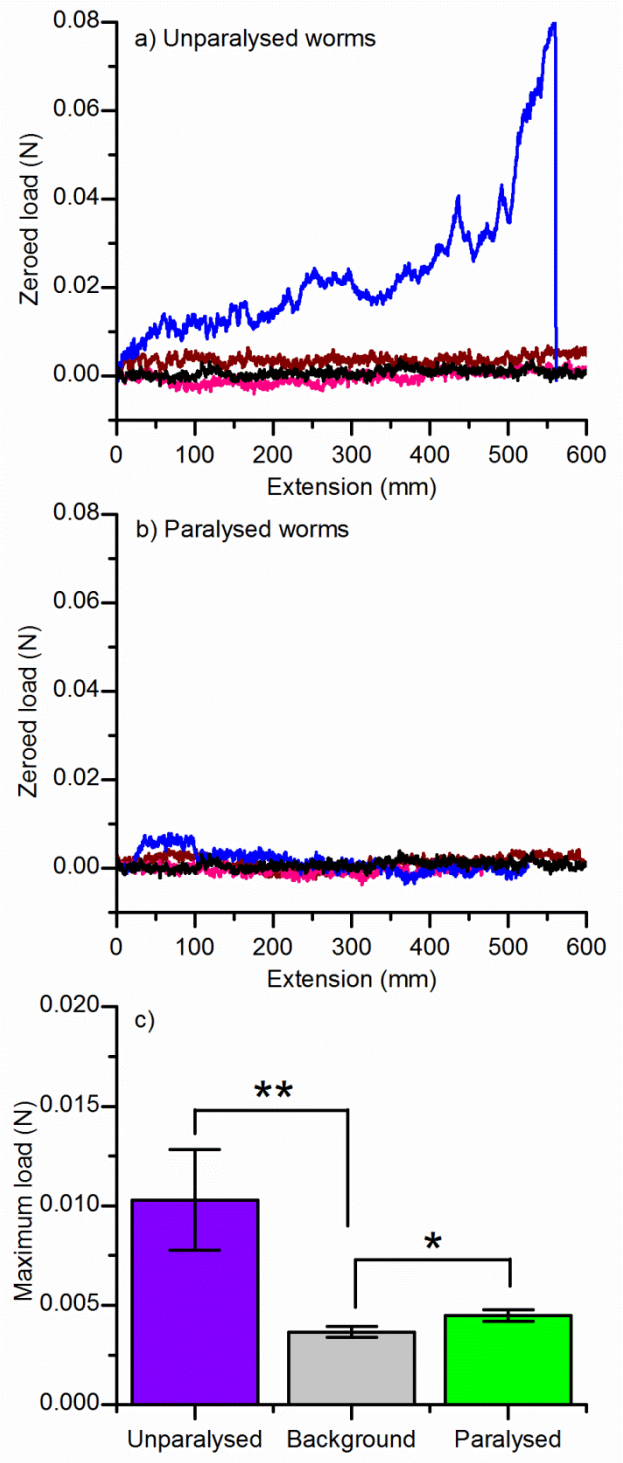

Figure 4.5. Silkworm force over reeling. Zeroed load over extension for **a)** unparalysed worms (6 worms, 30 reelings): blue line gives maximum load curve, red the median, pink the minimum and black a representative background curve (out of 12); **b)** Paralysed worms (8 worms, 27 reelings); **c)** Average maximum load for the moving crosshead for background (no worm attached) and paralysed and unparalysed worms, where errors bars give the standard error of the mean between worms. Unparalysed silkworms show a maximum load significantly higher than the background level (i.e. no worm attached; Moods sign test, $p<0.01$**), as do paralysed worms (Mann Whitney $p= 0.0197$*).

In contrast, the silkworms injected with the paralysis peptide were unable to apply a high force during reeling. These worms were semi-paralysed – they were able to move and spin silk, but there appeared to be a lasting effect of the paralytic peptide in the muscles that exert load onto the silk. As yet, a full understanding of the details of the silkworm's press system is missing to explain these findings. Regardless, the method of paralysis spinning prevents fibre breakage during reeling, allowing reeling for over seven hours (our record was >500 m).

The significant difference between the background and paralysed reeling load represents the force taken to pull the fibre out of the worm. It can be explained in part by the inherent viscosity of the silk dope as it flows[12]. Silkworm anatomy is also likely to contribute to this force as the press is applied when the muscles are relaxed[128]. Immediately after paralysis, the silk shows a ribbon shape (Figure 4.6), consistent with a compressive action of the press on the silk. When spinning restarts in the semi-paralysed state, the press constrains the thread without cutting it. The silk press will therefore be acting as a friction break on the silk during paralysed reeling. This could be further explored using a more sensitive load cell during reeling.

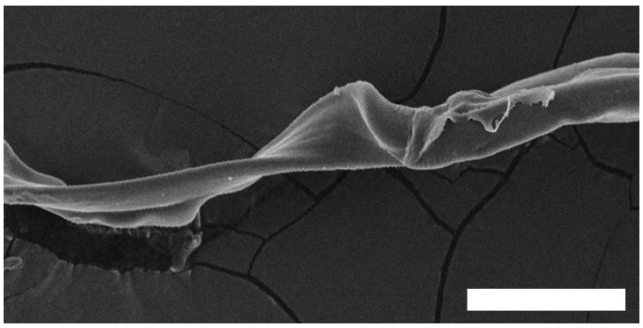

Figure 4.6. SEM image of a flattened silkworm thread following injection of the paralysis peptide, where white bar denotes 50 µm. Reprinted with permission from Mortimer, B., *et al.* Biomacromolecules 14 (10): 3653-3659. Copyright 2013 American Chemical Society

Only one reeling speed was measured using this set-up. Different reeling speeds may lead to different results. In particular, personal experience reeling unparalysed worms suggests that silkworms are more likely to break the silk at slower speeds, so behavioural influence may be more pronounced at these speeds. The force required to pull the silk out of the worm is also expected to increase with increasing reeling speed[12].

Overall, these experiments have shown that the behavioural application of load by the silkworm during reeling can be removed by injecting the silkworm with a paralytic peptide. This is important as variable load during reeling has been shown in spiders to affect mechanical property variability[185, 193]. By removing the effect of behaviour on mechanical property variation, the effect of applied processing conditions can be investigated. This is investigated in the next section by reeling paralysed and unparalysed silkworm silks at different speeds.

4.4.2 Reeling speed

The data in Figure 4.7 support the hypothesis that silkworm behaviour influences silkworm silk mechanical properties. Some unparalysed worms broke the thread during reeling. In specimens close to the break (most commonly before 15 mm s^{-1}), it appears that the animals were applying load to the fibre. Research on spider silks has shown that higher reeling force increases modulus and breaking stress and decreases breaking strain[185, 193]. The unparalysed data agree with this, showing higher strength and modulus (see Appendix Figure A.3) and lower extensibility compared to paralysed silkworm silks at 15 mm s^{-1}, suggesting a higher reeling force. Importantly, if the specimens surrounding a break are excluded from comparison, the paralysed and unparalysed worms show more similar properties, suggesting more comparable reeling loads (Appendix Figure A.4).

Paralysed worms give the best indication of the relationship between forced reeling speed and mechanical properties (as their reeling load is consistent; Figure 4.5b). This observation is underpinned by the consistency of silk-area data for paralysed worms (Figure 4.7d), which shows a non-linear relationship and is consistent with findings in spiders[204].

The mechanical data from silks taken from paralysed worms shows an ‘optimum’ speed for maximum stress and breaking energy. This feature is also observed for spider silk[88]. Moreover, silkworms can also be reeled ‘too fast’, resulting in a deterioration in properties above a certain

speed (100 mm s^{-1} for spiders[88], 20 mm s^{-1} for silkworms (Figure 4.7)). For silkworms, the maximum thread toughness was seen at 10 mm s^{-1}, at the average natural spinning speed[127]. Toughness is likely to be the mechanical property on which natural selection acts as the cocoon structure will be selected for high energy absorption ability for protection against predators[74]. Both the composite structure of the cocoon and the fibre properties will contribute to this energy absorption[129]. Individual fibres will therefore be selected to have high toughness at biologically relevant reeling speeds. Therefore, the relatively poor breaking energy above 20 mm s^{-1} is unlikely to have an effect on fitness, as these reeling speeds will not be used by the worm.

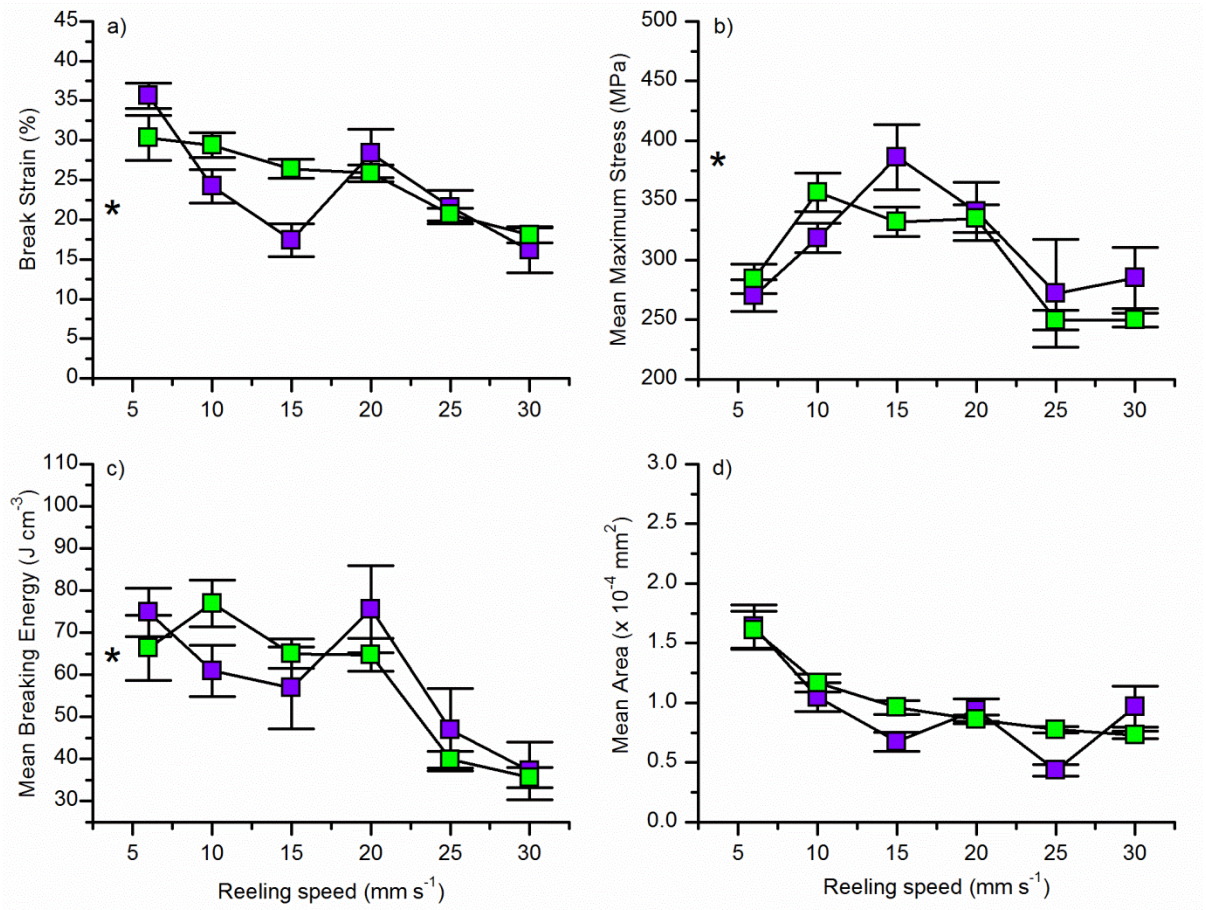

Figure 4.7. The effect of reeling speed on the mechanical properties of paralysed (green) and unparalysed silkworm silks (purple: includes data where the silkworm broke the thread): **a)** the break strain, **b)** maximum stress, **c)** breaking energy and **d)** mean cross-sectional area. Stars give a comparison to mean values for naturally spun silk (not shown in d). Error bars give the standard error of the mean. Number of specimens measured is given in Appendix Table 13.

The patterns of mechanical properties observed here differ from previously published literature data on the effect of reeling speed on silkworm silk properties, which shown higher stiffness,

strength and toughness with increasing reeling speed[127, 203]. This will be due to differing methods in area measurement and insufficient control of worm 'behaviour' in the previous experiments. The methods presented here will provide more robust data as silkworm behaviour was controlled, with consistently low fibre loading during reeling (Figure 4.5b), giving a much more reliable relationship between mechanical properties and reeling speed.

Taking silks from one paralysed worm, Figure 4.8a compares the mechanical property envelope of forced reeled silks taken at different speeds compared to naturally spun cocoon silk. In support of Figure 4.7, silks reeled from paralysed worms at the intermediate speed (here 15 mm s^{-1}) displayed the highest average toughness. Importantly, the toughness is also similar to the naturally spun silk, but the forced reeled silks show a slightly higher variability.

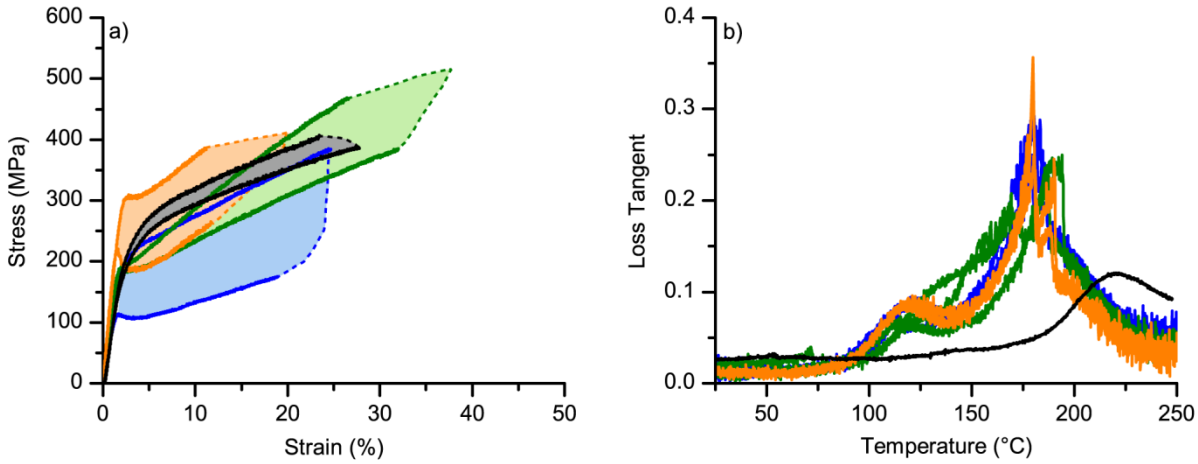

Figure 4.8. Differences between forced reeled silks from one paralysed worm reeled at different speeds: **a)** stress-strain profile showing the envelope of properties per material type. Blue denotes 6 mm s^{-1} (n=7), green 15 mm s^{-1} (n=5) and orange 25 mm s^{-1} (n=5) and black denotes naturally spun silk. **b)** Loss tangent taken from DMTA temperature scan run by J. Guan, showing 2 or 3 repeats per speed.

Naturally spun and forced reeled silks from the same worm spun at different speeds were then measured by J. Guan for their dynamic mechanical properties (Figure 4.8b). The higher the temperature of the loss tangent peak, the more ordered the polymer structure is, due to the higher glass transition temperatures of stronger bonded structures[179]. The height of the loss tangent value also indicates the relative amount of the type of polymer structure present. Hence, this can be interpreted as naturally spun silks having drastically higher amounts of order

in their composition compared to forced reeled silk. Furthermore, the paralysed silkworm forced reeled silks show large amounts of disorder, and evidence of multiple types of structure, indicated by the presence of multiple tan delta peaks. The effect of reeling speed on the structure of forced reeled silks is also minimal, with a slight increase of order for the 15 mm s^{-1} reeled silk. It has been assumed that the trends in the dynamic mechanical properties are representative as the stress-strain trends for this individual worm are similar to the average trend (Figure 4.7).

These results raise questions about the inherent differences between naturally spun and forced reeled silks. Whereas the stress-strain profiles between forced reeled silks and naturally spun silks are similar, especially under more natural processing conditions (i.e. match average natural spinning speed), the DMTA data suggest their structures are very different, forming two different 'classes' of materials. The next section investigates the differences between naturally spun and paralysed silkworm forced reeled silks further.

4.4.3 Naturally spun versus forced reeled

4.4.3.1 Fibre morphology

Differences between the fibre morphology of the two silk types are presented in Table 7. Differences in cross-sectional area are particularly important for understanding the variability in the stress-strain profiles seen in Figure 4.8, as variation in area directly influences variation in engineering parameters (excluding strain).

Forced reeled silks are thinner than their naturally spun counterparts (Table 7), which is in part due to a more even sericin coating (Chapter 2, Figure 2.4). For naturally spun silks, the interlayer bonding that was present in the cocoon is not completely removed during cocoon unravelling. This uneven coating may be removed by degumming[226].

Furthermore, cross-sections show that the brins themselves are smaller in forced reeled silks when compared to naturally spun cocoon silks (taking into account protease digestion). This is hypothesised to be due to the silk press contributing a load that decreases fibre diameter. Other factors that may reduce forced reeled silk size is an increased draw ratio during reeling (speed that silk leaves the spinneret versus reeling speed), which is a subject for further investigation.

Paralysed worms appear to have the press consistently applied, leading to the thinner and less circular cross-sections (Table 7). Unparalysed worms have control of their silk press, enabling them to increase silk duct lumen diameter[128], making fibres more circular on average. The implication of this finding is that unparalysed worms are not only able to apply load during reeling using external mechanisms (Figure 4.5), but they can also decrease load by removing their silk press. Combined, this increases the variation in reeling load. These relationships hold across the range of reeling speeds (Table 7).

Table 7. Shape and area comparison of silks. Feret's shape coefficient gives a ratio of the largest and smallest diameters of the shape, where a value of 1 is circular.

Silk type (speed in mm s^{-1})	**N**	**Area**			**Feret's shape coefficient**		
		Mean (x 10^{-6} mm^2)	**Standard Deviation (x 10^{-6} mm^2)**	**Coefficient of Variation (%)**	**Mean**	**Standard Deviation**	**Coefficient of Variation (%)**
Naturally spun	145, 67	3.79	0.65	17	2.25	0.57	25
Unparalysed (6)	69	2.0	1.2	58	1.52	0.33	22
Paralysed (6)	67	1.57	0.59	37	1.66	0.42	25
Unparalysed (30)	44	0.76	0.43	57	1.48	0.24	16
Paralysed (30)	67	0.72	0.19	26	1.77	0.63	36

Given the morphological differences in the fibre cross-sectional areas between forced reeled and naturally spun silks, variability at different scales along the fibre length was investigated

(Figure 4.9). This ensures the accurate allocation of cross-sectional area for stress calculations; another source of variation in mechanical properties.

Forced reeled silks are more consistent than naturally spun silks in their cross-sectional area over their length (Figure 4.9), in agreement with previous literature[181]. This is primarily due to the decreased variability in cross-sectional area as well as less variability in sericin coating (Table 7). For naturally spun silk, the variation in spinning speed due to the natural figure of eight head movement may also contribute[127].

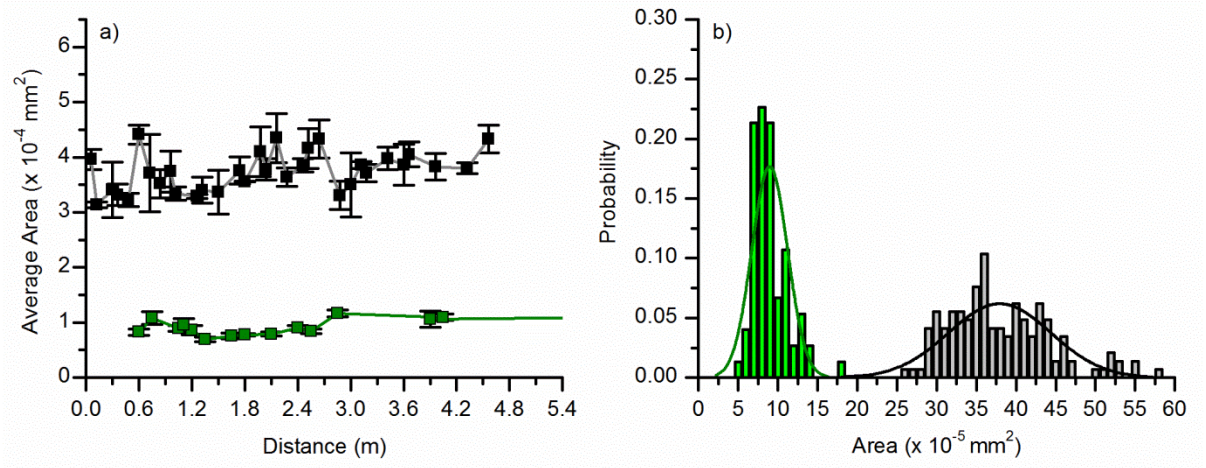

Figure 4.9. a) Average area over distance for naturally spun (black) and paralysed forced reeled silkworm silk from one worm reeled at 20 mm s^{-1} (green), error bars (standard error of the mean) can be seen as variation at the millimetre scale, variation across the x axis as variation at the metre scale; **b)** Probability distributions of area data (bars) and random normal distributions with equal mean and standard deviations of measured data (lines) of paralysed silkworm forced reeled (green; n=75, area=8.97 x 10^{-5} mm^2 ± 2.26) and naturally spun silk (black; data given in Table 1).

The SEM cross-sectional area measurements cannot be modelled with a normal distribution, which was unexpected (Figure 4.9, Anderson-Darling normality test, $p<0.05$). There is a slight right skew in both distributions. This appears to be an artefact of the method where overestimation is more likely than underestimation. This will therefore slightly underestimate the stress-linked mechanical properties of the silks.

These data have led to the outlined methods for area allocation and minimum number of specimens required for a representative area, outlined in Chapter 2. It should be noted that

degumming would decrease variation for naturally spun silks, most likely decreasing the number of specimens required. As sericin contributes little to the mechanical performance of fibres[129], repeating this technique on degummed fibres would quantify the variation of the fibroin cross-section in naturally spun silks, which directly contributes to the mechanical properties. Repeating this method on silks from multiple individuals (both forced reeled and naturally spun) would also validate the conclusions.

4.4.3.2 Thermal properties – thermogravimetric analysis (TGA)

Aside from the morphology of the fibres, the thermal properties of paralysed silkworm forced reeled silk and naturally spun (native and degummed) silks were compared by N. Hawkins in the TGA to support the findings in Figure 4.8b showing that forced reeled silks are more disordered than naturally spun silks (Figure 4.10). This technique gives information on the water content of the silks (taken by the difference in weight up to 100 °C) and the polymer structure, which influences the temperature at which thermal decomposition starts (dramatic loss in weight at high temperatures).

The water content of the forced reeled silks (three repeats, slack storage) was higher than naturally spun and degummed naturally spun silk (c. 7 %, 6 % and 4.5 % respectively). Since water is associated with hydrogen bonding to disordered silk[179], this suggests that forced reeled silks are intrinsically more disordered, with higher amorphous fractions. The earlier onset of thermal decomposition in forced reeled silks also supports the proposition that they are more amorphous. Polymers with a greater proportion of amorphous structures have lower thermal decomposition temperatures due to higher vibrational energy in their less rigidly-bonded polymer chain backbone[179, 230]. A higher amount of disorder in forced reeled silks when compared to naturally spun silks also explains the lower and more numerous temperature loss tangent peaks in forced reeled silks seen in Figure 4.8b.

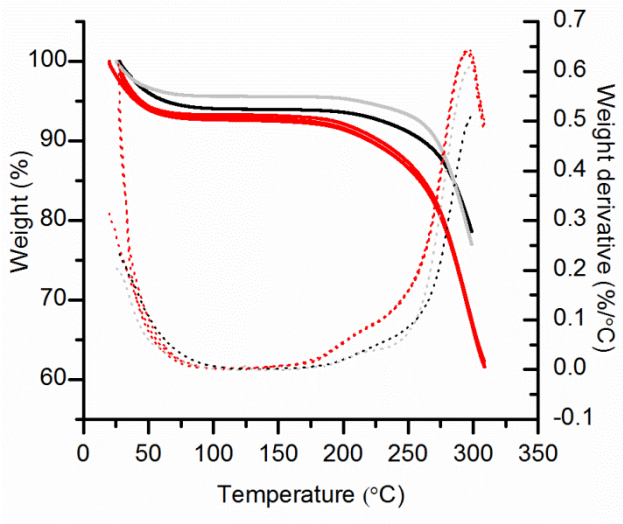

Figure 4.10. TGA plot from N. Hawkins of naturally spun (black), degummed naturally spun (grey) and 3 repeats of a non-postdrawn silk (slack; red) forced reeled silks. The solid lines give the weight loss over temperature and the dotted lines give the weight derivative over temperature.

4.4.4 Processing conditions

As already shown with reeling speed (Figure 4.7), forced reeling allows a range of processing conditions to be applied to manipulate the properties and structures of the silks. Looking exclusively at paralysed silkworm silks, where variation due to behaviour is removed (Figure 4.5b), a range of other processing conditions were investigated. Due to the time constraints in setting up the reeling procedures, each treatment shows data from only one worm, where the worms are different between treatments. With the use of paralysis, inter-worm variation is reduced (Figure 4.7) but may still affect the data. Therefore trends, rather than the values, will be analysed here.

Applying varied processing conditions can be used to investigate whether the mechanical property envelope can be further extended beyond the effects of reeling speed, giving information on the limitations and potential of forced reeled silks, important for the application of these silks in engineering and medicine[15]. Additionally, the effect of processing conditions on the structural disorder of the forced reeled silks (Figure 4.8 and Figure 4.10) is also investigated (see 4.4.5), to infer how the material structure is influenced by these processing conditions, and

if the structural disorder of forced reeled silk can be manipulated to approach that of naturally spun silk.

Figure 4.11 shows that forced reeled silks have a greater variety of mechanical properties compared to naturally spun silks, usually accompanied by higher specimen variability within each treatment. All forced reeled silks were from paralysed worms reeled at 20 mm s^{-1}. Applying a greater postdraw and higher stretch rate to forced reeled silks leads to the strongest properties seen, which were accompanied by greater specimen variability in the post-yield region. These data also indicate sensitivity to specimen storage conditions such as silk tension (d) and specimen storage humidity (d and e; mainly affecting specimen consistency).

Higher postdrawn specimens (x 1.16 in b) displayed higher average failure stresses. This is due to higher fibre stiffness caused by a higher molecular orientation, which in turn is enhanced by the increased stretching force. Additional techniques such as birefringence could support this assertion. Interestingly, the postdraw not only affected the mechanical properties, but also the fibre cross-sectional areas. Reeling from the same worm and applying the same amount of stretch (x1.16), allowing less time to respond to this stretch (i.e. faster stretch rate) lead to a significant decrease in fibre cross-sectional area (from 2.60 x 10^{-4} mm^2 to 1.44 x 10^{-4} mm^2; $p<0.01$ Moods sign test).

Additionally, the postdrawn specimens showed high variability throughout the stress-strain profile, resulting in variable stress and strain to failure. This is in contrast to the non-postdrawn specimens in d and e, which followed more consistent stress-strain contours, and only varied in their failure points along the contours. The postdrawing itself may be causing this effect by increasing structural variability. The different secondary structures (such as different helix or random coil structures) formed during spinning can be stretched to different extents by the postdraw process, thereby enhancing structural differences.

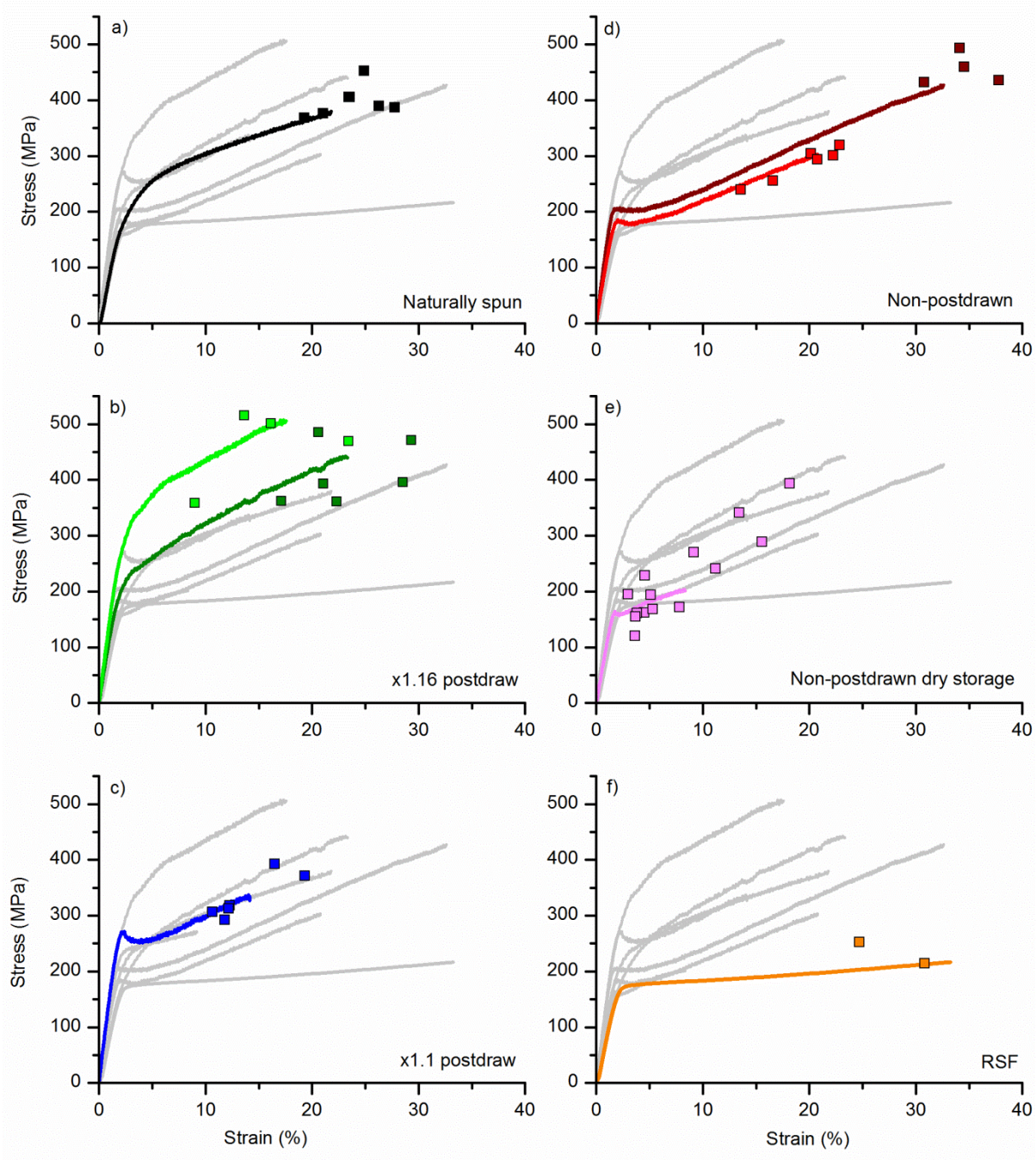

Figure 4.11. Stress-strain plots in order of decreasing strength: **a)** naturally spun (black); **b-c)** postdrawn silks: x1.16 slow and fast (light and dark green respectively) and x1.1 slow (blue); **d-e)** non-postdrawn silks: tension and slack (dark red and red respectively), and dry storage (pink); **f)** RSF silk, provided by J. Guan (orange). Scatter points give the breaking points of other specimens measured from the same treatment. Specimens on the same plot are comparable as they are from the same worm. All worms were paralysed for forced reeling and reeled at 20 mm s^{-1}.

Maintaining tension in the non-postdrawn specimens gave consistent, high failure stresses and strains, thereby producing the highest toughness seen in any of the fibres drawn. These fibres were the most similar to naturally spun threads, but with an increased post-yield plastic flow in

the disordered structures resulting in slightly higher energy uptake, i.e. area under the stress-strain curve.

Storing the non-postdrawn specimens under dry conditions induced a different kind of variability. Many of these fibres were slightly embrittled by the dry conditions, with associated low failure stress near the yield stress[138]. Without water acting as a plasticiser for silk, the silks become less ductile (Chapter 3)[179]. Some of the specimens, however, appear to have rehydrated back to the humidity of the measuring conditions (c. 40 %), decreasing the influence of brittle failure. Alternatively, dry-storage could lead to embrittlement of the sericin binder coating on the fibres, which weakens the whole fibre structure when cracks are initiated in the sericin layer and propagate through the whole fibre (Chapter 3).

A disordered (largely amorphous) RSF fibre is shown for reference in Figure 4.11f. These fibres have little to no post-yield modulus due to their structural morphology. In contrast with silks, they have larger and wider distributed ordered regions in the amorphous matrix[209], leading to little contribution of the ordered regions after yield.

To further investigate the mechanical property scope of paralysed silkworm forced reeled silks, poikilothermic worms were heated or cooled during reeling at two reeling speeds (Figure 4.12). In general, reeling temperatures above room temperature are not significantly different from the room temperature control. Cold reeling, however, produced silks that are significantly less extensible and have a lower maximum stress at the higher reeling speed of 20 mm s^{-1} ($p<0.01$, Mann-Whitney one tailed test), but were not significantly different from the non-cold specimens at 10 mm s^{-1}.

Cold body temperatures effect silkworm silk properties due to the lower energy available for rheological flow of the silk dope during spinning, thus reducing the energy available for disorder to order structural transition of the silk proteins[12]. Additionally, there may also be influences of

metabolic ion pumping, which influence fibre formation during the spinning process[9]. Finally, there are known to be enzymes present in silkworm silks with tanning and cross-linking functions[180], however, the data here do not support the effect of temperature on the enzymes at these timescales. The activity of these enzymes would be expected to increase fibre stiffness[180].

The trends seen here are unlike those found with tropical spiders[88], where spider silk breaking energy increases as spider body temperature increases from 5 to 40°C, assigned to an increase in breaking strain. (This is different from the effect of temperature on the dried silk fibre, where increasing temperature in spider silk leads to higher stiffness[231].) It may be that silkworm silks respond differently to body temperature during reeling as their protein composition and duct morphology is different to spider silk[8, 128]. In particular, extension of silkworm silk may be at its limit at c. 45%, which is the highest strain recorded from all processing conditions (Figure 4.11). Additionally, as a wide temperature range is common for tropical spiders (compared to domesticated silkworms: 25 °C recommended[139]), the change of silk properties at different temperatures may have been selected for.

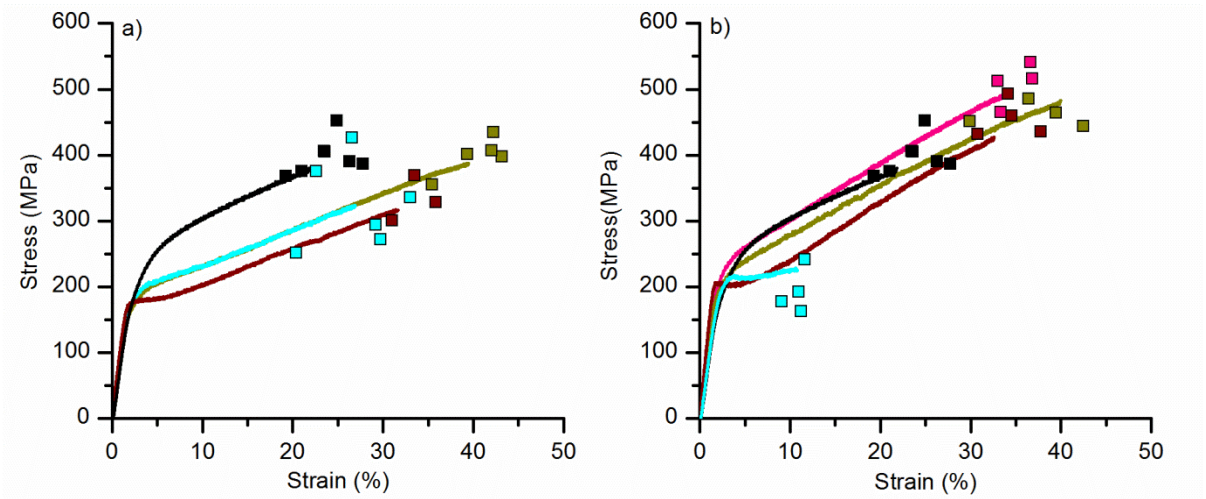

Figure 4.12. Effect of worm temperature on the mechanical properties of paralysed silkworms reeled at **a)** 10mm s^{-1} and **b)** 20 mm s^{-1}. Black curve gives a reference naturally spun silk specimen. Temperature of worm: 'cold' (blue), room temperature (dark red), 'warm' (dark yellow) and 'hot' (pink). Scatter points give the breaking points of other specimens measured from the same treatment.

This finding also highlights the importance of controlling silkworm acclimatisation to room temperature after removing worms from the cool storage incubator. This was controlled for in these experiments, where worms were not reeled for an hour after removing (Chapter 2).

Another interesting feature of the stress-strain curves in Figure 4.11 and Figure 4.12 is the post-yield plateau in stress seen immediately after yield, which indicates molecular chain elongation. Coiled molecules relax through yield until they are stretched sufficiently to sustain the applied load with the equilibrium post-yield modulus[224]. Postdraw removes this feature, as well as higher temperature on average. All naturally spun silks yield gradually, with no post-yield dip. It would therefore be expected that postdraw and higher temperature would increase the structural order of the forced reeled silks.

4.4.5 Structural basis of properties

This last section uses data from J. Guan, using DMTA to explore the extent to which processing conditions affect the amount of structural disorder of forced reeled silks (Appendix Figure A.5, Figure 4.13, Appendix Supplementary Discussion). Overall these data support Figure 4.8, showing that all forced reeled silks have complex combinations of partially disordered fibroin structures that have been introduced by the forced reeling spinning process. By comparing reeling speeds (Figure 4.8) and the effect of postdraw (Appendix Figure A.5 and Figure 4.13), it appears that post-treatment can only partially compensate for this increased and variable disorder. Postdrawing had the strongest effect, but silk retained strong evidence of multiple types of disordered structure. The highest level of disorder was seen in the non-postdrawn specimens that had been slack-stored.

The greatest order seen in forced reeled silks emerged following annealing to 180 °C (Appendix Figure A.5b). Importantly, this suggests that thermal treatment under mechanical load would be the most effective way to create ordered structures in silk. Not surprisingly, this feature is

similar to the common practice of annealing synthetic polymer fibres such as PET under load at elevated temperatures in order to increase the orientation and crystal fractions, which in turn increases stiffness and strength[232]. Similarly, annealed silks show stiffer mechanical properties, with lower breaking strains, explained by the higher order and lower water availability (Chapter 3, Appendix Figure A.6).

Processing conditions therefore influence the properties and structures of forced reeled silks to cover a spectrum of disorder ranging from the disordered artificially spun RSF to the more ordered naturally spun silks (Figure 4.13).

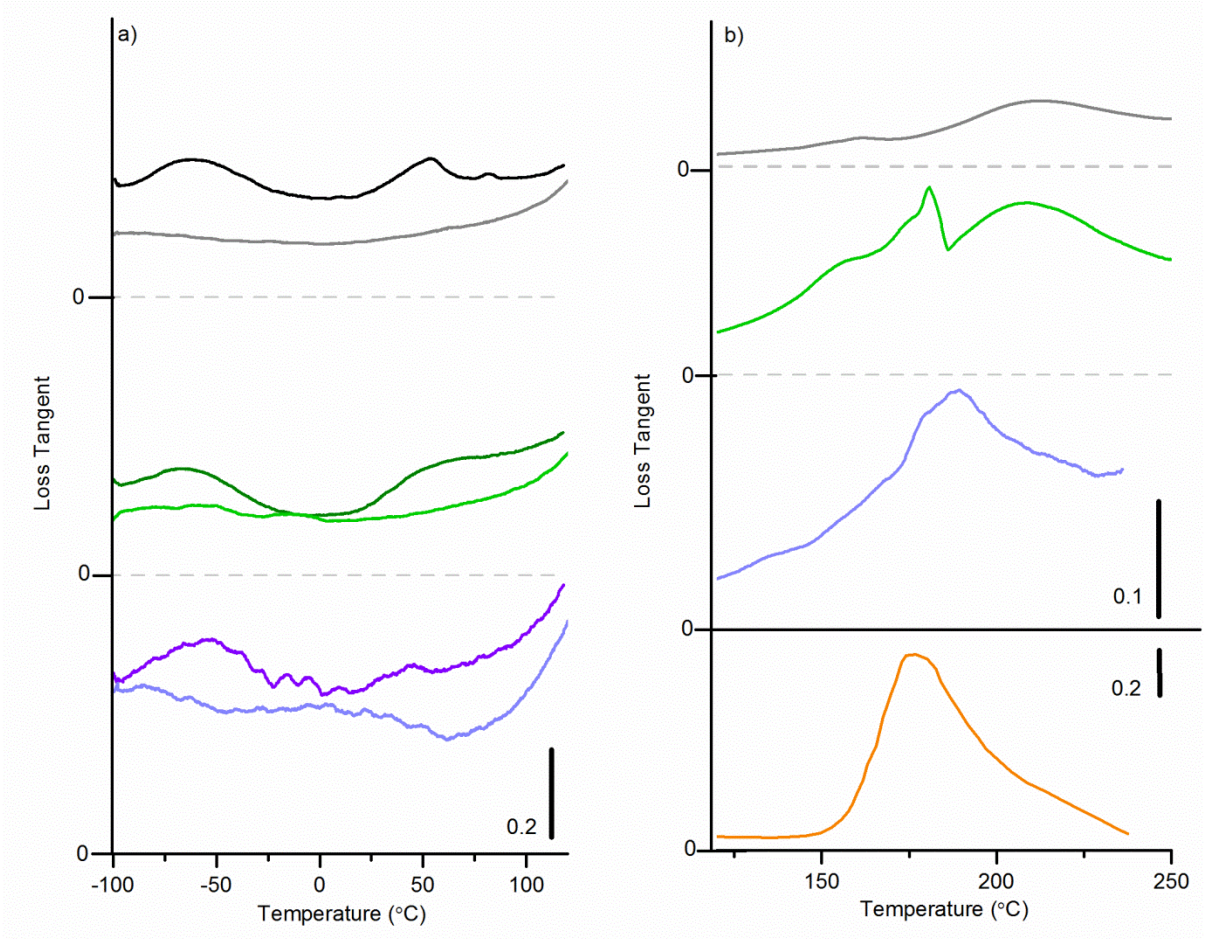

Figure 4.13. a) Loss tangent over temperature pre- and post-120 °C annealing (dark and light respectively) on naturally spun silk (black and grey), postdrawn (x1.16 fast; dark and light green) and non-postdrawn (dark and light purple) forced reeled *B. mori* silks. Bar gives y axis scale; **b)** the post-120 °C annealed loss tangent, including RSF (orange). Black bar gives y-axis scale for the top and bottom section.

The postdrawn forced reeled silk in Figure 4.13 showed an interesting rapid change around 175 °C. This change started out like an RSF structure peak and then jumped rapidly to a more ordered structure similar to natural silk, which has the higher level of coordinated hydrogen bonding. This specimen further supports the assertion that the loss peaks are associated to specific hydrogen bonded structures, and that combinations of temperature and mechanical load can anneal the silks, giving better bonded states. In the specific bonding arrangement of this postdrawn silk, the structure can dynamically reassemble under specific load and temperature conditions. This type of dynamic reassembly is likely to also be the mechanism behind the post-yield dip seen for many forced reeled silks in Figure 4.11. The specific conditions leading to this dynamic reassembly have not been asserted, but are likely to be linked to the stress and humidity history of the silk, both of which affect hydrogen bonding structure[135, 177, 179].

4.4.5.1 Naturally spun versus forced reeled silk structure-property links

Compared to naturally spun silks, forced reeled silks were more variable in many aspects of their structure and properties - and in some cases seem more akin to derived RSF fibres. Previous research has suggested that such variation in mechanical properties might be attributable to topological 'defects' such as surface imperfections present in the silks[34], which may be exacerbated by behavioural control of the silk press during non-paralysed reeling[35]. The data presented here suggest that this variation may be attributed to the amount of randomly distributed disordered protein structures present. The precise mechanism of the differences in structures between naturally spun and forced reeled silks is currently unknown, but is likely to be a product of both behavioural and physiological control exerted by the silkworm during processing.

Behaviour during reeling may introduce the disorder. The paralytic agent used in this chapter is believed to inhibit muscular control around the spinning apparatus, specifically the silk press (Figure 4.5). This inhibition prevents the animal from using its behaviour to fine-tune the ratio of

applied force and reeling rate during fibre production. A lack of feedback and control during silk production could propagate rheological flow instabilities in the silk dope in the duct, as well as preventing any postdraw processing of fibres.

Furthermore, forced reeling may impact the silkworms' physiological control, i.e. the exposure of the dope to chemical processing in the duct (changes in pH and ions), known to affect silk's self-assembly properties[233-237]. For example, recent research suggests that specific chemically-induced links between terminal groups on the protein chains might allow the flow field in the duct to stretch the macromolecules into an aligned structure. This mechanism is therefore vital to promote structural order and inter-chain hydrogen bonding and it is possible that it may be controlled during natural spinning, but not during forced reeling[17-18].

4.5 Conclusions

In summary, the use of silkworm paralysis can eliminate the effects of silkworm behaviour on forced reeled silk mechanical properties. This allows silk to be reeled for hundreds of metres without breaking, with less variable properties due to the consistent reeling load. This opens up the use of silkworm paralysis for industrial-scale reeling.

The removal of the influence of silkworm behaviour on silk properties allows the effect of a range of different processing conditions to be investigated, including reeling speed, postdraw, storage conditions, worm temperature and annealing. Forced reeled silks showed sensitivity to all these processing conditions, with direct effects on mechanical properties. This has revealed the large performance scope of forced reeled silks, from RSF-like properties, to fibres tougher or stronger than naturally spun silk. Based on these data, there appears to be a limit of the strength of *Bombyx*-derived silks of c. 600 MPa and an extension of 50 %.

Processing conditions also influence the thermal properties of the forced reeled silks, which can be used to infer the structural basis of mechanical property differences. Processing conditions

alter the position of the forced reeled silks on a spectrum of disorder, from the highly disordered RSF to the most ordered naturally spun silk. In particular, postdraw and annealing under mechanical load can ameliorate the structural disorder of forced reeled silks.

This chapter highlights the extent to which forced reeled silk mechanical properties can be manipulated, allowing the production of silks with desired mechanical properties for tailored engineering or medical applications. However, there is a trade-off. Forced reeled silks are inherently variable, with the exception of their fibre morphology. This variability stems from the structural disorder, which can only partially be ameliorated.

Compared to naturally spun silk, forced reeled silks are a different class of *Bombyx*-derived silks. Despite using the same dope from the same spinning apparatus, disorder is introduced to the silk by unknown internal processes of the worm. The most ordered and least variable *Bombyx*-derived silks come from naturally spun silks. Furthermore, the toughest silks were found at the average natural spinning speed. This shows how the spinning apparatus, rheology and behaviour of the worm have been shaped by evolution to allow optimal silk properties and structural order in natural contexts.

Chapter 5 High-rate ballistic impact of silks

5.1 Synopsis

This chapter builds on the low-rate experiments from Chapters 3 and 4 to study the mechanical properties of silks at higher strain-rates. *Bombyx* naturally spun and forced reeled silks are compared to *Nephila* major and minor ampullate silks, as well as nylon. Rate-dependence is an important source of variability in mechanical properties of polymers, and is relevant for the mechanical performance of silks during impact events, such as pecking of the cocoon, or prey impact into the web. Furthermore, these properties are important for harnessing the toughness of silks in high-rate engineering applications, such as air bags or composite panels.

This chapter is adapted from a published paper (Drodge et al. 2012[132]), where my contribution was preparation of all the silk specimens, high-rate testing, low-rate testing, SEM cross-sectional area characterisation and data interpretation. Details on the experimental method and analysis techniques developed by D. R. Drodge and C. R. Siviour are given in Appendix B. D. R. Drodge, C. R. Siviour, C. Holland and F. Vollrath contributed to experimental design and data interpretation.

5.2 Introduction

Due to their viscoelastic nature, the mechanical properties of polymer fibres are expected to change as a function of their deformation rate, or strain-rate[130]. This has important implications for the biological function of spider silks, as the mechanical performance of silks in the web will change depending on the speed of the deformation event, from slow wind blasts to fast prey impact. In fact, many webs have to cope with prey impact not just from insects, but fast-moving vertebrates such as birds and bats[106]. Rate-dependence also has implications for the silks involved in protective functions in cocoons, which have to deal with varied impact rates, for example attempts of predators or parasitoids to penetrate the cocoon[75].

There is conflicting evidence on the trend in mechanical properties of silks over strain-rate (Chapter 1)[47, 97, 133-134]. In particular, the trend in strength and toughness is unclear given current data, making understanding the link between rate-dependent properties and their biological function impractical.

This chapter uses high-rate ballistic impact on polymer fibres to offer some insights into these differences and contribute to the understanding of polymer rate-dependence. In particular, a previously described ballistic impact method[134] is further developed to assess whether pre-stress affects the high-rate mechanical properties. In this method, a fibre is impacted transversely to produce propagating stress waves, whose behaviour can be used to infer fibre properties. Static pre-stress and impact speeds are varied to change the dynamic stress imposed on the specimen. The data obtained have implications for the pre-tensioning (i.e. static stress) of polymer fibres for high-rate applications. It is also important for understanding orb web function, where radial threads are tensioned, which is likely to influence impact performance for catching fast-moving prey with high kinetic energies[109-110].

5.3 Materials and Methods

5.3.1 Specimen preparation

Spider silks were obtained from *Nephila edulis* through the forced reeling of immobilised spiders, described in (Chapter 2). Several *Nephila* individuals were reeled for both major (8 spiders) and minor ampullate silk (5 spiders, 4 of which also gave major), where major was a single filament and minor was a double. Some spiders were reeled for their major ampullate silk from both glands, so the silks could be used for different experimental methods for comparison. Other materials were also measured: mulberry silkworm *Bombyx mori* naturally spun silk, *Bombyx* forced reeled silk at 10 and 20 mm s^{-1}, and nylon. All silks were unravelled from a spool mounted at the top of the testing rig for the high-rate experiments. Therefore, specimens were

not kept at reeled tension at all times of their preparation. Nylon was unravelled from its spool and individual fibres were unravelled from the three-fibre twine. Density and diameter for nylon are given in Appendix A.

Nail varnish was used to fix specimens at the beginning and end of reeling onto the spool for accurate SEM and stress-strain properties. Details of methods for SEM and stress-strain measurements are given in Chapter 2. For *Bombyx* silks, specimens were also fixed to the spool mid-way through experiments to keep an ongoing measurement of the cross-sectional area and tensile properties over specimen length (see Chapter 4, Table 7 for naturally spun silk results). Mean area was used for analysis and quasi-static stress-strain area allocation.

5.3.2 Ballistic impact experimental set-up

A diagram of the experimental set-up for ballistic impact is given in Figure 5.1. The set-up involves firing a projectile (a chisel-ended nylon cylinder), from a clamp-release gas gun into the centre of a long single fibre held under a static pre-tension and imaging its two-dimensional deformation during impact.

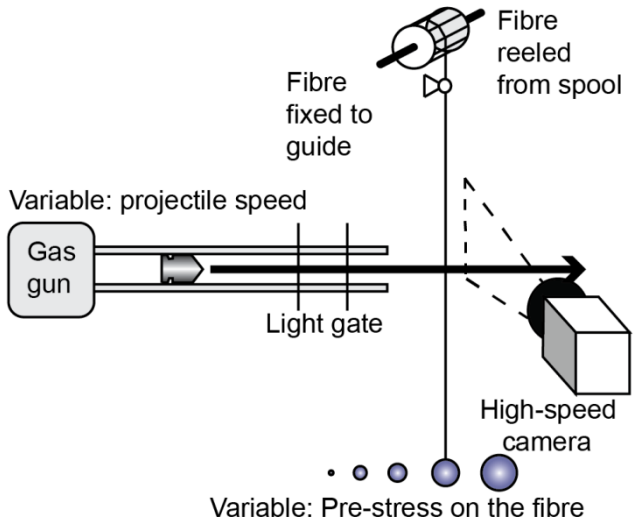

Figure 5.1. Nylon projectiles are fired from a gas gun at a single fibre. Either the pre-stress on the fibre is varied, or the projectile speed. The fibres are unravelled from a spool and fixed to a guide the top. A weight (static load) is hung from the fibre and the fibre is kept vertical by a guide at the bottom. Specimens were up to 2 metres long. Fibre deformation is imaged using high-speed cameras, where the fibre is lit up by high-power flashes. Timings of cameras and flashes were controlled using a light gate on the gun barrel.

Two variations of this technique were used. The first 'vary speed' method uses a low, constant pre-stress on the fibre (usually under 10 MPa, up to 60 MPa) and varies the impact speed of the projectile (from 20 m s^{-1} to 450 m s^{-1}). The second 'vary static load' method keeps the projectile speed constant (c. 115 m s^{-1}), but varies the pre-stress on the fibre by applying different static loads (10 MPa to 1150 MPa). The first method varies the stress applied by producing a differing amplitude longitudinal wave at different impact speeds, where all applied stress is dynamic. The second changes the stress through applying a static load, so stress is applied statically and then dynamically.

In both cases, the impact of the projectile causes a longitudinal tensile stress wave to propagate along the fibre. This is accompanied or followed by a transverse wave. Using appropriate high-speed imaging, the speed of the observed transverse wave is measured and this gives a direct measurement of the fibre tension due to the combination of the static stress and longitudinal wave. By combining this stress with a suitable strain measurement (also from the high-speed images), high-rate stress-strain co-ordinates can be constructed (Figure 5.2). More detail of experimental set-up is given in Appendix B.

Spools with reeled specimens were hung from the top of the testing rig above a guide. The guide is a retractable cylindrical rod with a notched end. A small pre-weighed amount of blue tack of 0.03 g was added to the fibre end which enabled easy unravelling from the spool to the length required. If a low weight is used (up to 0.2 g), the fibre at the top near the spool is blue-tacked to the guide rod, where the fibre runs through the guide notch and bends 90 degrees onto the rod before fixing. If a higher weight is used, the fibre is additionally superglued into the notch to prevent slipping. Where possible, the specimens are not cut to allow the fibre to be easily located for the next experiment. In cases where a larger static load is needed, the additional weight is added after the fibre is fixed at the top (spool end). Labjacks were used to allow controlled application of the weight and prevent higher stresses being reached. The bottom end

of the fibre falls vertically within the notch of a lower retractable guide. This ensures that, although it is not fixed at the bottom, the fibre is unable to swing. Specimens were tested as soon as possible after the static load was added (usually less than 20 seconds) to reduce the effect of creep between specimens and minimise specimen breaking or weights falling off.

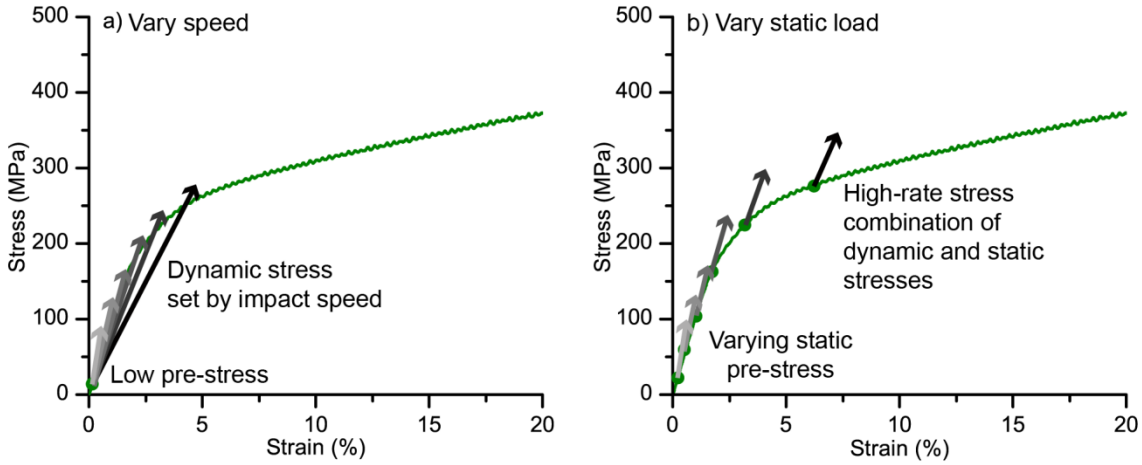

Figure 5.2. Comparison of the loading of specimens using: **a)** the vary speed method or **b)** the vary static load method. For the vary speed method, the pre-stress is kept low and the high-rate stress-strain co-ordinates are governed by the impact speed, where higher speed (longer arrow) leads to a larger jump in conditions. Using this method, the stress applied is almost wholly dynamic. The vary static load method applies pre-stresses of different amounts and adds an elastic jump in properties from impact of a set speed. Using this method, the stress is applied statically and then dynamically. The quasi-static stress-strain curve is from naturally spun *Bombyx* silk, used here for illustrative purposes.

The measured parameters from high-speed imaging were velocity of the projectile (V), measured from the light gates or the camera images, and the observed transverse wavespeed (C_w) – the speed of the transverse wave/kink in the fibre during the early stages of deformation (the horizontal motion visible in Figure 5.3). Longitudinal waves also propagate in line with the axis of the fibre, but cannot be imaged.

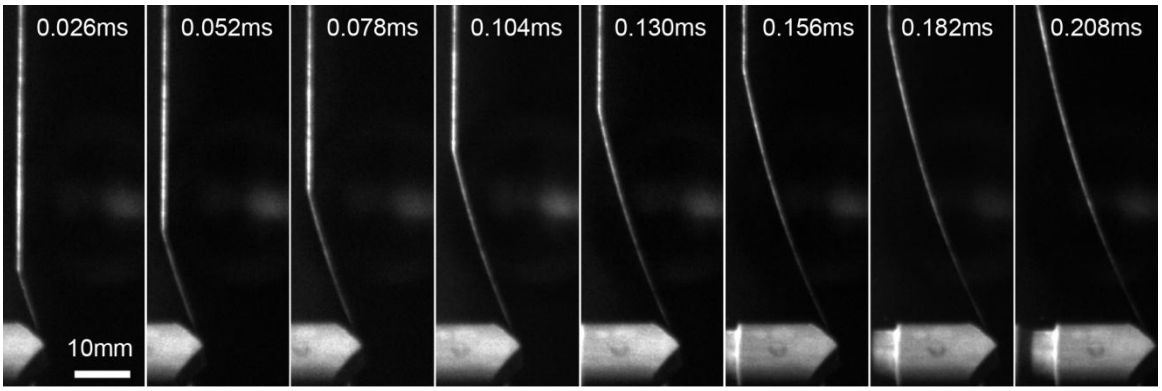

Figure 5.3. High-speed images of the silk and projectile in the early stages of deformation, where timing between pictures is given at the top. The observed transverse wavespeed (C_w) is the speed of the propagation of transverse motion in the silk, visualised by looking at the speed that the fibre 'kink' moves up. Only the section above impact is imaged, as the deformation is symmetrical about the impact point.

Specimens were usually two meters long to ensure that the observed transverse wave is not affected by the reflection of the usually faster longitudinal wave from the guide. Spider silks were slightly shorter, but were long enough to ensure imaging of the transverse wave is before the longitudinal wave has reflected back (see Table 8). The lengths were varied in this case to conserve silk, to get the maximum amount of data points from a limited supply of silk from each spider (usually around 50 meters from one gland).

Table 8. Length of fibres used for different projectile speeds for spider silks specimens.

Projectile speed, *V* ± SE Mean (m s^{-1})	51.1 (0.7)	112.9 (1.5)	148.0 (1.1)	208.8 (2.3)	277.8 (3.3)	335.5 (1.9)	396.4 (3.7)
Specimen length (m)	1.20	0.84	0.84	0.62	0.62	0.46	0.46

For the speed method, either Helium or Nitrogen propelling gases were used, where the former allows higher speeds to be reached as it has a lower density at any given pressure. The pressures of the propelling gases were controlled to set projectile speed (examples given in Table 8). In order to fire the gun, projectiles were initially held in the clamps using a clamping gas pressure higher than the propelling pressure. The propelling reservoir was then filled to the required pressure, at which point the clamps were released.

A diaphragm was placed at the end of the gun barrel, to prevent air disturbances from moving the thread before the arrival of the projectile. At low velocities (up to 115 m s^{-1}), a layer of tinfoil was used, and at higher velocities, layers of mylar tape were used. Both were kept in place using gaffer tape.

Following each experiment, the broken ends of the specimens following impact were mounted for SEM imaging.

5.3.3 Ballistic impact analysis

Details of the analysis equations used are in Appendix B, which are published in Drodge *et al.* (2012)[132]. Data analysis is performed using the projectile velocity (V), observed transverse wavespeed (C_w), the density (ρ), the mean cross-sectional area (used to work out stress, σ, and mass per unit length, μ), the static tension in the specimen (T_0) and the quasi-static stress-strain curves. A representative quasi-static stress-strain curve is selected based on the variability seen between equivalent specimens, where the median properties are chosen. This curve is then used to work out a pre-strain (ε_0) and pre-stress (σ_0) on the specimen given the weight added to the fibre.

In brief (more detail in Appendix B), the high-rate stress (σ_1) is the sum of the initial tension (T_0) and tension due to the passage of the longitudinal wave following impact (T_1), divided by a cross-sectional area. The high-rate strain (ε_1) is calculated by summing the initial strain (ε_0) to the strain caused by the relative motions of the longitudinal and particle velocities (C_l and W respectively). The transverse wave does not affect strain, but takes up slack caused by the passage of the longitudinal wave[238], and hence allows strain to be reassigned.

The equations make the assumption that the material stiffness does not vary during the impact loading step (straight lined arrows seen in Figure 5.2). These equations are therefore unable to model plastic flow behaviour following yield and is only sensitive in changes of C_w relative to V

(if, indeed, any plastic flow occurs at these strain-rates). Low static tensions were therefore used to minimise jumps in properties following impact to beyond yield, where plastic-flow decreases modulus. An additional assumption is that the slowest longitudinal wave component propagates more quickly than the transverse wave; if either the tension or impact speed is high enough, this will no longer be the case, and a different approach is required[239]. Appendix B outlines other assumptions of the equations and compares alternative analyses, including a justification for why this analysis technique was chosen. Data points for the vary speed method were excluded if the calculated modulus (*E*) was not similar to the trend in increasing impact speed seen from other equivalent specimens, which suggests an incorrect measurement.

For the vary static load method, high tensions are often above yield, or the stress following impact reaches above yield. Since publication in Drodge *et al.* (2012), it has been suggested that these loading conditions invalidate the assumptions made in the equations, as plastic flow is not modelled by the equations, which is further discussed in Section 5.4.2.

5.4 Results and Discussion

5.4.1 Vary speed

The mechanical response of polymers to high-speed impact differs from their measured response at a low-rate of deformation (Figure 5.4). For nylons and silk, the high-rate stress-strain co-ordinates follow an approximate straight line, in line with the quasi-static initial modulus. This is because both the stress and strain high-rate co-ordinates are calculated from the longitudinal wavespeed, which is governed by the elastic modulus in the current analysis (see also Chapter 6). All *Bombyx* silks show similar properties, as they have similar elastic, or initial moduli (see Chapter 4).

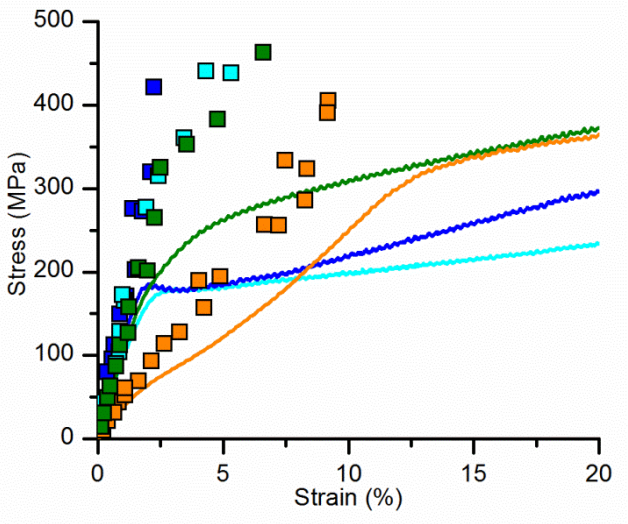

Figure 5.4. High-rate stress-strain co-ordinates calculated from vary speed experiments on naturally spun *Bombyx* silk (green), forced reeled *Bombyx* silk at 10 and 20 mm s^{-1} (cyan and dark blue respectively), and nylon (orange).

This analysis suggests that fibres are stiffer at high-rate following yield compared to the quasi-static curve. Previously published high-rate stress-strain curves of spider silks measured at a range of strain-rates also show increased apparent stiffness[47, 97], but importantly, also show a yielding behaviour[133]. Plastic flow post-yield absorbs energy from impact, but this behaviour cannot be quantified using the equations in the analysis method. Alternative analysis equations outlined in Appendix B do show a yielding behaviour, but make different assumptions in their analysis. Therefore the equations used to generate Figure 5.4 model the elastic and sonic components of fibre impact, they do not fully model the high-rate stress-strain response if yielding is involved, with important implications for the energy absorption ability of these fibres following impact.

The high-rate properties of spider silks are more variable than *Bombyx* silks or nylon, where major ampullate silks are more variable than minor ampullate silks (Figure 5.5). Even for major ampullate silk from the same spider reeled in a single session, the response following impact can be very different (dark blue and cyan in Figure 5.5). The general trend in properties is linear, resulting in higher stiffness post-yield, like the materials shown in Figure 5.4. Some higher speed data with minor ampullate silk appear to show a stress plateau following yield, matching the

quasi-static trend, but at a higher stress value. This indicates that the structure of the silk may be changing post-yield, discussed in the next section.

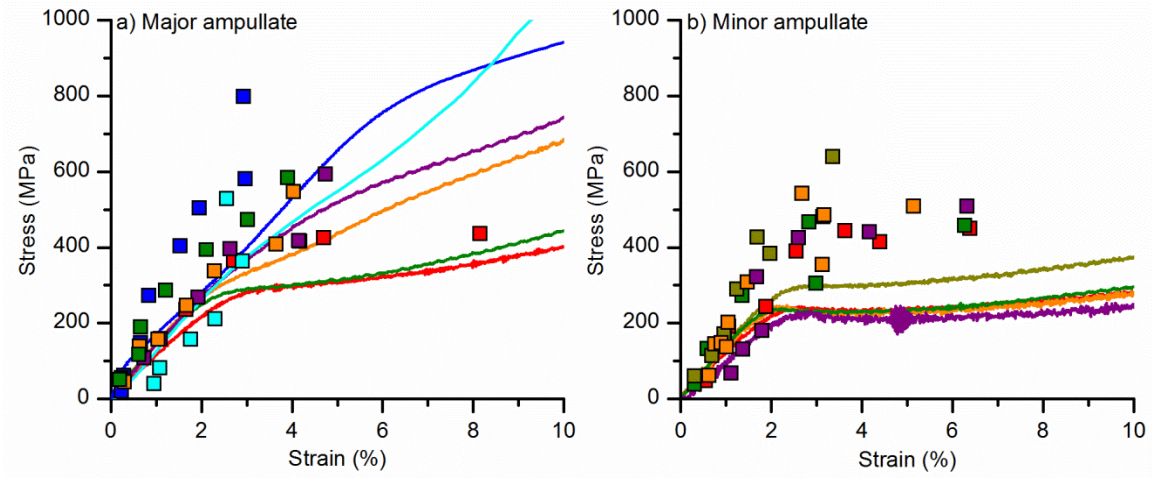

Figure 5.5. High-rate stress-strain co-ordinates for the vary speed data of: **a)** *Nephila* major ampullate silks (single fibre) and **b)** *Nephila* minor ampullate silks (double fibre). Different colours denote silks from different individual spiders. Cyan and dark blue are from the same spider but different glands.

The variability in major ampullate silks can be explained in part by errors introduced by the thin fibre diameters used, which affect the measurement of C_w. Air drag at the high speeds of impact affects all the experiments, but has a larger effect for thin diameter cylinders, as the ratio of drag forces to those due to inertia or internal stress increase as the fibre diameter is reduced[240]. Air drag causes the silk fibre to curve in the region affected by the transverse wave, which absorbs energy, alters strain measurement and has the potential to affect the wavespeed, increasing the error in the C_w measurement. The curvature of the different material fibres during impact is currently under investigation, and has the potential to provide strain measurements during yield, as well measuring drag coefficients.

Additionally, major ampullate silks are particularly sensitive to humidity due to their MaSp2 composition due to their proline content [87, 91, 135, 241]. The humidity sensitivity directly influences the modulus, which in turn alters the longitudinal wavespeed directly, and transverse wavespeed indirectly through changes in tension. The silks are therefore sensitive to small changes in the testing conditions (room humidity and temperature), which increases variability

in properties, exacerbated by the loose fibre storage for these experiments. This variability has interesting implications for the use of major ampullate in the web as the main energy absorbing and sonic wave propagating component[81, 96] – factors which are further investigated in Chapters 6 and 7.

5.4.2 Vary static load

The vary static load method produces comparable results to the vary speed method for naturally spun *Bombyx* silks (Figure 5.6a). This is in contrast to nylon, where the two methods produce different results, where the vary static load method follows a more quasi-static response after yield (discussed in Appendix B).

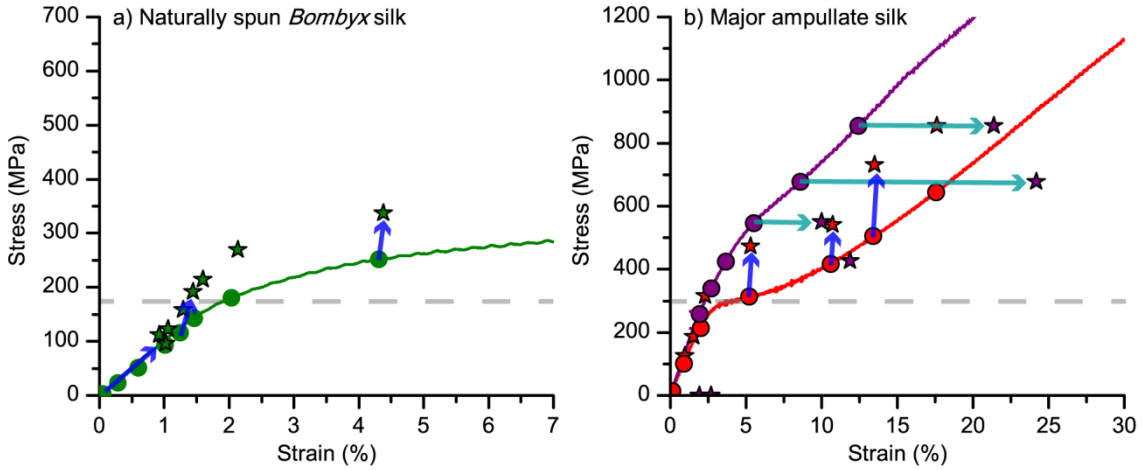

Figure 5.6. High-rate stress-strain co-ordinates (stars) for the vary static load data for: **a)** *Bombyx* naturally spun silk and **b)** *Nephila* major ampullate silk from two different spiders. Closed circles give the pre-stress and pre-strain co-ordinates from the static weight added to the fibre, on the quasi-static stress-strain curve. Dashed line gives the approximate stress where fibres have yielded. Arrows give the elastic jump in properties following impact.

However, the high static loads produce high-rate properties that highlight the limitations of the analysis method, especially evident for spider major ampullate silks (Figure 5.6b). Impact speed is constant using this method, so introduces a set amount of energy to be absorbed following impact. As the equations are elastic, the energy absorption is therefore modelled as an elastic jump in stress, seen for the *Bombyx* silk and the red major ampullate silk high static load high-

rate stress-strain co-ordinates (Figure 5.6). A small amount of strain may accompany this jump, which is variable due to problems quantifying purely elastic strain post-yield.

An alternative deformation at high-rate is suggested by the purple spider silk curve in Figure 5.6b, which shows no increase in stress at high-rate following yield. This is explained by stretching of coiled structures following yield. Many silks show a post-yield plateau, or even dip, following yield in their quasi-static curves, which is caused by this effect (see Chapter 4). In simple terms, the purple silk stretches its structures following impact, as it has not done this at yield, whereas the red silk takes stress following yield, as it has already stretched out its structures.

These classes of high-rate co-ordinates (vary stress, red; or vary strain, purple) appear to be a two-state phenomenon: for all spider silks measured (6 individuals), the post-yield high-rate stress-strain co-ordinates showed either an increase in stress with no strain, or an increase in strain with no stress.

In reality, post-yield plastic flow strain may be absorbing energy, but this cannot be modelled with the current model equations. Current thoughts are that post-yield deformation in the impacted fibre occurs in two sections: first the purely elastic deformation behind the longitudinal wave front, but ahead of the transverse wave; second, the deformation behind the transverse wave front, which has high plastic strain that develops with time as a curve. By detailed analysis of this curve shape and length, it should be possible to calculate the post-yield strain at stress values calculated simply from the transverse wavespeed.

Biologically, this is very important. If plastic flow occurs during high-rate impact, the energy absorption ability of silks following impact will be increased. Additionally, as only the silk within the transverse wave will yield, it also means that damage due to impact will be localised. This may help explain why webs are usually pre-tensioned[242] – to allow yield to take place following

impact to increase energy absorption and limit damage to the web. These effects have previously been modelled by taking yield into account in terms of a change of modulus[109, 243], but an understanding of the role of sonic waves in these phenomena have not previously been presented.

These data therefore highlight the need for further research on the analysis methods to accurately calculate high-rate stress-strain co-ordinates for specimens where the static stress is high and above yield, which is more common in the spider silks.

5.4.3 SEM of shot ends

The ends of the fibres following ballistic impact were also compared, which showed large variability (Figure 5.7 and Figure 5.8).

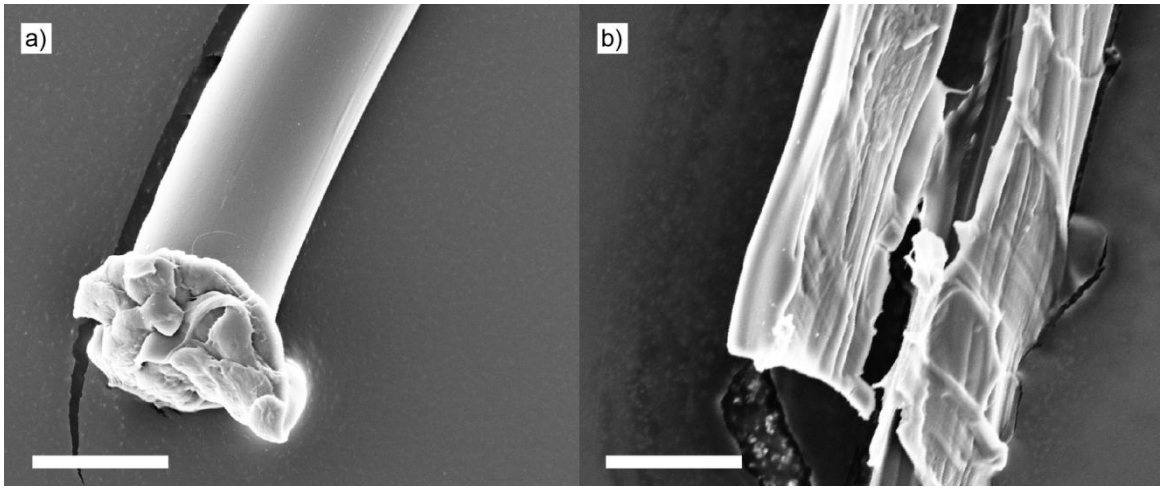

Figure 5.7. Fibre ends following ballistic impact, where white bar denotes 20 µm: **a)** nylon (pre-stress 245 MPa, impact speed 116 m s^{-1}); **b)** *Bombyx* naturally spun silk (pre-stress 4 MPa, impact speed 118 m s^{-1}).

Whereas nylon does not show any evidence of micro-structures, *Bombyx* silk shows evidence of brin separation and fibrillation following impact, where sericin appears to have covered the brins. The energy absorbed therefore also contributes to thermal changes in sericin and macromolecular rearrangement between fibrils.

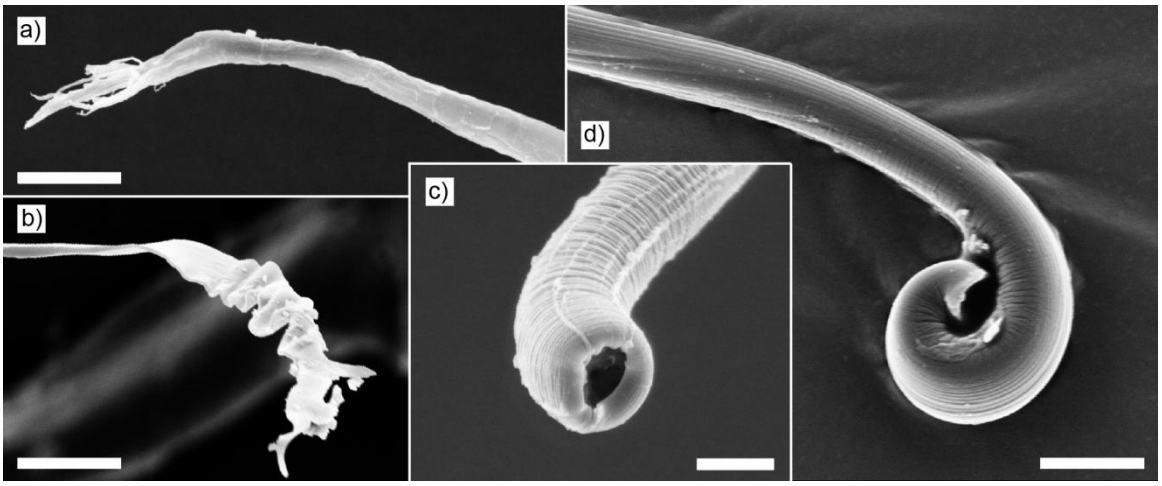

Figure 5.8. Spider silk fibre ends following ballistic impact, where white bar denotes 10 µm: **a)** minor ampullate (pre-stress 195 MPa, impact speed 118 m s^{-1}); **b)** minor ampullate (pre-stress 60 MPa, impact speed 330 m s^{-1}); **c)** major ampullate (pre-stress 424 MPa, impact speed 110 m s^{-1}); **d)** major ampullate (pre-stress 10 MPa, impact speed 111 m s^{-1}).

Spider silks showed more variability in structures, which are unlike the broken ends following impact at slower strain-rates[133]. Minor ampullate showed flattening and larger scale splitting (Figure 5.8 a and b), indicating brittle failure, plastic flow or even thermal softening within these regions. Major ampullate repeatedly showed a skin-core effect (both skin and core can be seen in Figure 5.8c), where transverse wrinkling is seen, suggesting different forces are taken between the skin and core parts of the spider silk, or that there is movement of the skin relative to the core. This is an interesting feature for further study because the tension state of the skin will affect crack propagation through the fibres[244]. Longitudinal lines are also seen, suggesting fibrillation. Fibrillation in spider silks is commonly seen following processing treatments (e.g. anaeasthesia[140]), and a skin-core effect has previously been explored elsewhere[245], but has not been a focus of explaining spider silk properties.

5.5 Conclusions

Analysing the high-rate properties of viscoelastic thin silk fibres during high-rate impact is a challenge due to the implicit assumption of the model equations that the material is purely elastic. The analysis methods have shown that the deformation following impact can be modelled by elastic jumps in stress and strain. When impact speed is varied and static load is

low, the assumptions of this analysis method give consistent results, with high-rate stress-strain co-ordinates following a linear elastic relationship. However, high speed and high static loads highlight the limitations of an assumption of an elastic response. At high static loads, the jump in stress-strain co-ordinates at high-rate is either mainly in stress or mainly in strain, not a combination of the two. The fibre can either elastically jump in stress, or stretch out coiled structures to introduce significant strain. The theoretical analysis does not quantify any standard post-yield plastic strain (if any exists), and this will be the next step in developing the data analysis.

Further research is needed to quantify these post-yield effects, but the current analysis captures the elastic component through describing the effects of the sonic wave propagation, both longitudinal and transverse, following impact. Silk's stress or sonic wavespeeds are further explored in the next chapter, where the elastic propagating waves measured here are compared to wavespeeds measured from acoustic standing waves.

Chapter 6 Sonic properties of silks

6.1 Synopsis

This chapter uses the technique outlined in Chapter 5 to further investigate the sonic properties of silks. The sonic wavespeeds of spider silks are quantified and compared to *Bombyx* naturally spun silk, as well as synthetic nylon and copper beryllium wire. Important for the biological function of spider silks, the consistency of vibration signalling is investigated, including the effect of tension, specimen length, number of fibres and fibre diameter. The physical basis of these properties is discussed, important for the interactions between spider silk's mechanical and signalling functions. The data presented here are useful beyond biology as a study of one of nature's high performance, multifunctional materials, providing insights into how materials can be engineered to have signalling functionalisation.

This chapter forms a published paper (Mortimer *et al*. 2014 in *Advanced Materials*). My contribution was designing the experiments, preparing all specimens and testing them, as well as data interpretation and preparation of the manuscript. C. Holland, C. R. Siviour and F. Vollrath helped with aspects of experimental design, data interpretation and manuscript editing, and J. Windmill and S. Gordon helped with vibrometer measurement and manuscript editing.

6.2 Introduction

From ancestral trip-wires to the highly evolved orb webs, silks play a key role in spider ecology and behaviour as both a structural material and a medium for information gathering and communication[246-247]. The focus of this chapter is major ampullate silk, which exhibits exceptional mechanical performance for its size and serves as not only scaffolding[15, 56, 86], but also the primary communication material of the orb web[119-120, 248-249].

Silk vibration is used for hunting, predator avoidance, and courtship across most spider families[30, 119-120, 248-257]. For example, many orbweavers are positioned in the web hub to detect vibrations on their radial threads from across the prey capture region[96, 119, 258-260]. Some spiders will actively pluck the radial threads as an object-location strategy or in response to intruders or mates[119-120, 255, 261-264]. Spiders detect vibrations using slit sensilla, most notably in their metatarsal organs[265-266]. Barth and Geethabali[267] measured displacement sensitivity as a function of frequency in wandering spiders. They identified dramatic increased sensitivity with increasing frequency, with displacement thresholds as low as 100 nm at frequencies approaching 1 kHz, the highest frequency measured.

The signalling and mechanical roles of major ampullate silks make these fibres multipurpose. This means there are likely to be as yet undefined evolutionary trade-offs that may limit the optimisation of mechanical and sonic properties – important information to consider when using spider silks as inspiration for new-age materials. Hence, understanding the physical basis of spider silk's sonic properties will be key to understanding the evolutionary interactions between mechanical and signalling performance.

Fibres propagate both longitudinal (compression/tension) and transverse waves[267], where the former consists of vibrations along the fibre length, and the latter those perpendicular to the fibre (see Figure 6.1)[268]. Theory shows that the longitudinal wavespeed is determined by material properties, whereas transverse wavespeed is additionally governed by applied tension (see section below)[269]. Behavioural experiments with orbweavers show that these spiders are more likely to respond to longitudinal over transverse waves when their webs are vibrated[119, 270-271].

The sonic properties of a spider's silk are difficult to measure in the natural web context, as the vibrational 'landscape' is highly complex involving the geometry of interacting silk strands of different tensions and types (e.g. stiffer ampullate silks and elastic capture spiral silks)[47, 97, 242].

Previous studies have measured wavespeeds in parts of the web using Brillouin light scattering, and web propagation speeds using laser vibrometry, both showing variable results[120, 272]. Vibration propagation distance has also been measured in webs, showing lower attenuation of longitudinal compared to transverse waves[96, 120-121]. Damping, caused by a combination of internal material effects and external factors, also contributes to attenuation, which has been found to differentially affect the two types of wave[109, 121]. Modelling techniques have used these data in part to infer web function, but few are validated by experimental data and none take into account the ad hoc variation of silk properties, which is controlled by spider processing through their behaviour[97, 109, 121, 242, 273-275].

Given the complications of the experimental measurement of wave propagation in webs, here silk fibres are investigated independent of the web, allowing accurate matching between material and vibrational properties prior to interpretation in the complex web engineering structure. Physical theory is combined with the complementary experimental techniques of laser vibrometry and ballistic impact to confirm the physical basis of the sonic properties of a range of materials. By comparing spider silk to other materials, the constraints on the evolution of signalling properties in terms of material structure can be inferred. Where these limitations are apparent, the means that the spider might employ to adjust the balance between structural support and signalling functions are discussed. The experimental techniques presented here provide novel contributions towards understanding complex web vibration and spider evolution and the approach provides important insights into nature's design of stimuli-responsive multifunctional polymeric materials.

6.3 Materials and Methods

6.3.1 Specimen preparation

Spider silks were obtained from two orb weaver species, *Nephila edulis* and *Araneus diadematus* through the forced reeling of immobilised spiders, described in Chapter 2. *Nephila* of different sizes (larger are older) were reeled where silk diameter scales with spider size: 'Big', 'Medium' and 'Small' diameters of single major ampullate silks are 6.97, 4.23 and 3.38 μm respectively. Both single fibres and bundles of major (MA) and/or minor (MiA) silk were reeled from spiders. Other materials were also measured for comparison: *Bombyx mori* cocoon silk, nylon and metal wire (diameter and density given in Appendix A). Longer specimen lengths were needed for longitudinal experiments due to the fast wavespeeds involved; different lengths were used between materials to keep the resonance at similar frequencies. For silkworm cocoon silk, specimens of different lengths were additionally measured under the transverse set-up (Table 9).

Table 9. Specimens and specimen lengths investigated.

Specimen	**Transverse tests gauge length (mm)**	**Longitudinal tests gauge length (mm)**
Silkworm cocoon silk	5, 12.5, 50, 180	180
Nylon	12.5	140
CuBe wire	12.5	220
Nephila – big (1MA; 2MiA)	12.5	-
Nephila - medium (1MA; 2MiA; 2Ma and 2MiA)	-	180
Nephila - small (1MA; 1MA supercontracted; 1MA and 2MiA)	12.5	-
Araneus (2MA and 2MiA)	12.5	-

For the small specimens of spider silk (12.5 mm or under), silk was reeled onto a spool, then glued under tension using cyanoacrylate onto dividers before fixing onto frames[140]. Non-spider silk specimens were glued loose into frames. For the long *Nephila* specimens, silk was obtained by reeling the spider at 20 mm s^{-1} directly onto the frames. A spool was used to control the reeling speed and frames were placed onto a laboratory jack, which was raised when the reeling was paused. Silks were glued at both ends into frames by sandwiching between cardboard using superglue. Minimal tension was applied and silk specimens were reeled horizontally, parallel to the jack.

All specimens were imaged for cross-sectional area in a scanning electron microscope (SEM; see Chapter 2). The materials were also tested under quasi-static tension (Appendix Figure A.7). All fibres were measured at a rate of 1.5 mm min^{-1} until failure occurred (5 N load cell, model 5512, Instron, UK).

6.3.2 Laser vibrometry

To control tension during vibrometry experiments, specimens were clamped at both ends into a Deben Microtest tensile stage with a 2 N load cell. For the transverse experiments, the load cell was engaged and a constant tension was applied during the experiments. For the longitudinal experiments, the load cell was disengaged because it was found to affect fibre vibration, so extension was used to control tension. Above yield, three minutes were left before measurement, so the amount of creep was consistent. Between 3 and 7 specimens were measured for each material type, and two measurements were taken per fibre (low then high tension).

Some major ampullate silks were supercontracted for experiments. These silks were loaded into the tensile testing clamps and a 50 % slack was introduced. They were then breathed on 7-8 times to introduce a high humidity onto the fibre, which then supercontracted and shortened. If

the fibres were still slack, jaws were opened until visibly taut, or an increase in load was seen. The supercontracted length was taken as the fibre length.

During the vibrometry experiments, silk strands were vibrated using sound, amplified (TA-FE370, Sony) and transmitted from a loudspeaker (ESS Air Motion Transformer) that was positioned either perpendicular or parallel to the silk fibre axis for transverse and longitudinal waves respectively (Figure 6.1). A reference microphone (Bruel & Kjaer 4138) was positioned near the silk, perpendicular to the speaker. A ~50 dB sound pressure level broadband linear chirp of frequencies 1-30 kHz was generated by the micro-scanning Laser Doppler Vibrometer system (PSV 300, Polytec), which measured the silk's nanometre movement with a fitted close up unit (OFV 056). The noise floor of the vibrometer system was typically 0.3 µm s^{-1} (48 pm) for 1 kHz increasing to 3 µm s^{-1} (16 pm) for 30 kHz. The maximum vibration amplitude measurement for these experiments was 50 mm s^{-1} (7.96 µm at 1 kHz to 0.265 µm at 30 kHz).

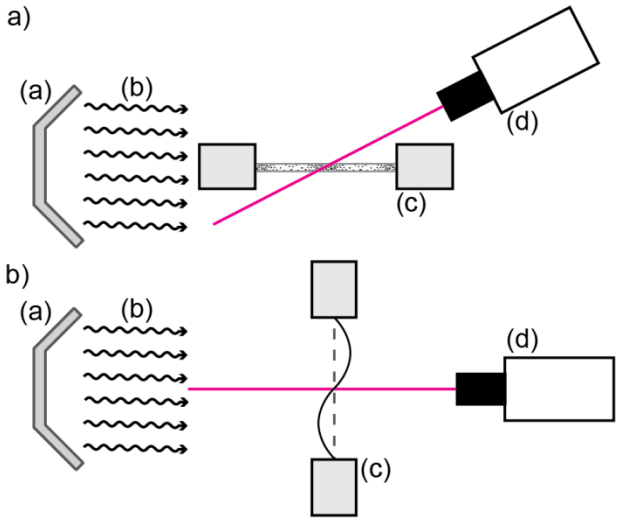

Figure 6.1. Experimental set-up for laser vibrometry (view from above) for **a)** longitudinal and **b)** transverse experiments. A speaker (a) emits sound (b), vibrating the silk clamped between a tensile stage (c) with displacement measured by a laser vibrometer (d).The microphone was placed as close as possible at the intercept between the silk thread and the laser beam, perpendicular to the speaker.

For longer silk specimens, a lower range loudspeaker (L20AT, Nikkai) was used from 100-2000 Hz. The displacement amplitude of the silk was measured at several points (15 averages per point) along the length of the fibre to confirm the wave shape and mode of the vibration (Figure

6.2). Then, just the middle of the fibres was measured, where the amplitude was greatest for first mode resonance.

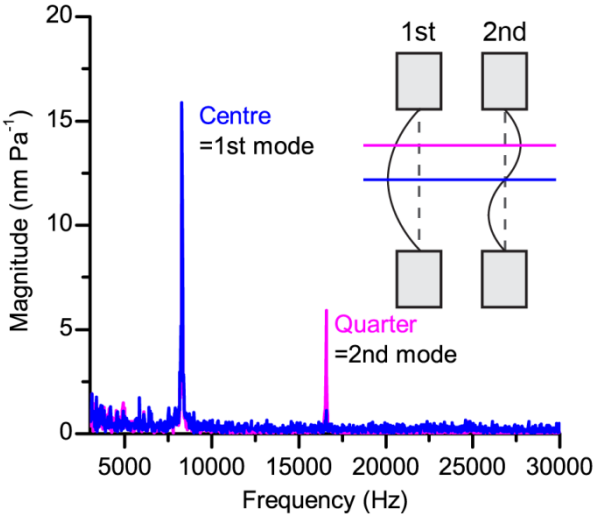

Figure 6.2. Example output from vibrometer, plotting frequency against magnitude of movement. Peaks represent resonant frequencies, which will change depending on the mode and position of imaging. Here, CuBe wire is imaged both at the centre (blue) and quarter (pink). Two peaks can be seen, corresponding to the 1st or fundamental mode at the centre and the 2nd mode at the quarter, which is twice the frequency of the fundamental mode.

Following the transverse vibrometry experiments, the specimens were tested in tension at a deformation rate of 1.5 mm min^{-1} to the full extension of the tensile stage (10 mm; ranges from 5.6 % strain for 180 mm specimens to breaking for 5 mm specimens; Appendix Figure A.7). These force-extension profiles were aligned with non-paused force-extension curves to give the stress, strain and length of the fibres during the vibrometry experiments. For longitudinal experiments, the extension was used to infer the strain, stress and length using a reference non-paused force extension curve.

Data from the laser vibrometer were analysed in Origin software (v. 8), where magnitude (nm Pa^{-1}) versus frequency (Hz) plots were used to infer resonant frequency (Figure 6.2). Frequencies below 3 kHz were cut off, as there is increased noise at these frequencies, presumably due to the movement/resonance of the apparatus at these frequencies. Equally, frequencies above 20 kHz show low amplitude (so rarely were higher modes seen in these regions). To make sure

resonance occurred in optimal regions, specimen lengths were altered, aiming for fundamental resonance around 8 kHz.

To smooth the curves, the magnitude versus frequency data were filtered using Origin's in-built FFT filter in low pass mode, using an ideal filter. The cut-off time in seconds was selected as 0.004. CuBe wire data were not smoothed due to sharper peaks and a greater signal to noise ratio (see Figure 6.2). The column data were then run through Origin's in-built peak-finding algorithm. Most data used a threshold of 40 % increase in height over 20 local points. Due to variation in the signal to noise ratio (especially for the longitudinal data), the threshold height or number of local points were sometimes decreased to allow the analysis of visibly obvious peaks, so manual filtering was also used. This does not affect the characterisation of peaks, so data are comparable between materials. The outputs were manually checked to locate the fundamental mode. Any adjoining peaks (peaks with no gaps between them) were treated as a single peak.

The frequency at the centre of the fundamental mode resonant peak (f in Hz) was used to calculate the wavespeed (C in m s^{-1}; Equation 1), using the silk length (l in m).

$$C = l \times f \times 2 \quad (1)$$

The resonant peak shapes were analysed to give peak width, height and area, where transverse wave peak heights and areas were transformed to allow for comparison (see below). The angle of c. 30 ° used for longitudinal measurements is corrected for when working out longitudinal peak height/area.

The transverse amplitude data were transformed to account for the different diameters of the fibres. For a given pressure, the force per unit length on the fibre drives the vibration, so to account for this, amplitude data are divided by the fibre's diameter. Since the fibres were all the same length, only the force per unit length needs to be considered.

The force on the fibre can be calculated from Equation (2):

$$F = \frac{1}{2} C_D \rho l d v^2 \quad (2)$$

Where C_D is the drag coefficient, ρ the density of air, l the length and d the diameter of the silk fibre and v is the speed of the incoming air. As the speed and density of the incoming air and fibre length are equal between materials, and the drag coefficient is comparable between materials due to the fibre shape, the transverse peak height (in nm Pa^{-1}) is divided by only the fibre diameter (in nm) to give a force per unit length (F) for comparison between fibres (in Pa^{-1}). Peak areas are also divided by the fibre diameter to give a similar parameter that can be compared between fibres.

Average total diameter for two fibres of equal size (diameter D) was taken to be D·(3/2); a combination of one big fibre (diameter D) and two smaller fibres (diameter d) was taken as (D+d)·(2/3); and a combination of two big fibres (diameter D) and two smaller fibres (diameter d) was taken as (D+d). These calculations give a diameter that is roughly average and representative between multiple fibres that twist relative to each other, as an accurate calculation of the diameter facing the on-coming sound front from the speakers is not possible.

6.3.3 Ballistic high-rate analysis

Longitudinal and transverse wavespeeds can additionally be calculated using experimental data from high-rate ballistic impact on single fibres. Specimen preparation and full methods are given in Chapter 5. Here, wavespeed data taken from spider silks with a low pre-stress on the fibre (c. 10 MPa, in the elastic region) at an impact velocity of 220 m s^{-1} were compared. For nylon and silkworm silk, the wavespeeds were compared across a range of low pre-tensions on the fibre (keeping impact speed constant, see Chapter 5).

6.3.4 Theoretical equations

Both transverse and longitudinal wavespeeds can be calculated in theory from known material parameters and applied conditions[268].

The longitudinal wavespeed (C_L) is given by:

$$C_L = \sqrt{\frac{E}{\rho}} \quad (3)$$

Where E is the storage modulus (Pa) and ρ is the density. E is taken as the quasi-static modulus for CuBe wire (1200 GPa; independent of pre-stress), whilst for nylon, silkworm silk and major ampullate silk it is taken from previously published data[177]. Storage modulus is a measure of the spring stiffness of the material, which scales with the pre-stress on the fibre[177]. The storage modulus of minor ampullate silk was taken from Blackledge *et al.* (2006)[45], where its relationship with pre-stress is unknown.

The transverse wavespeed (C_t) is related to the material properties by:

$$C_t = \sqrt{\frac{T(1+\varepsilon)}{\mu}} = \sqrt{\frac{\sigma(1+\varepsilon)}{\rho}} \quad (4)$$

Where T is the tension on the fibre (N), ε is the strain on the fibre and μ is the mass per unit length of the unstretched fibre (kg m^{-1} calculated by multiplying the density by the cross-sectional area). All parameters were measured during the experiments, with the exception of density (values given in Appendix A). The strain parameter acts as a correction for the mass per unit length as the fibre is stretched.

6.4 Results and Discussion

6.4.1 Physical basis of sonic properties

In order to confirm the applicability of basic wave equations to the sonic properties of silk fibres, longitudinal and transverse wavespeeds are experimentally measured using high-rate ballistic impact[132] and laser vibrometry in a range of materials and then compared to their theoretical values (Figure 6.3).

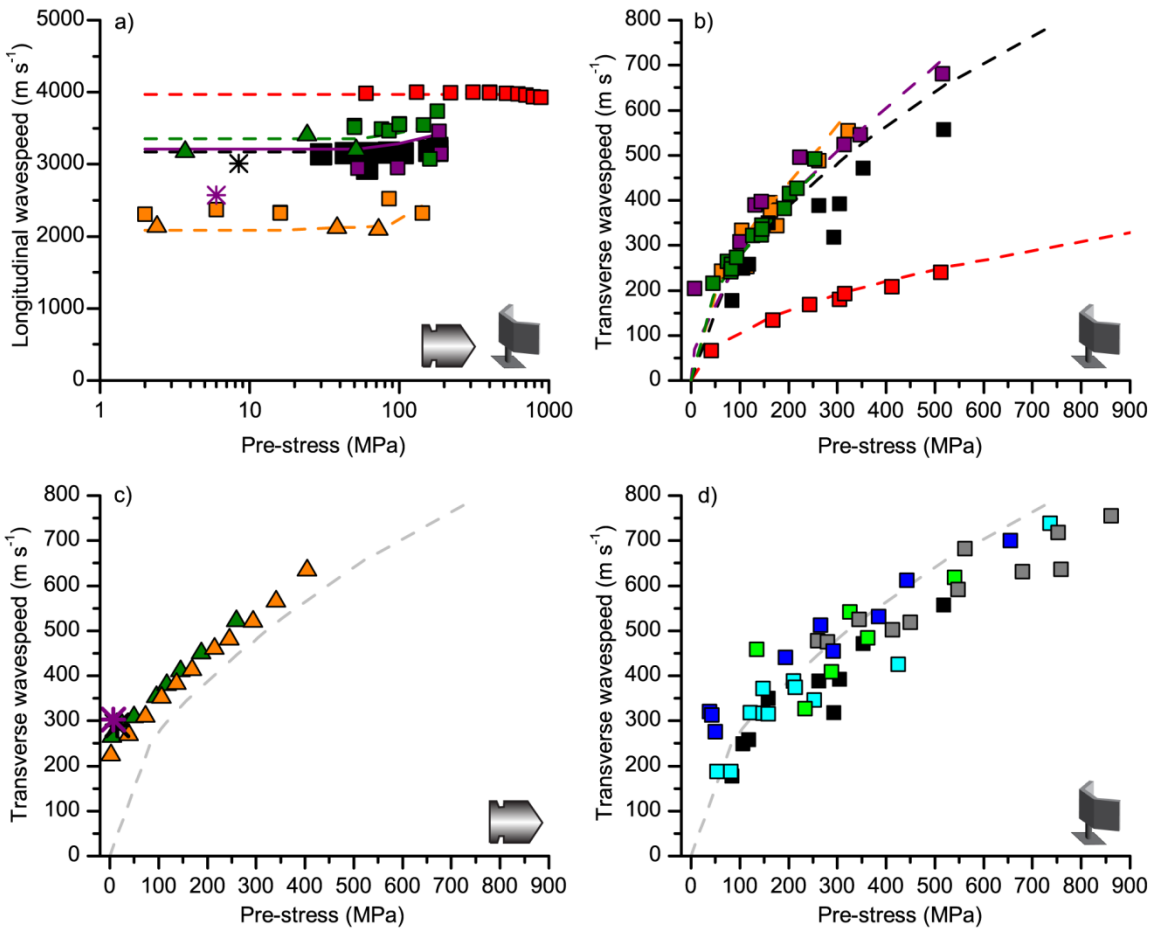

Figure 6.3: Wavespeed as a function of pre-stress. **a)** Longitudinal wavespeed (log axis) and **b)-d)** transverse wavespeed. Theoretical calculations are given by dashed lines, vibrometry data by squares (shown by speaker symbol), ballistic impact data, adapted from Drodge *et al.*[132], by triangles (shown by bullet symbol), and ballistic impact data for spider silks at low tensions and 220 m s^{-1} by stars. Materials: copper beryllium wire (red), *B. mori* silkworm silk (dark green), nylon (orange), *Nephila* major ampullate (MA) spider silk (big size, black; small size, dark grey; small size supercontracted, blue), *Nephila* minor ampullate (MiA) spider silk (purple), mixture of *Nephila* silks (2 MA, 2 MiA: cyan), and *Araneus* spider bundle (2 MA, 2 MiA: green). For b) and c), the grey dashed line gives a reference spider silk theoretical curve.

As silks and nylon have similar densities due to comparable polymeric structures, storage modulus is key to the differences in longitudinal wavespeed. For the transverse wavespeed, its response to stress is similar for all the polymeric materials tested (Figure 6.3b-d), due to their similar densities. In terms of the consistency of signalling, indicated by a fibre's response to tension, longitudinal wavespeed in both natural silks and synthetic polymers slightly increases in response to increasing static pre-stress above c. 50 MPa, by up to 16 % by 200 MPa (range 6 to 16 % for the different materials). This is because the storage modulus has a shallow linear relationship with pre-stress[177, 276]. Transverse waves are less consistent than longitudinal waves

as their wavespeed is sensitive to pre-stress, showing an increase in wavespeed of up to 102 % from 50 to 200 MPa (range 83 to 102 % for the different materials).

For all materials tested, the longitudinal wavespeed calculated from the two independent experimental techniques shows close agreement to theory, thus validating the approach (Figure 6.3a). The high-rate data show some small differences when compared to the vibrometry data and theory, explained by artefacts in the way in which longitudinal wavespeed is calculated, where small errors in the high-rate stress-strain coordinates are converted to large errors in the modulus and wavespeed (see Chapter 5)[132].

Although the transverse experimental data support the application of the theoretical equations in this context, there are some deviations. For example, the theory applies to standing waves specifically, and therefore describes the acoustic data well (Figure 6.3b and d). The high-rate data do not intercept at zero as the transverse waves are propagating rather than standing (Figure 6.3c). Even at zero pre-tension, there is a longitudinal pre-cursor wave that propagates ahead of the transverse wave and causes additional stress in the fibre[132].

In summary, the measured longitudinal and transverse wavespeeds for major (and minor) ampullate silk are 2940-3230 and 117-557 m s^{-1} respectively, comparable to previous theoretical calculations on *Nephila* silks (longitudinal 2111-2183 m s^{-1}, transverse 109-421 m s^{-1})[120, 269]. However, previously measured vibration propagation speeds in *Nephila* webs are slower (longitudinal 107-1070 m s^{-1}, transverse 70-100 m s^{-1}; frequencies of forced waves 10-1000 Hz)[120]. This can be explained by material dispersion of the relatively low-frequency, high-amplitude forced vibrations (see 6.4.2 and Figure 6.5), and also practical difficulties in measuring web silk fibres and keeping factors such as tension constant during the contact vibration used in these studies.

6.4.2 Consistency of wave signalling

Given the experimental confirmation of the physical basis of the sonic properties, signalling consistency of spider silks compared to other types of materials can be further explored by analysing the shape of the resonant peaks as determined by laser vibrometry (Figure 6.4). The peak width and height give information on the bandwidth of resonance and the influence of internal and external damping, where more damping would lead to wider and flatter peaks[268]. The resonant peak area reflects the capacity for vibration information transfer.

Data given in Appendix Figure A.8 show that, surprisingly, tension has no significant effect on peak shape. This may be explained by the small displacements used here. Higher displacements are expected to lead to internal damping due to plastic flow of polymer chains, causing a flattening of peak height[130]. Internal damping will be exacerbated by high tensions, not reached here due to limitations of the tensile stage (Appendix Figure A.7). Internal damping is expected to affect longitudinal more than transverse waves, because it directly affects modulus, on which the wavespeed depends (Equation (3)).

The resonant peak area for longitudinal waves is approximately consistent for all the materials tested (Figure 6.4e). Affecting both wave types, the polymers show wider peaks than the metal alloy as there is an increased distribution of structures within polymers, more consistent in the nylon than in the silks[130]. In contrast, the resonant peak area for transverse waves is not consistent between materials, where spider silks have a larger peak area (Figure 6.4f). The inconsistency stems from the additional factor of external damping acting from air resistance on transverse waves. This is supported by the sensitivity of transverse resonant peak width to fibre diameter and to the number of fibres present. Thinner spider silks show broader peaks, explained by external air damping effects, where smaller fibre diameter leads to a larger relative damping factor, broadening the resonant peak[240]. Importantly, the thinner spider silks

additionally have higher amplitude peaks as they couple more readily with the air relative to their mass per unit area.

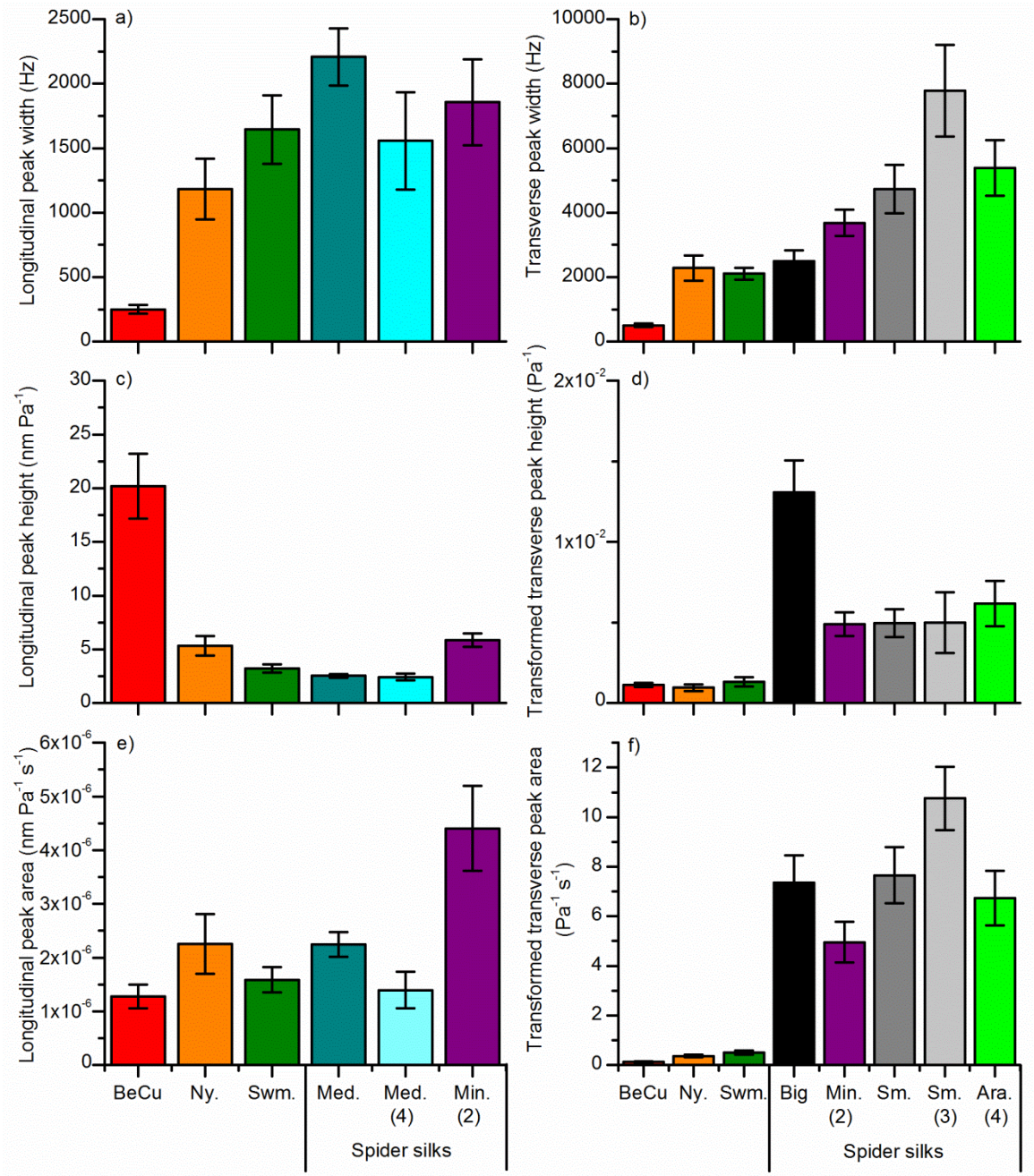

Figure 6.4. Resonant peak width data for **a)** longitudinal and **b)** transverse waves; height data for **c)** longitudinal and **d)** transverse waves; area data for **e)** longitudinal and **f)** transverse waves. Height and area outputs are transformed for transverse waves. Given there were no observable effects of tension, average values of all data points for each material type are given where error bars give standard error of the mean. Abbreviations: BeCu is copper beryllium wire, Ny. is nylon; Swm. is *B. mori* silkworm silk where two fibres are bound together; Big, Med. and Sm. refer to the size of the *Nephila* spider being reeled, and so the relative diameters of the silk fibres; Min. is minor ampullate silk and Ara. is *Araneus* silk. Numbers in brackets on the x-axis give the number of fibres present (no number means there is only a single fibre, numbers greater than two include a mix of major and minor ampullate silks).

Importantly, multiple fibres of spider silk show the broadest transverse wave bandwidth out of all materials tested. Increased peak width is due to differential sharing of the load between different fibres, leading to diverging transverse wavespeeds. Divergence is enhanced by including fibres of different diameters and types, such as filaments of both major and minor ampullate silks. Peak broadening could be a property useful for the spiders, as resonance can occur over a broader frequency range. The animal could increase transverse resonant peak area by combining multiple fibre types in a web or even a single thread (as can be found in some web radial threads[97]), thus increasing capacity for information transfer.

Another important factor affecting signalling consistency of materials is the sensitivity of wavespeed to frequency, known as dispersion. Theory suggests internal and external factors will cause a small amount of dispersion by damping the harmonic motion for either wave type[268]. To investigate the relationship between wavespeed and frequency experimentally, transverse resonance of silkworm silk specimens of different lengths were measured (Figure 6.5). Transverse wavespeed is approximately constant with changing frequency, but wavespeed is slowed down slightly at low frequencies (<1 kHz). Interestingly, this fits in with trends seen in plant material, which are dispersive at low frequencies, but non-dispersive at higher frequencies[277].

Theory suggests dispersion will have a greater effect on longitudinal than transverse waves, as the modulus term that directly affects longitudinal wavespeed (Equation (3)) is sensitive to frequency in polymers (log relationship)[142]. This frequency dependence may slightly decrease wavespeed for longitudinal waves at low frequencies, explaining previous observations of slower wave propagation speeds at low forced frequencies[120]. However, it should be noted that the overall effect of dispersion for any wave type will be very small, so wavespeeds are only marginally sensitive to frequency.

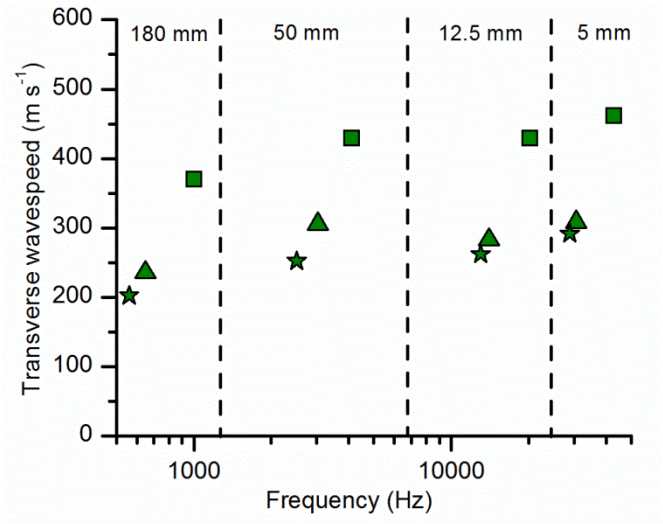

Figure 6.5. Dispersion in transverse waves. Frequency (log scale) versus transverse wavespeed for different length silkworm silk specimens at different tensions: squares 170 (± 5.3) MPa, triangles 66 (± 2.4) MPa and stars 49 (± 3.8) MPa. The dashed lines separate the specimens of different lengths, given by the label.

Overall, the resonant peak shapes and the dispersion data highlight the importance of damping on the consistency of signal transmission. Experimental measurement of the relative contributions of internal and external damping in single silk fibres and their relationship with tension is an area for further research and will give a full picture of how damping affects different wave types.

6.4.3 Evolution of spider silk as a signalling material

For the first time the sonic properties of single fibres of silks independent of the web have been quantified. This allows the physical basis of sonic properties to be confirmed and the consistency of signal transmission and information transfer to be measured. These data provide interesting insights into the evolution of spider silks' sonic properties.

The transverse wavespeed of spider silk is determined primarily by its density, and hence differs little from other polymers. Density depends on the material structure, which constrains the shaping of transverse wavespeed by natural selection. In contrast, the value of the longitudinal wavespeed is tuned by the storage modulus, or spring stiffness, which differs between the

materials tested. Therefore, in principle, the storage modulus could be selected in spiders to adapt the longitudinal sonic properties.

However, storage modulus also dictates mechanical properties, so the wavespeed will be constrained by the dual functions of the storage modulus. Storage modulus in silk varies according to protein structure[135, 278]. Yet material structure can be modified by both environmental and processing conditions[87, 135, 177, 278-279], which enables the spider to behaviourally tune the storage modulus for best performance (use-specific) under variable conditions (see 6.4.4).

The differences in signalling consistency of transverse and longitudinal waves allow their possible roles in the web to be inferred (Table 10). Longitudinal waves have greater scope for signalling uses as they propagate reliable, damage tolerant signals to the spider regardless of the tension, humidity and strain history of the web. This supports previous studies of webs showing lower attenuation for longitudinal compared to transverse waves, explained by lower external damping and minimal wave reflection at junctions[96, 109, 120-121, 269]. As attenuation has direct effects on wave amplitude, longitudinal waves may therefore aid spider vibration detection in the web and possibly discrimination of signals[119-121]. This difference in consistency and attenuation may explain behavioural data showing that spiders are more likely to respond to web-borne longitudinal waves[119, 270-271].

In contrast, transverse waves are highly sensitive to small changes in tension, meaning that the transverse wavespeed is difficult to control, and is affected by both passive mechanisms, including wind, caught objects and even humidity conditions, but also active mechanisms such as web pre-tension and number of fibres. Transverse sonic properties may be a disadvantage in terms of consistent signalling, but could be an advantage for real-time probing of web condition (e.g. damage and tension) via reflection due to changes in impedence[120-121].

Table 10: Summary of findings. Asterisk gives an inferred effect that is not directly tested.

Wave type	Longitudinal	Transverse
	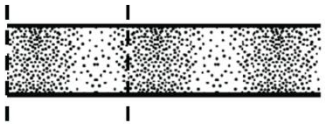	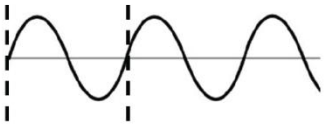
Wavespeed variation between materials	Governed by storage modulus	Does not vary between polymers as densities and response to tension is similar
Wavespeed sensitivity	Storage modulus, (slight effect of tension), (slight effect of frequency)*	Tension, (slight effect of frequency)
Resonance sensitivity	Distribution of structures in the material	Fibre number, fibre diameter, distribution of structures in the material
Hypothesised use in web	Vibration propagation of all kinds, where any resonance will be above 1 kHz	Web condition signals, resonance at short silk lengths from silk plucking
	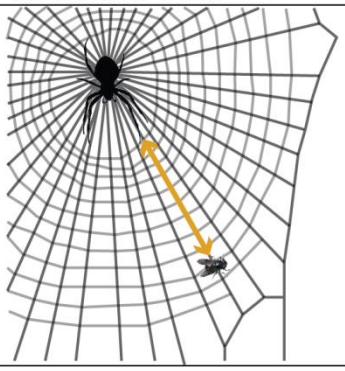	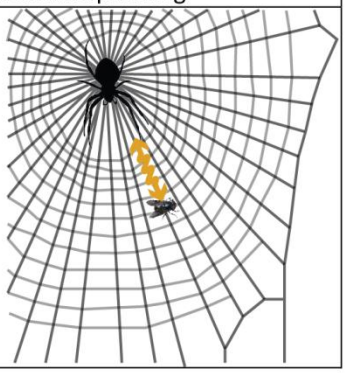

Interpreting the measured wavespeeds within the context of *Nephila's* web geometry, possible frequency ranges for the different wave types in a web can be calculated. For a 0.7 m web under tension[82, 242], the minimum resonant frequencies are 1150 Hz for longitudinal and 75 Hz for transverse waves, assuming the vibrating source is the maximum displacement point of the wave. This calculation further supports use of longitudinal waves over transverse waves for information gathering in webs, when the influence of dispersion and resonance is considered. Firstly, transverse waves are likely to be less consistent in signalling as they are affected by dispersion due to their low resonant frequencies and are subject to geometrical dispersion due to the distribution of web tensions[242]. Secondly, longitudinal waves will not resonate close to prey-generated vibration frequencies (typically under 1 kHz)[97, 120, 270]. This means that silk

resonance is unlikely to interfere with prey-driven vibrations. This may be an advantage for detecting diverse and inconsistent vibration signals, particularly the broadband signals produced by prey[120, 271]. Therefore, longitudinal resonance at high frequencies may have a selective advantage over resonance under 1 kHz[120]. This would enable prey-generated signals to propagate without resonant amplification, which may incur additional processing by the spider prior to interpretation.

Together, these interpretations may provide an explanation as to why spider vibration sensors have the highest displacement sensitivity at 1 kHz (~100 nm)[267, 280-281] in spite of prey not causing vibrations at such high frequencies[97, 120, 270]. The answer stems from the behaviour of silk plucking by spiders; the results predict that following silk-plucking, longitudinal (and potentially transverse) waves will resonate close to or above 1 kHz at web-like lengths[119-120, 255, 261-262, 264]. In principle this could be used to determine an objects' (or 'intruders'') radial thread location, as the frequencies will be higher on threads with a reflection point.

6.4.4 Silk as a multifunctional material

Moving beyond the web and comparing silk to other materials, spider silk is shown to be a superb example of a high fidelity, behaviourally tunable, multifunctional fibre. To facilitate comparison, a performance map of silks akin to an Ashby plot is presented, comparing the consistent and controllable longitudinal wavespeed[282] (Figure 6.6).

Spider major ampullate silks occupy a unique niche of properties (Figure 6.6). Whereas a metallic alloy has one modulus and so one longitudinal wavespeed, polymers have a range, shaped by the sensitivity of their storage moduli to tension[177, 276]. Of particular significance is the discovery that spider major ampullate silk has the largest wavespeed range out of any known material due to the range of moduli available (3 to 30 GPa)[87, 135, 177]. At the high end, similar to other polymers and silks, the storage modulus can be increased by tension and other processing

conditions, such as the speed of silk production (i.e. spinning rate)[87, 177, 278-279]. This provides active controls for the spider to alter the storage modulus and with that, the resulting wavespeed and mechanical properties of its silks. At the lower end, wetting major ampullate silk causes supercontraction, drastically decreasing modulus[87, 136]. This provides a passive control, which can reset properties periodically, for example when dew descends at night[90]. Importantly, following the passive supercontraction, the silks can be actively stretched to again increase their moduli[283]. Spiders can therefore choose the extent to which the silks are stretched, giving them access to the whole range of moduli through their behaviour, allowing them to shape the balance between mechanical and signalling properties as required.

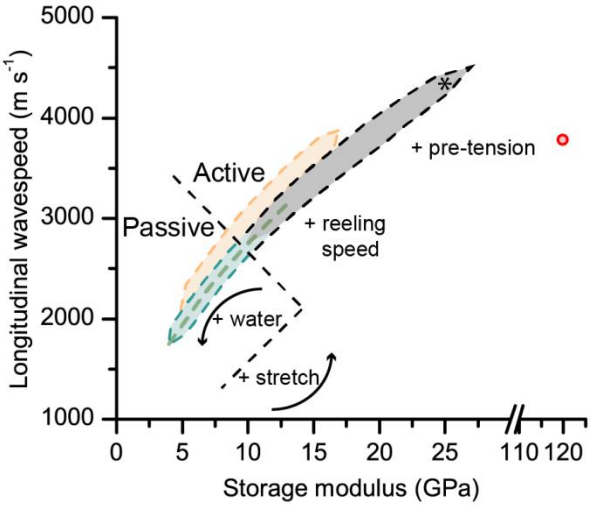

Figure 6.6: Storage modulus versus longitudinal wavespeed for different materials. Polymers and silks follow a (root) dashed line, so shaded area is given to allow different materials to be distinguished. Metal wire has a single coordinate. Materials: copper beryllium wire (red), silkworm silk (dark green dashed line), nylon (orange), *Nephila* major ampullate spider silk (dry: black, wet: cyan). Asterisk gives low tension, dry Aciniform spider silk[45]. For the major ampullate silks, modulus can change with passive and active controls (separated by dashed line): for passive control, wetting the silk allows supercontraction, lowering wavespeed; in active control, modulus can be altered by processing conditions such as reeling speed, but also by applying tension or stretching, which increases the longitudinal wavespeed.

6.5 Conclusions

In conclusion, by studying vibrations in spider silks in comparison with other materials, evolutionary trade-offs between mechanical and signalling functions are indentified, both governed by storage modulus. Storage modulus, in turn, may be adjusted actively by the spider via its spinning behaviour in response to abiotic and biotic conditions, or it may be passively affected by climatic factors, such as humidity. The approach presented here is interdisciplinary and by combining experimental, empirical and theoretical investigations, vibration transmission in multifunctional materials is investigated. This is applicable beyond the silk model system to a wide range of multipurpose biomaterials that aim to balance both signalling and mechanical functions. In this way, spider silks may provide interesting and important insights beyond the specific adaptations of the web to provide inspiration for the design of stimuli-responsive smart materials[284-285].

Chapter 7 Future outlooks

7.1 Introduction

This chapter applies the techniques developed in previous chapters to some specific unanswered questions associated with spider silks. The first section investigates capture spiral silks. Understanding the mechanical and vibrational properties of these composite silks will be vital for building an understanding of orb web function. Building on research from Chapter 6, the second section investigates the mechanical implications of combining multiple fibres of spider silks, relevant for the orb web and draglines of spiders. The last section looks in detail at the signal thread of the sector web spider *Zygiella*, who uses a single bundle of spider silk as her main vibration sensory input.

The capture spiral is made of a core flagelliform silk, coated in an aggregate glue coating[46, 115]. The mechanical properties and stickiness of these silks are affected by humidity[46, 286], where high humidity increases prey catching efficiency[117]. However, there is large variation in the literature of the mechanical properties of these silks, leading to vastly different estimates of their toughness[46-48, 97, 287]. The traditional view is that capture spiral silks are the main energy absorbing component of the web[47, 97], but other authors suggest that the radial threads fulfil this function and the capture spiral silks are used exclusively for retaining caught prey[81]. Additionally, the vibrational properties of capture spiral silks are unstudied, although the capture spiral has been shown to increase damping on the radial threads[120-121]. This chapter therefore aims to explore the possible causes of the mechanical property variation, with a focus on diameter measurement, and to measure the vibrational properties of capture spiral silks.

Spider silk draglines and radial and structural threads of orb webs contain multiple fibres of silks[97], commonly thought to contain major ampullate silk, with some evidence of minor ampullate as well[93, 288-289]. From my own observations of forced reeling *Nephila*, *Araneus* and

Zygiella, both major and minor are often coextruded. In the case of *Nephila*, the larger pregnant spiders are more likely to contain minor ampullate, and even aciniform silk, presumably to cope with their larger mass (hypothesis untested). Multiple fibres affect the vibrational properties (see Chapter 6), but the effect on the mechanical response remains relatively understudied, especially the effect of combining silks with different properties, like major and minor ampullate bundles. Yarns of spider major ampullate silk have been measured at high-rate[134], and bundles of polymer fibres have been measured at different rates[290], but there are little data in the literature on the tensile mechanical response of bundles of spider silks.

Zygiella x-notata is the sector web spider, which builds modified orb webs with a free sector (Figure 7.1). The signal thread is built last and runs between the hub and a retreat[291]. The spider sits in the retreat with one or two front legs on the signal thread[119]. The spider will run to the hub when prey hits its web or in response to web vibration, indicating the signal thread's use to transmit vibrational sensory information to the spider[119, 271]. *Zygiella* takes longer to locate prey in the web compared to orb weavers such as *Nephila*[119], but the use of the retreat allows the spider to protect itself from predators and parasitoids[292]. Studies have previously looked closely at *Zygiella* web building behaviour[291, 293-295], but none have looked in detail at the structure and properties of the signal thread, which I aim to begin to address here.

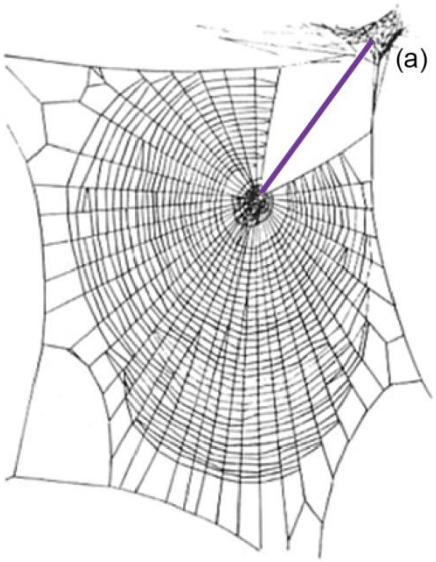

Figure 7.1. Typical web from *Zygiella x-notata*. The web is a modified orb web, a sector is kept free in a top corner, where the signal thread (purple) runs from the hub to a retreat (a). Adapted from Foelix 2010[86].

7.2 Materials and Methods

7.2.1 Specimen preparation

7.2.1.1 *Nephila* silks

Capture spiral silks were mounted from a single *Nephila edulis* web that was built under lab conditions (see Chapter 2). Threads were stuck onto compass points using their own stickiness and cut. The specimens were then contracted until just above being slack (imaged using a dissection microscope) and were mounted onto 5 mm cardboard frames. Specimens were mounted in this way to make sure that all capture spiral threads were at a comparable tension, as the tension differs throughout the web[242]. This ensures all specimens have a comparable starting point for their stress-strain curve, which should reduce strain-related variability between specimens.

Bundles of major and minor ampullate silks that were naturally coextruded by the spider for use as their dragline were also mounted onto 10 mm frames for SEM imaging and tensile testing (these were also measured in Chapter 6).

7.2.1.2 *Zygiella x-notata*

Signal thread silks were obtained from *Zygiella x-notata* webs (Figure 7.1). Details on the housing and sourcing of the spiders are given in Chapter 2. *Zygiella* were fed exclusively on adult *Drosophila*. Spiders were photographed and weighed to give size data.

Dividers fixed onto a micromanipulator were used to remove signal threads from the web, which were superglued to give as large a specimen as possible. In all cases, two 12.5 mm specimens could be mounted from the dividers into cardboard frames, kept under tension at all times. Webs were photographed before removing the signal thread. In many cases, at least three signal threads built on different occasions were collected from an individual spider.

A large *Zygiella* (0.0312g) was also forced reeled for her silk, as described in Chapter 2.

7.2.2 SEM imaging

Capture spiral silks were imaged in their contracted state in 5 mm cardboard frames in the ESEM. Wet mode was used at a humidity of 40 % (1 °C, 250 Pa settings), using a cyclic pump-down between 750 and 250 Pa six times. For comparison, capture spiral silks were imaged in the SEM following sputter coating (150 seconds).

Zygiella specimens were also imaged in the SEM following sputter coating. Specimens under tension in their frames were imaged for their diameters. Broken ends from stress-strain experiments were also imaged, allowing approximate number of threads to be measured (two repeats per signal thread). Diameter measurement from broken ends will be an underestimate as specimens have been pulled apart.

7.2.3 Laser vibrometry

The laser vibrometry methods developed in Chapter 6 were further adapted here. Capture spiral silks were loaded into the tensile testing clamps and the cardboard was cut. The specimens were

then breathed on 7-8 times to introduce a high humidity onto the fibre, to saturate the silks. Tension was controlled by changing specimen extension, up to 200 % strain. Tensions in capture spiral silks are very low, so tension was calculated outside the vibrometry set-up using a high resolution load-extension curve from specimens mounted from different webs and measured in a Zwick Z0.5 tensile tester with a 5 N load cell. Variability in stress-strain curves of capture spiral silks mounted and measured using this method is low, even between spiders and testing rates (Appendix Figure A.9).

Zygiella specimens were kept under tension, and the first reading was taken straight after frames were cut, under 'natural tension'. Further tension was then added by extending the specimen using the tensile tester (strain, not stress controlled). Preload was calculated by using the post-break tension at zero load. Fibres were measured for their transverse wave properties in the middle of the silk fibre, over frequencies of 1-30 kHz. As cross-sectional area is difficult to measure due to the multiple fibres of thin size, resulting in a complicated shape, load data were analysed instead of stress data.

Data from the laser vibrometer were analysed similar to Chapter 6. Due to the low frequencies involved, the data output did not have to be FFT filtered. The peak finding algorithm used at 20 % height increase over 20 points, to allow measurement of smaller visible peaks. Fundamental mode frequencies were calculated by the relationship between higher mode peaks, assuming only odd modes are seen where the fibre was imaged at the centre. The reference sound pressure versus frequency data was particularly important for the thin *Zygiella* silks, as they were sensitive to small changes in the acoustic sound front. The reference data were therefore checked carefully and used to discount peaks where a dip in sound pressure could be seen (which increases the magnitude output of the silk). Any adjoining peaks (peaks with no gaps between them) were treated as a single peak. The frequency of the highest section of a peak

was used to calculate the wavespeed. Height and area of peaks were not analysed, so no transformation is used.

7.2.4 Stress-strain

Capture spiral silks and *Zygiella* forced reeled and signal thread silks were measured in a Zwick tensile tester. Multiple fibres of *Nephila* ampullate silks were measured in an Instron tensile tester.

7.2.5 *Zygiella* signal thread repair

After signal threads were taken from new webs built by *Zygiella*, the webs were filmed to record the spiders' signal thread repair behaviour (Panasonic HDC-TM700). In particular, the number of times the spider moves between the hub and retreat is recorded, termed 'number of runs'. Correlations were made between the number of runs and other parameters using Excel, which calculates an R^2 value, where 1 is a perfect linear relationship and 0 is a random relationship.

7.3 Results and Discussion

7.3.1 Capture spiral silks

Imaging the fibre using the ESEM gives pictures dissimilar from that in the SEM (Figure 7.2). The flattened shape of the silk fibre in the ESEM image suggests that the fibre is either immersed in water or the fibre is stuck onto the Peltier chip below the specimen. Further experiments in the ESEM would determine what is causing this shape. Nevertheless, Figure 7.2a clearly shows the composite nature of capture spiral threads – with an internal core of flagelliform fibres, which appear to be a double strand, coated in blobs of aggregate glue[115]. Whether the third layer is an artefact of the fibre being stuck to the surface (layer of water perhaps) or is a feature of the fibre is unknown. But as the double core strand cannot be seen in the SEM and the metal coating is thin, it does suggest a third coating is involved. In contrast, the SEM image shows

shrivelled glue blobs on a smooth fibre, interpreted as an artefact of the high vacuum and low humidity conditions. These images look different from previous light microscope images, explained by differences in hydration and fibre tension[46].

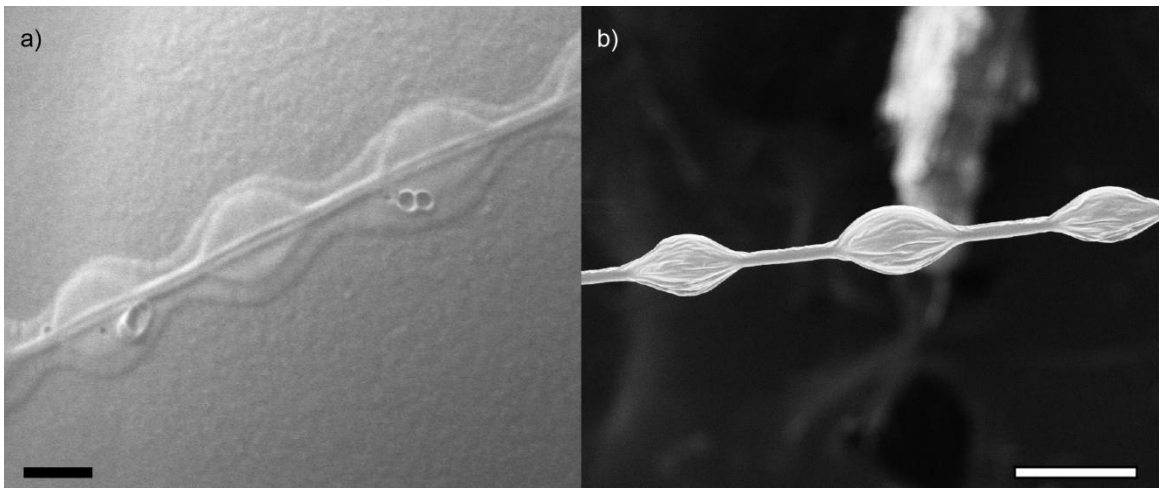

Figure 7.2. Images of capture spiral silks in the: **a)** ESEM in wet-mode at 40 % RH and **b)** SEM under high vacuum, following sputter coating. Black bar denotes 20 µm, white bar denotes 100 µm. Bubbles in a) suggest charging due to electron damage. This was seen repeatedly for the glue coating only, both in the ESEM and SEM if the coating cracked.

The aim of these images is to measure the diameter of the core fibre, which takes the load during tensile testing[286]. These fibres are from different webs, but the diameter of the SEM fibre and the ESEM fibre and coating are approximately equal. Although more evidence is required, it may be that SEM images cannot be used to make an accurate diameter measurement as they do not show the flagelliform core fibres without a coating. The error involved in the SEM diameter measurements requires further study. ESEM may provide information on flagelliform coating, but more experiments are needed to determine ideal imaging conditions, with minimal artefacts. Due to the thin diameters involved, casing in superglue and sectioning (as in Chapter 2) was not attempted, but could be a method for future consideration.

There is large variability quoted in the literature of capture spiral silk mechanical properties, with strength from 0.4 to 1.7 GPa and extensibility from 150 to 360 %[46-48, 97, 286-287]. This can be explained by a combination of: the method of mounting capture spiral silks, causing problems measuring the initial length; their humidity sensitivity, affecting all properties; and the difficulty

in imaging the silks without artefacts, which affects stress-related parameters through diameter measurement.

An alternative method that might provide insights on the mass per unit length of the capture spiral is measuring their vibrational properties. In contrast to all other measured silks, the resonant peaks of 12.5 mm capture spiral silks are very low (Figure 7.3), giving the lowest calculated transverse wavespeeds at 3-23 m s^{-1} (ampullate silks are 150-700 m s^{-1}; Figure 6.3). This is explained by the very low tensions involved (inferred from load-extension curves to be 2 x 10^{-5} – 2 x 10^{-4} N, Appendix Figure A.9). This supports previous research showing that capture spirals damp vibrations in the radial threads of the web[120-121], as wavespeed will be dramatically reduced in these silks.

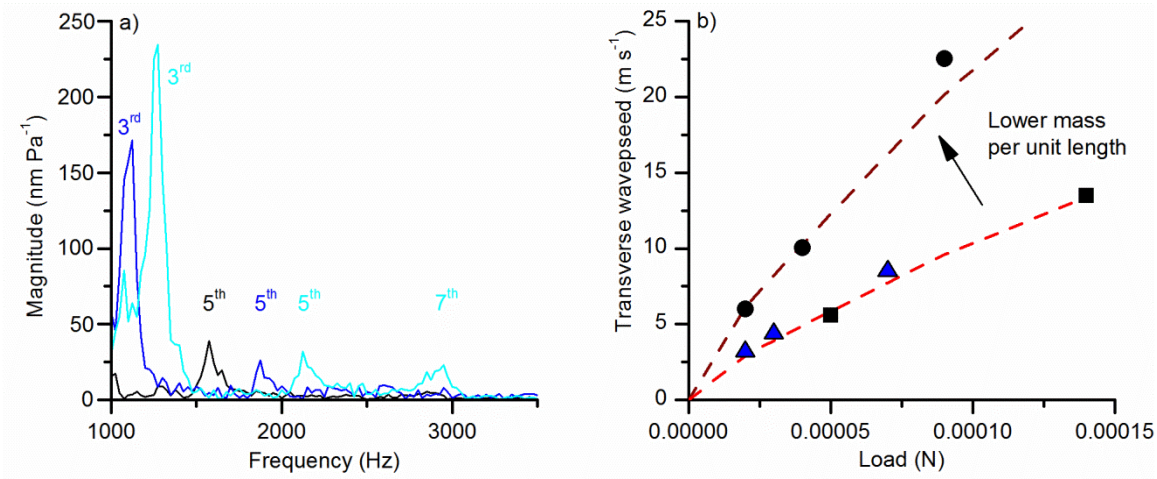

Figure 7.3. Vibrational properties of capture spiral silks: **a)** resonant peaks from 2 x 10^{-5} N (black), 3 x 10^{-5} N (dark blue) and 7 x 10^{-5} N (cyan) of one specimen of capture spiral silk, which is representative of all the silks measured. Mode number is labelled on the peak, which is calculated by taking the information of all peaks into account. **b)** Transverse wavespeed over load. Different shape symbols represent different silk specimens, blue triangle gives the specimen measured in a). Dashed lines give the fitted theory curve for the measured points, where the higher curve requires a lower mass per unit length.

The method allows mass per unit length to be calculated from the wavespeed and the tension, using the theoretical equations for transverse wavespeed (Chapter 6, Equation 4). For the three specimens measured across a range of tensions, two had a similar modelled mass per unit length, and so wavespeeds, but one had a lower modelled mass per unit length. This is explained by a smaller volume coating, or fewer aggregate glue blobs. Both density and area over length

are expected to change as more aggregate glue is added, so further ways to interpret the mass per unit length change are not possible without further study. As the technique is so sensitive, it may also provide a way to monitor changes in tension without using a load cell.

7.3.2 Stress-strain properties of combined spider silks

The stress-strain response of naturally co-reeled major and minor ampullate silks are given in Figure 7.4, which can be interpreted as the mechanical behaviour of spider draglines. In theory, load should be taken by fibres in proportion to their relative stiffness[296]. Minor ampullate silks are on average less stiff than major ampullate silks pre- and post-yield[92-93]. The area allocation of the sum of the fibres is used to calculate stress, which matches between spider silk bundles of different compositions (Figure 7.4a and b).

These curves have implications for their role in the dragline or web. The increased extension of the minor ampullate has a noticeable effect – as more energy can be absorbed up to c. 50 % extension. These silks are therefore a 'last resort' in the dragline (and possibly radial threads), allowing more energy to be absorbed and high extensions to be tolerated without breaking.

Interestingly, major and minor ampullate silks also vary in their response to high humidity – where major ampullate silk supercontracts and minor ampullate does not[91-92]. This means that in some cases minor ampullate silk will be stiffer than major, and so be expected to take proportionally more load. This will also contribute to the benefit of major and minor ampullate bundles, as there will be a stiff fibre taking part of the load regardless of the humidity. Data in Chapter 5 also show that major ampullate silks are more variable than minor silks under impact, so using bundles may improve performance over a range of conditions. More experiments are required to understand the stress-strain variability of multiple types of spider silks across species and their relative use in different parts of the webs by spiders of different sizes.

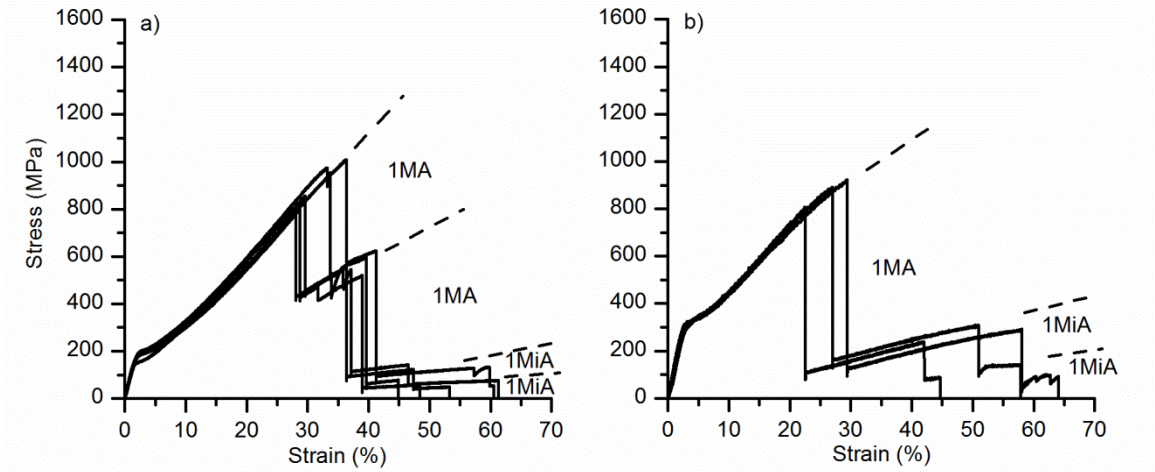

Figure 7.4.Stress-strain responses of bundles of major and minor ampullate *Nephila* silks: **a)** two major ampullate (MA) and two minor ampullate (MiA); **b)** one MA and two MiA bundles.

7.3.3 *Zygiella* silks

Building on the techniques in the previous section, the stress-strain responses of forced reeled *Zygiella* silks are also analysed (Figure 7.5). Through inference from dissection microscope imaging prior to reeling, bundles are two major and two minor ampullate silks, which fits in with SEM images showing two larger and two smaller fibres (Figure 7.7a). Some fibres were double the load of others. Area allocation assigned the whole or half the total area (total being 2 major and 2 minor) to make these curves align, suggesting that some tested specimens had different silk compositions (perhaps through breaking of fibres during mounting).

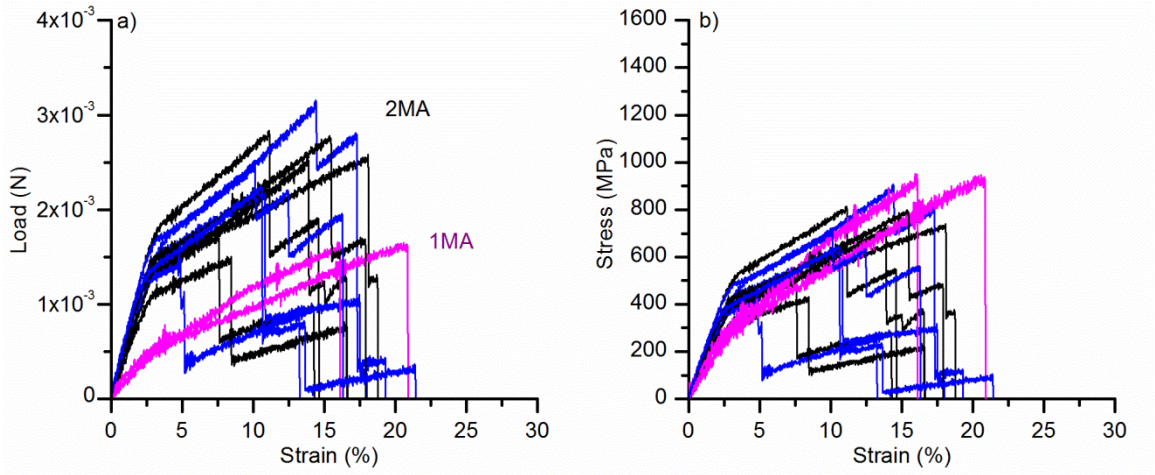

Figure 7.5. Mechanical responses of bundles of two major and two minor ampullate silks from *Zygiella*. **a)** load and **b)** stress, where pink curves (where the load is half) use half the total area, and black or blue curves use the whole area. Black and blue indicates specimens with two or three breaking points respectively.

Comparing both species, the stress-strain contours are similar (Figure 7.4 and Figure 7.5), and load correlates with fibre diameter. Unlike the *Nephila* silks, the *Zygiella* silk breaking pattern does not show high extension for major or the more noticeable minor ampullate fibres. On average for *Zygiella*, fibre breaking is distributed around 15 % breaking strain. Stress-strain curves showed a mixture of one (pink, low load), two or three breaking points, so fibres did not always break individually. Unlike *Nephila*, there is more variation in the load taken by different *Zygiella* fibres following the initial break, indicating more variability in fibre strength within and between ampullate silk types. Overall, this suggests that *Zygiella* ampullate silks have different properties to *Nephila* silks, which may be explained by the differing natural function of ampullate silks.

These forced reeled silks are compared to the stress-strain properties of signal threads from the same spider, shown in Figure 7.6a. On average, signal threads had higher breaking loads, due to the multiple fibres used (Figure 7.7b) and showed evidence of post-yield hardening, which can be caused by the interaction of strands together, whether mechanically or electrostatically[114, 297].

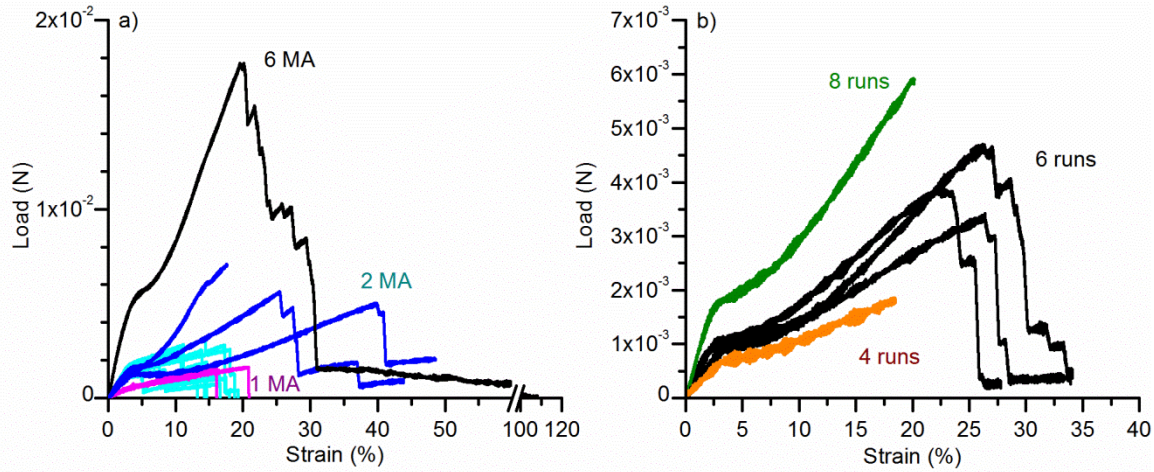

Figure 7.6. Load-extension curves of *Zygiella* silks: **a)** forced reeled and signal threads from the same spider, where pink shows the curve where one MA is taking the load, blues is two MA (cyan forced reeled, dark blue signal thread) and black is 6 MA (MiA is ignored for simplicity). **b)** Stress-strain curves of signal threads from one spider, where the number of runs was recorded. Orange is 4 runs, black 6, and green 8 runs, which correlate with initial modulus (in N).

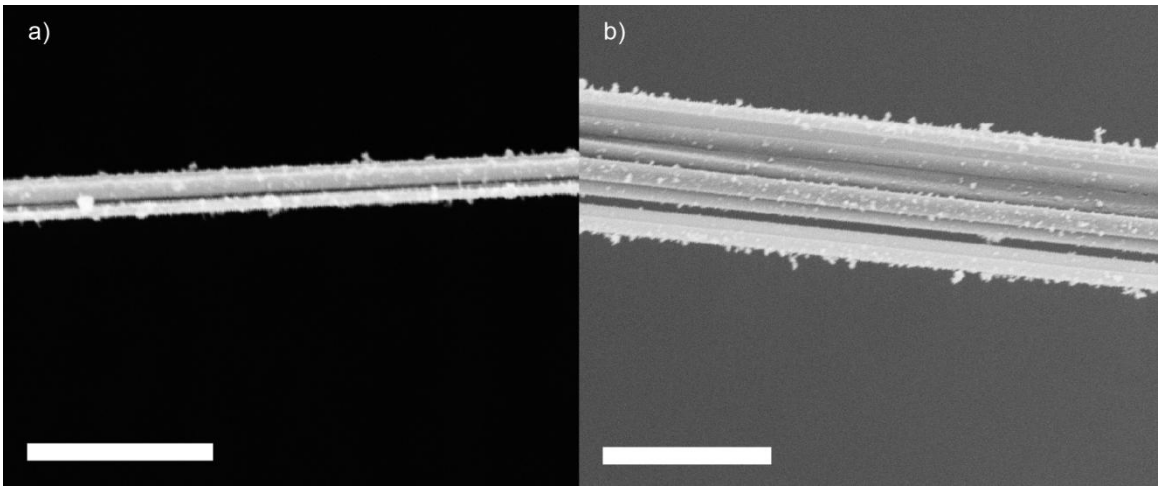

Figure 7.7. SEM image of *Zygiella* silks: **a)** forced reeled, where a doublet of larger silk (assumed MA) and a doublet of smaller silk (assumed MiA) are coextruded, and **b)** naturally spun signal thread taken from a new web, where multiple silks are used. White bar denotes 10 µm.

Stress-strain data from signal threads can be combined with other data to infer the number of silks present in a signal thread. Initial modulus (in N) is used to infer the number of fibres taking the load, correlated against the forced reeled silks of known fibre composition. Taking the data from four spiders and 11 specimens, initial modulus correlates with the number of times the spider moved between the hub and retreat during signal thread repair (termed 'runs'; $R^2 = 0.78$; example from one spider given in Figure 7.6b). Number of runs also correlates with the number of broken ends seen in the SEM ($R^2 = 0.74$), whereas the number of breaks seen in the stress-strain response had no relationship, implying that some fibres were not involved in taking load before breaking ($R^2 = 0.02$).

The close relationship between modulus, number of broken ends and number of runs is encouraging. Every time the spider moves, more silks are added, meaning more are seen on the broken ends, giving a number always a multiple of two. This relationship is not perfect, so spiders will vary in how many silks they add each time – most likely whether they add two minor ampullate silks during a run.

Between different signal thread repairs, the number of SEM broken ends varies from four to 14 (number of runs varies too), highlighting that repair behaviour is flexible within and between spiders. There is no correlation between number of runs and time taken to repair, $R^2 = 0.12$.

Signal thread building behaviour in new webs has a similar level of variation. The only difference between repair and new signal thread was in their pre-tension, where the latter was higher and never zero. Pre-tension also correlates with the load modulus (R^2 = 0.74), suggesting that pre-load may lead to a similar pre-stress between signal threads of different sizes.

This has interesting implications for the importance of the signal thread composition, as the variability supports that the number of threads is not conserved by spider behaviour, suggesting that it is relatively unimportant. This is regardless of spider size – the total diameter of the signal thread does not correlate with spider size (measured by carapace width, R^2 = 0.12), although the diameter of a single silk thread has a weak correlation (R^2 = 0.5). Draglines laid during movement between the hub and retreat are incorporated into the signal thread, so the number is likely to change throughout the day as prey is caught. The pre-tension is likely to lead to a roughly constant pre-stress, which may be important for ensuring consistent transverse or longitudinal vibration. Further experiments are required on the structure of the signal thread, particularly its integration with the web in terms of bridging threads and vibration transmission from different areas of the web.

The sonic properties of *Zygiella* signal threads were further investigated over a range of pre-tensions (Figure 7.8). Not seen in any of my previous research on spider silks (Chapter 6), signal threads have multiple, separate peaks not caused by resonant harmonics. This suggests that the multiple fibres involved have different masses per unit length, caused by different cross-sectional areas, and/or tension being shared by the fibres unevenly (by differing moduli or differential pre-tensioning). In terms of the transverse signalling, this is potentially beneficial as signals from prey can be amplified over a wide range of frequencies through resonance. In theory, longitudinal wave signalling should not change as storage modulus is unaffected by number of fibres (see Chapter 6).

For the signal threads shown in Figure 7.8a, more load increases the number of peaks and simultaneously increases and decreases the resonant frequencies seen. In this special case, more load correlates with a simultaneous increase and decrease in area contributing to mass per unit length (Figure 7.8b). This can be explained by the multiple fibres of signal threads – some can be recruited to vibrate as load is added, but others may separate and vibrate independently. This trend was not seen in all cases, and Figure 7.8b shows the transverse wavespeed versus the load for three signal threads from the same spider. More repeats are needed to fully investigate the effect of tension on the vibrational properties, as it gives information on the ability of fibres within a bundle to take load, separate or be recruited as load is added.

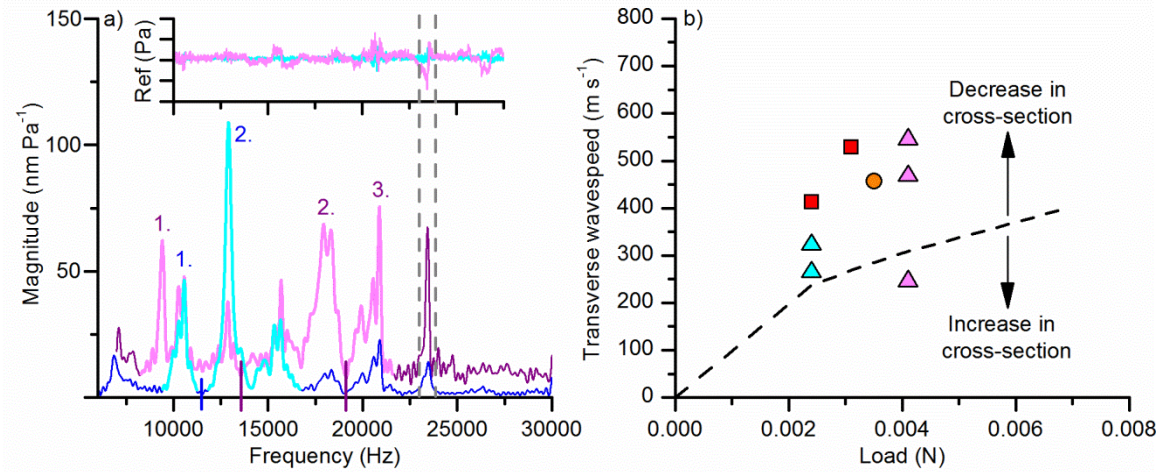

Figure 7.8. The vibrational properties of *Zygiella* signal threads: **a)** resonant peaks of one signal thread at 0.0024 N (blues) and 0.0041 N (pinks). Light colours give the data determined to be a peak. The different peaks are labelled with numbers and the gaps between them denoted by a line across the x axis. Inset is a frequency versus reference plot, which gives the relative sound pressure of the acoustic sound front at different frequencies. Around 23 kHz, there is a dip in the reference which corresponds to a peak in the magnitude data (shown with grey dashed line), so this peak was excluded. **b)** Transverse wavespeed versus load for three signal threads from the same spider (red; orange; and blue and pink give the low and high load data used in panel a)). The area used to work out the theoretical dashed curve used the measured whole cross-section (a technique that succeeded only once), which seems to be an overestimate. Data points below this line require a higher area, and above require a lower area.

7.4 Conclusions

In conclusion, the combination of electron microscopy, tensile testing and laser vibrometry allows several complicated and problematic questions to be investigated relating to spider silk form and function. In the case of capture spiral silks, consistent techniques need to be developed for fibre mounting and diameter measurement. In this way, the mechanical and vibrational properties can be investigated with low variability to infer their functional role in the orb web. Multiple fibres of spider silk are often utilised in the web, and here there is support that the load taken by a fibre bundle is proportional to the number of fibres present and their relative stiffness. This appears to differ between species and is a question deserving further in-depth study. Lastly, the signal thread of *Zygiella x-notata* appears to be flexible in composition, with apparently weak selection pressures to conserve the number of threads present. A higher number of threads may have beneficial effects for transverse vibrational signalling, but in theory will not affect longitudinal vibrations, to which *Zygiella* preferentially responds[119].

Chapter 8 General Conclusions

This Thesis contributes towards the understanding of mechanical and sonic property variation of single fibres of silk. The Thesis has concentrated on the effects of environment (Chapter 3), applied processing conditions (Chapter 4), deformation rate (Chapter 5), tension and number of silk strands (Chapter 6 and 7). Data have been presented on spider silks, including major and minor ampullate silks and capture spiral silks from three species of spider and *Bombyx mori* silkworm silks, both naturally spun and forced reeled. In addition, two synthetic materials have been tested: nylon and copper beryllium wire. These comparisons allow links to be made to the material structure, which varies across the materials studied, and to the biological function in the case of silks. In turn, this research helps answer questions on the evolution of silk and the possible applications of silk in engineering and medicine. A key aim of the research was to study single fibre properties to help understand the natural structures on which natural selection acts.

This chapter draws together the previous chapters in order to summarise the findings on variation in properties for silks, how variation can be controlled both in nature and in industry, and finishes with a discussion on how these results shed light on silk's natural structures (webs and cocoons) and the further research that is needed to progress this understanding.

8.1 Variation in properties of silk single fibres

This section summarises the Thesis and discusses the variation in mechanical (Chapters 3-5, 7) and sonic properties (Chapters 5-7), which is additionally represented in Table 11. Section 8.2 discusses the ways that this variation can be controlled in nature to give the biological function, and to create functionalized materials or devices in industry.

Table 11. Summary of findings in Thesis.

Chapter	Property	Materials	Variable	Key findings
3	mechanical	*Bombyx* cocoon silk	Testing humidity, metal coating, ESEM pump-down method	Silk mechanical properties can be used as a humidity sensor, response to humidity is rapid when there is no coating
4	mechanical	*Bombyx* cocoon silk, forced reeled *Bombyx* silk	Reeling conditions (reeling speed, silkworm paralysis and temperature), silk processing conditions (postdraw), storage conditions (dry, slack/tension)	Silkworm paralysis removes the effect of behaviour on mechanical properties, forced reeled silks are more disordered than naturally spun silks and processing conditions alter this order, *Bombyx* silk mechanical properties have a large range within limits
5	mechanical and sonic	*Bombyx* cocoon silk, forced reeled *Bombyx* silk, major and minor ampullate *Nephila* silk, nylon	Strain-rate, pre-stress, impact speed	Polymers' elastic response does not stiffen at high strain rates, pre-stress affects the material response at high-rate, major ampullate silks (slack stored) are the most variable
6	sonic	*Bombyx* cocoon silk, major and minor ampullate *Nephila* and *Araneus* silk, nylon, copper beryllium wire	Transverse vs longitudinal, pre-stress, spider size, number of silk fibres, fibre length	Longitudinal waves are more consistent than transverse waves, longitudinal waves are governed by the storage modulus that also governs mechanical response, major ampullate silk has one of the largest ranges of longitudinal wavespeeds available
7	mechanical and sonic	*Nephila* capture spiral silk, Major and minor ampullate *Nephila* and *Zygiella* silk, *Zygiella* signal threads	Imaging conditions, tension, number of silk fibres	Variability in capture spiral silk stems in part from diameter measurement, the mechanical and vibrational properties of bundles of silk gives information on their structure and interaction

8.1.1 Mechanical properties

Mechanical property variation has been shown to be influenced by a range of factors, including: humidity (e.g. ESEM environment, wet postdraw; Chapters 3 and 4), tension (e.g. slack pump-down in the ESEM, slack vs. tension storage; Chapters 3-5) and time or rate (e.g. humidity exposure time, postdraw rate, deformation rate; Chapters 3-5). These factors interact to influence silk structure during deformation, with direct effects on mechanical response. Their effect can be broken down into an energy component and a time component. Energy components include a catalyst, in this case water as a plasticizer, mechanical force and thermal energy. The time over which these energies are applied then affects their influence on silk structure.

Starting with water as a catalyst, plasticizers are small molecules that can form and negotiate hydrogen bonds within the polymer structure[130]. Therefore, as demonstrated in Chapter 3, silks in low humidities show a brittle failure response, as polymer chains cannot slide as easily relative to each other. In high humidities, silk mechanical properties show a softening behaviour as water reduces the extent of strength-inducing hydrogen bonds between polymer chains[298]. A recent study has shown that small molecules of different sizes have different plasticizing effects between comparable silk specimens (where water is the smallest molecule studied, then methanol, and ethanol as the largest)[224]. This has been attributed to variation in the free volume of the amorphous region of the silk, which allows or prevents molecules from accessing the silk structure. Therefore, lack of water can lock hydrogen bonds in place, presence of water can influence hydrogen bonding mobility, affecting silk structure, but also silk structure can influence the effect of water.

Humidity interacts with mechanical forces, like tension, to create new structures, with the potential to create order, create disorder or increase variability in structure. An example of creating order through tension and water is found in Chapter 4, where water is used as a

catalyst to promote postdraw, increasing strength and order within the silk structure. When this force was applied at a faster rate, more order was created. The ability to improve strength with water and tension is supported with the wet-reeling of spiders[183]. Disorder can be created when tension is removed, where room humidity (c. 40 % RH) is enough to promote hydrogen bonds to move. For example, slack stored silks showed more variable and less tough mechanical properties compared to silks stored under tension, creating the lowest amount of order seen in forced reeled silks (Chapter 4). Tension and humidity interactions also influence variability in structures, shown in the stress-strain contours of postdrawn silk (Chapter 4), and the high-rate properties of major ampullate silk following its slack storage (Chapter 5).

However, over time and change in humidity, these structures can be altered again. Silk specimens that have been under a vacuum will rehydrate to room conditions quickly, and likewise for saturated specimens, although this process is slower (Chapter 3). Dry stored silks showed large variability in properties between specimens, explained by the partial hydration of some silk specimens to the testing humidity (Chapter 4). Therefore, the tension and humidity history of the silk explains property variation through their influence on hydrogen bonding structure.

The interaction between water and mechanical force is of paramount importance in the spinning of silk into a dry fibre[2]. By investigating reeling speed, the force acting on the dope over time was altered, with direct effects on properties and structure (Chapter 4). There was an optimum in toughness, with some evidence of increased order at the natural spinning speed of 15 mm s^{-1} for silkworm silks, suggesting a predisposition for the spinning apparatus to create optimal structures at this reeling rate. The effect of reeling speed was influenced by worm behaviour, which alters the mechanical force or energy on the silk fibre, and worm temperature, where a dope with less energy (cold body temperature) was unable to form ordered structures at a higher spinning rate.

The effect of mechanical force over time on mechanical properties was investigated in Chapter 5. The elastic components of the polymer structures did not stiffen significantly over a change in strain-rate from 0.005 to 5000 s^{-1}, supporting that the ordered structures are not influenced by the time over which mechanical energy is applied. In theory, the disordered regions of a polymer should be more rate-dependent, as they show plastic deformation that will be hindered when there is less time for flow/energy dissipation[130], and more research is needed to quantify this. However, an interesting outcome from this research is the uncoiling of structures following yield. These structures have direct effects on the mechanical performance of the fibre, which is a sum of the elastic, plastic and uncoiling deformation. The formation of these structures will also be due to the humidity and tension history of the silks, and can be visualised in the stress-strain curve by the post-yield dip or plateau seen for some forced reeled silks in Chapter 4.

Thermal energy is the last form of energy investigated, which, if high enough, can break and form hydrogen bonds without the need for water - as shown by the DMTA scans, where new bonds and structures are formed over the course of the scan. Annealing with applied static tension was the processing condition inducing the biggest change in order in forced reeled silk (Chapter 4), and has the added benefit of reducing variability in structures as well as creating order.

8.1.2 Sonic properties

The variability in sonic properties of silks depends on whether the waves are longitudinal or transverse. The longitudinal waves are governed by the storage modulus (Chapter 6), so are influenced by tension and processing conditions that increase storage modulus[142]. For major ampullate silk, the MaSp2 component means that the storage modulus and so longitudinal waves are additionally sensitive to softening due to supercontraction[91]. Supercontraction adds an extra complication to the sensitivity of humidity and tension history, which can explain why major ampullate silks tend to be the most variable in high-rate properties when slack (Chapter

5). As storage modulus is dictated by the ordered and rate-independent regions of the silk structure, the variable hydrogen-bonded structure of the amorphous regions, as described in Section 8.1.1., has no direct influence. This means rapid fluctuations in humidity and tension, or plastic flow will not have a dramatic effect on the longitudinal sonic properties. Additionally, the number or diameter of polymer fibres has no effect (Chapters 6 and 7).

This is in contrast to transverse waves, which are governed directly by tension (Chapter 6), meaning rapid changes in tension and humidity will have direct effects. Transverse waves are also a lot more sensitive than longitudinal waves to the damping effects of air, as their motion is perpendicular to the fibre axis. More research is required to quantify the damping for both types of waves (see Section 8.4.1), but for transverse waves this means they are additionally sensitive to number and diameter of silk fibres. Silk diameter and number additionally influence mass per unit length and tension when used in a bundle, spreading resonance across a broad range (Chapter 7).

8.2 Controlling variation in properties

The ways that this variation can be controlled and harnessed will now be discussed, linking to the natural function of the silks and their evolution, and then how the variation of silk may be harnessed for industrial applications. In nature, variation in properties is an adaptive trait, whereas in industry, consistency in properties most often has to be assured over variation.

8.2.1 Silk variation in nature

As discussed in Section 8.1, variation in properties stems from different regions of silk, affecting different aspects of silk properties. Ordered regions directly affect the elastic, storage modulus-dependent mechanical and sonic properties, whereas disorder affects mechanical performance, particularly energy absorption. All structures are controlled by the spinning process, which has

been shaped by natural selection to suit the niche of a particular species, but which can also be altered day-to-day to allow silk properties to match environmental conditions.

The potential silk structures that could be present in a silk fibre, ordered or disordered, is dictated by the primary sequence, as the arrangement and types of amino acid residues affect the secondary and tertiary packing of the protein and their potential interactions with water[32, 55, 91]. For example, silkworm silks will never be as strong as spider silks due to their primary sequence (Chapter 4). Both the duct morphology and biochemistry have co-evolved with the primary sequence to control the interaction between mechanical energy and water, dictating the structures present. Furthermore, the spinning apparatus directly influences the final diameter and so the potential strength of the silk fibre[83].

The ratio of order to disorder can then be controlled within the limits of the primary sequence through animal behaviour: mechanical energy is controlled by altering the speed of the head movement in the case of caterpillars, or the speed of a leg movement in the case of spiders[80, 127, 225]. The extent to which the biochemistry is varied or controlled by the animal day-to-day is an interesting open question for further study – the fundamental differences in the structures of forced reeled and naturally spun silkworm silks suggest some unknown control of fibre spinning (Chapter 4 and[224]).

Overall, silks are variable to allow tailoring of properties for diverse environmental conditions and functional uses, controlled by the animal's behaviour.

8.2.1.1 Silks compared to other materials

The observations in this Thesis regarding the effects of spinning and processing on structure and properties are echoed by all polymeric materials. Synthetic polymer structures are controlled through monomer type and distribution, processing 'energy', whether temperature or mechanical, and fibre processing (stretch, annealing and plasticizer effect)[299]. As polymers,

therefore, silks do not appear particularly unusual in their response to processing conditions, as it is a direct consequence of their polymer structure's ability to manage energy input over time.

However, major ampullate silk is unusual in terms of its supercontraction ability, dictated by MaSp2[91], which increases its sensitivity to tension and humidity history. Supercontraction is special in that it affects many regions of the fibre structure (with the exception of 'permanent order')[135], affecting most aspects of mechanical and vibrational properties, a mechanism which is lacking in other silks and polymers. Although supercontraction makes major ampullate silk more variable, it provides a mechanism for almost complete control of variability day-to-day; silks are contracted following dew every morning, and can then be stretched to controlled extents to set the structure and properties of the fibre[90-91]. Therefore major ampullate silk is one of the most variable, but controllable, materials known.

However, the assertion that the spider can control all aspects of the major ampullate silk is unlikely. The use of major ampullate silk within the web structure, differences between species and its co-extrusion with the less variable minor ampullate silk may provide more clues as to how variability is controlled and what selection pressures govern its maintenance (see Section 8.4.3).

8.2.2 Harnessing silk variation for applications

As silks are biodegradable, natural, high performance materials which are made at room temperatures and pressures[15, 300-302], there is a focus on harnessing the properties of silks for applications in engineering and medicine. Whereas in nature, variability is an important factor to increase an individual's fitness, in industry, variability should be completely controlled, or at least predictable, to provide consistent properties.

This Thesis has presented a range of research looking at *Bombyx* silkworm silks. Silkworms can be farmed[139] and the silk can be harvested in large amounts from the animal's own spinning

apparatus, which has obvious advantages. Silkworm paralysis is a real step forward in producing large amounts of consistent silks (Chapter 4). Through removing the effect of behaviour on properties, large amounts of silk can be harvested. The possible extension of this research is introducing the paralysis peptide into a strain of transgenic worms, where paralysis can be switched on for controlled reeling[199]. The challenge is processing these silks to have consistent properties. Annealing and stretching are the best processing candidates for consistency, effectively removing the mal-formed or disordered regions of the silk structure. An alternative may be to control the humidity sensitivity of the silk fibres through coating, which can have added functionality such as conduction of electricity (Chapter 3).

More unusually, and in trend with 'smart' materials, the variability of silk may be harnessed to make functional materials or devices. Silks have been shown to be excellent humidity sensors, which may be useful as humidity-sensitive switches (Chapter 3). Silks also change shape in contact with water or humidity, providing mechanical energy and potential shape-memory ability (Chapter 3 and 4). Also, as tension affects the high-rate and sonic properties of silks, properties could be tuned or switched depending on their pre-tension – useful for microphones or damage-limitation impact protection panels (Chapter 5-7)[79, 189, 303].

8.3 Towards understanding natural structures

The research with silkworm silks gives insights into the evolution of the cocoon. Cocoons are composite structures, and the interaction of sericin with fibroin is vital for their functionality. Through studying single fibres, I have shown that sericin is important for the hydration and the failure mechanism of the fibroin core (Chapter 3), which takes a majority of the mechanical load[129]. Furthermore, the natural spinning process produces fibres with the best mechanical performance and structural order compared to forced reeled silks, meaning the cocoon utilises fibres with optimal properties (Chapter 4). In combination with other research, this helps to inform on the function of the cocoon as a protective and environmental barrier.

Likewise, studying the properties of single spider silk fibres has given insights into the function of the orb web. The properties of silks at high-rate are sensitive to pre-tensioning, where elastic deformation is complicated post-yield by plastic flow and uncoiling of structures (Chapter 5). This means that damage due to energy absorption can be localised in the web by careful pre-tensioning of its fibres. Pre-tensioning additionally alters the sonic properties of the web. This Thesis proposes that longitudinal waves are used as information-carrying consistent vibration signals, whereas transverse waves are likely to play a role as impact or web-condition indicators, with little specific information content in their signals (Chapter 6). In signal threads in the webs of *Zygiella*, the amount of fibres appears to have little effect on their function (Chapter 7).

8.4 Future experiments

The research with spider silks has opened up many further questions important for understanding orb web function, which form the basis for my proposed future experiments.

8.4.1 Energy absorption

The relative importance of internal (plastic flow) and external (air drag) energy dissipation has direct effects on the energy absorption of the web, damage limitation and silk vibration. As already outlined in Chapter 5, the curvature of silk fibres over impact may be analysed to calculate plastic flow at high-rate and may also provide information on the air drag acting on the fibres, which can be compared to theory[240].

As outlined in Chapter 6, calculating the damping factor of longitudinal and transverse waves can provide information on the relative roles of internal and external energy dissipation on the propagation of vibrations. Using long fibres of spider silk (c. 60 cm) and contact vibration, the amplitude of sine waves can be tracked along the length of a fibre that is vibrating at a high harmonic (i.e. 7^{th} mode will have seven amplitude peaks along its length). The ratio at which amplitude decreases along this length will give the damping factor of the wave. It is expected

that longitudinal waves will only be subject to internal dissipation (as air drag does not act on displacements in line with the fibre axis), but transverse waves will be subject to both internal and external energy dissipation mechanisms.

8.4.2 Multifunctional orb webs

The mechanical and sonic properties of silk fibre interactions will be useful for building a model of web behaviour, building on this Thesis' research on single fibres. To gather data on the interactions of silk fibres, laser vibrometry will be used to study the vibrational properties of webs from *Nephila* and *Araneus*, which differ in their web geometry, specifically their use of minor ampullate silk (Figure 8.1). All orb-weavers use minor ampullate silk to form an auxiliary spiral to maintain web shape during building[304], but the Nephilidae leave the auxiliary spiral in their webs, whereas most other orb weaving spiders remove it upon completion.

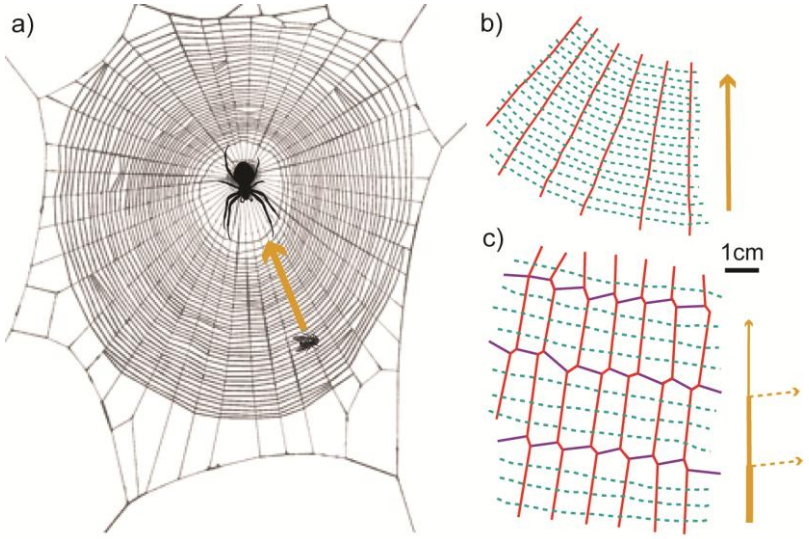

Figure 8.1[304-305]**.** Orb web architecture: **a)** webs catch prey and signal vibrations to the spider. Typical web sections of: **b)** garden orb weaver *Araneus* and **c)** golden orb weaver *Nephila*. Silks: major ampullate radial threads (red), flagelliform/aggregate capture spiral (green) and minor ampullate auxiliary spiral (purple). Arrow shows the vibration propagation direction to the spider in web centre.

This research would aim to establish how silk interactions in the differing web geometries influence vibration propagation, reflection and dissipation. Tensile testing of these silk junctions (radial to auxiliary spiral and radial to capture spiral in different directions) would enable me to

probe the mechanical implications of web silk interactions in different web geometries, particularly whether silk junctions absorb energy as they are separated.

The data collected would be integrated into finite element analysis simulations. This would enable me to model orb web vibration using natural geometries, compare them to vibrometry data and generate predictions on web function of other spider web geometries. From this, spider web engineering biodiversity can be used to propose novel hypotheses on the possible evolutionary trade-offs between efficient vibration signalling and prey-catching ability:

Hypothesis 1: Spiders with small prey (*Araneus*) remove the auxiliary spiral to enable detection of prey-generated vibrations.

Hypothesis 2: Spiders with large prey (*Nephila*) keep the auxiliary spiral to increase energy absorption.

Comparison of four species across orb weaver spider evolution would enable hypotheses on the direction of selection on auxiliary spiral use in the web to be investigated.

8.4.3 Major versus minor ampullate silks

Comparing the use and properties of major and minor ampullate silks between species will provide insights into the evolution of supercontraction, properties and web function. Importantly, since minor ampullate silks do not supercontract, it makes them more attractive candidates for biomedical applications, with implications for further research and development of novel silk-inspired bio-polymers. The research questions would break down into specific hypotheses regarding the multiple roles of webs:

Hypothesis 3: Control of supercontraction allows a broader range of wavespeeds in major compared to minor ampullate silk, explained by silk stiffness.

Hypothesis 4: Wet, dried, then stretched ampullate silks show repeatability of mechanical and vibrational properties.

These experiments address the scope and 'resetting' of properties caused by supercontraction[7,10]. I would use laser vibrometry to measure wave properties; tensile testing to measure fibre performance; and dynamic mechanical analysis to measure storage modulus of ampullate silks under different humidity conditions. Silk samples will be from *Nephila edulis*, *Araneus diadematus*, *Cyrtophora citricola* and *Euprosthenops* sp., representing three spider families and the full range of supercontraction ability[91].

The major ampullate silks' supercontraction ability can be correlated with web geometry and ecological factors reported in the literature such as species distribution, habitat environmental conditions and prey type. These correlations will highlight possible drivers of supercontraction diversity, which can be investigated further.

8.4.4 Beyond silks

The web can be viewed as a vibration landscape, where spider silk fibres interact to influence vibration transmission to the spider. Moving beyond silk, further research could investigate how other materials affect vibration propagation for other animal systems. Vibrations that propagate through materials are used as sensory information for a range of animals and even some plants[306-307]. Current research in this expanding field of substrate borne communication concentrates on the generating and detecting of vibrations, with little focus on the role of the material on vibrations, vital for communication, navigation and interacting with the environment[306]. Looking ahead to future projects, research could focus on the effect of materials on vibration communication for: animals that engineer their own materials (e.g. bees and wasps), animals that use plant material (a range of insects), or animals that use the ground (e.g. moles and elephants).

8.5 Concluding remarks

Silks are inherently variable natural materials, which are expertly spun and tuned by the animals that make them. This Thesis has contributed towards understanding the variability in properties, both mechanical and sonic, where spider silk balances both. The properties are explained in terms of the structures that govern them, both the elastic components that govern sonic properties, and the disordered components that govern their plastic behaviour. Although silks are comparable to synthetic polymers in terms of the viscoelastic origin of their properties, major ampullate spider silk has been shown to be an outlier in terms of both the high variability and control of variability that is available to the spider. These unique properties open up a range of questions regarding the evolution of spider silks and potential applications for silk-inspired smart materials. The next step for this research is to focus on the interactions of silk fibres within their natural structures, breaking down the multifunctional complexity of the spider's expertly engineered extended phenotype.

Appendix A Supplementary Information

A.1 Chapter 2

Table 12. Density and cross-sectional area data for different materials. Spider silks are taken from different *Nephila* spiders (labelled with number).

Material	**Density (kg m^{-3})**	**Cross-sectional area ± SE Mean (mm^2)**
Nylon	1140*	4.91×10^{-4}*
Copper beryllium wire	8250*	4.91×10^{-4}*
Bombyx naturally spun silk	1325[1]	$3.79 \times 10^{-4} \pm 5.4 \times 10^{-6}$
Spider major ampullate silk sp1	1325[1]	$1.89 \times 10^{-5} \pm 3.4 \times 10^{-7}$
Spider major ampullate silk sp2	1325	$2.72 \times 10^{-5} \pm 2.5 \times 10^{-7}$
Spider major ampullate silk sp3	1325	$2.88 \times 10^{-5} \pm 2.8 \times 10^{-7}$
Spider minor ampullate silk sp1	1325[1]	$4.94 \times 10^{-6} \pm 1.2 \times 10^{-6}$
Spider minor ampullate silk sp1	1325	$3.43 \times 10^{-6} \pm 5.9 \times 10^{-8}$
Spider minor ampullate silk sp1	1325	$2.45 \times 10^{-6} \pm 8.6 \times 10^{-8}$

[1] Density for silk taken from [308]

*densities and diameters taken from manufacturer's data sheet for the material

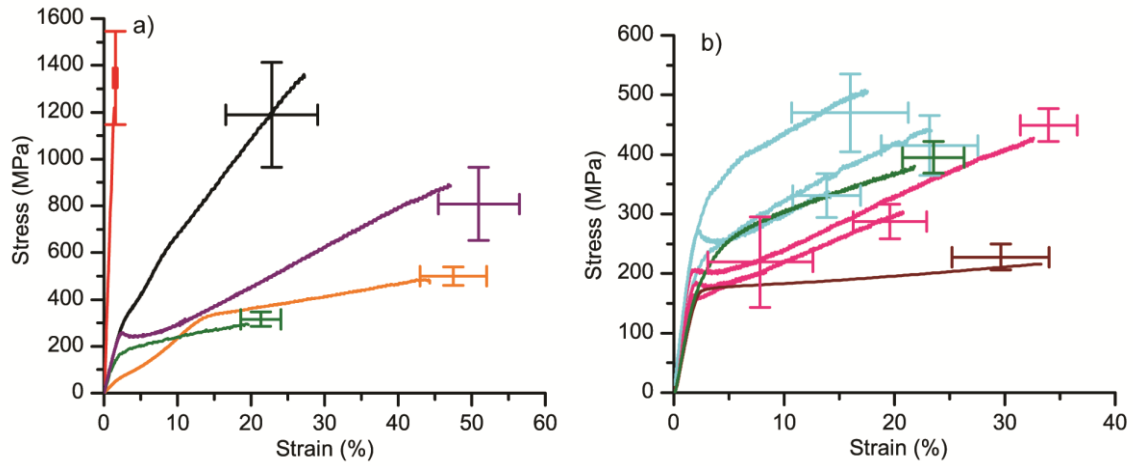

Figure A.1. Example stress-strain curves for **a)** copper beryllium wire (red), *Nephila* major ampullate silk (black), *Nephila* minor ampullate silk (purple), nylon (orange) and naturally spun *B. mori* silkworm silk (green), and **b)** postdrawn *B. mori* forced reeled silkworm silks (blue), non postdrawn silkworm silks (pink) and reconstituted silk fibroin (brown). Error bars give the standard deviation of stress and stress breaking co-ordinate for different specimens of the same material.

A.2 Chapter 3

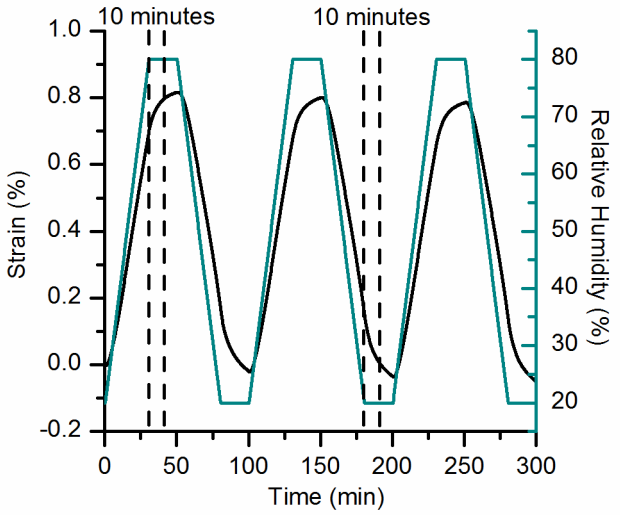

Figure A.2. Data provided by Nick Hawkins. Strips of cocoon 5 by 30 mm size are tested in a DMTA. The change in length is measured given a constant load of 0.01 N over a range of humidities. Temperature is held at 20 °C and humidity is ramped from 20 to 80 % at a rate of 1 % min^{-1} and held at the set humidity for 20 minutes. Dashed lines give the start and end of a ten minute period after the target humidity is reached.

A.3 Chapter 4

A.3.1 Supplementary figures and table

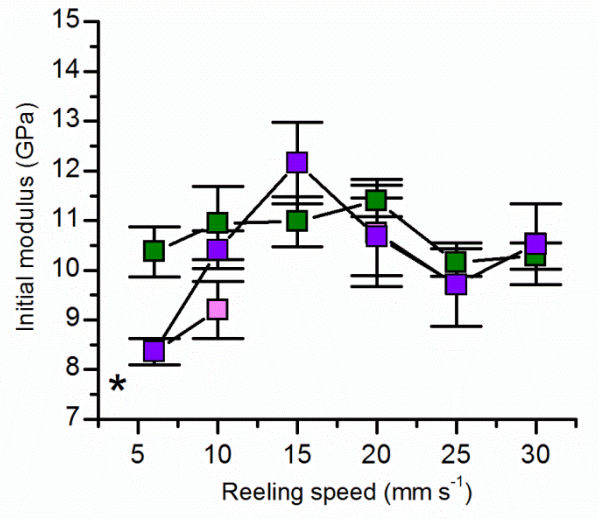

Figure A.3. The effect of reeling speed on the initial modulus of paralysed (green) and unparalysed silkworm silks (purple: includes data where the silkworm broke the thread; pink: excludes speeds before or after a break). Star gives a comparison to mean values for naturally spun silk. Error bars give the standard error of the mean. Number of specimens measured is given in Appendix Table 13 (no pink square at 15 mm s^{-1}, as all unparalysed silkworms broke the thread before or after this speed).

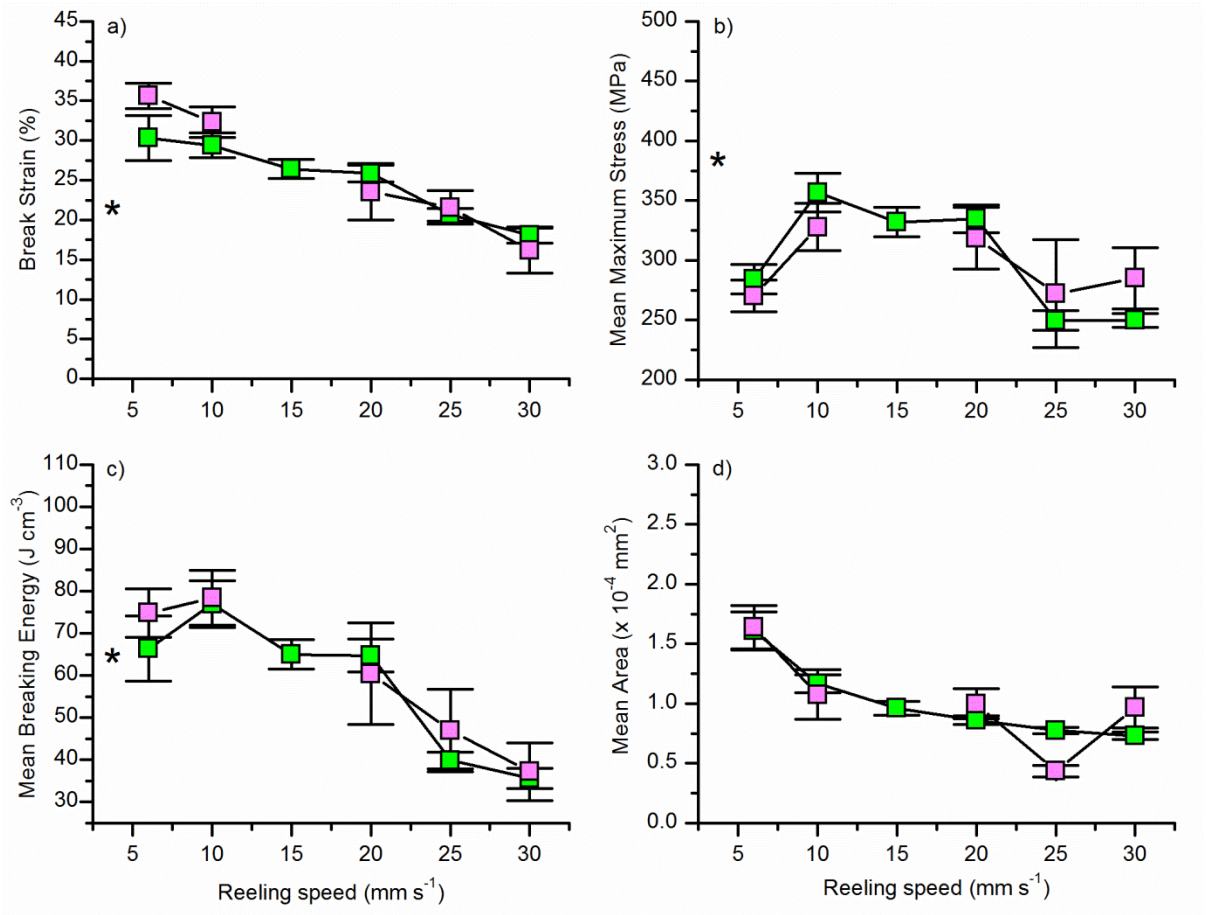

Figure A.4. The effect of reeling speed on the mechanical properties of paralysed (green) and unparalysed silkworm silks (pink: excludes speeds before or after a break): **a)** the break strain, **b)** maximum stress, **c)** breaking energy and **d)** mean cross-sectional area. Stars give a comparison to mean values for naturally spun silk (not shown in d). Error bars give the standard error of the mean. Number of specimens measured is given in Appendix Table 13 (no pink square at 15 mm s^{-1}, as all unparalysed silkworms broke the thread before or after this speed).

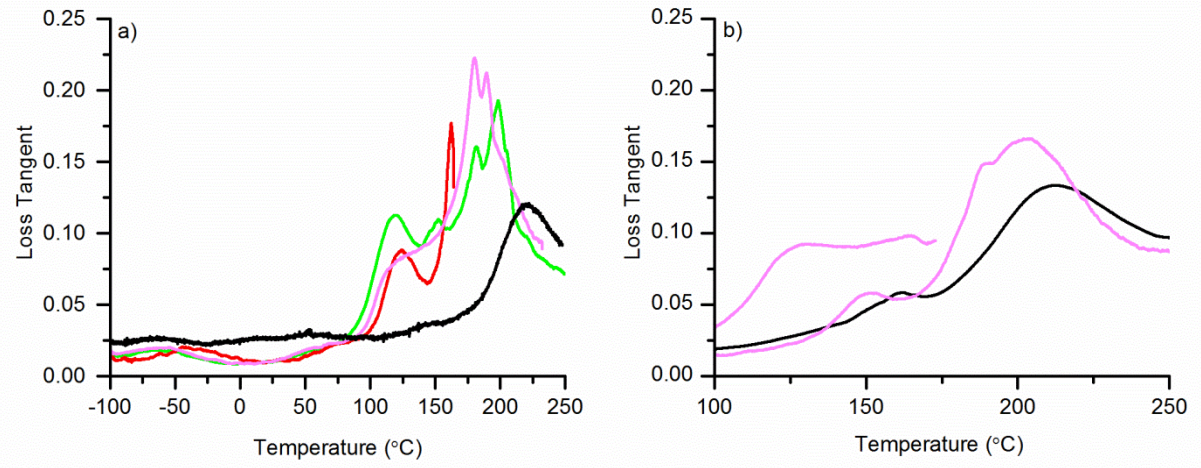

Figure A.5. Loss tangent profiles of various forced reeled *B. mori* silks from 3 different reeling conditions run by J. Guan, **a)** ramp straight up for slack-stored non-postdrawn silk (red; broke midway through sampling), dry-storage non-postdrawn silk (pink) and x1.16 slow postdrawn silk (light green); **b)** the loss tangent profile of dry-storage non-postdrawn silk (pink) before and after annealing to 180 °C, in comparison with standard naturally spun silk (black). One repeat of 2 or 3 is shown per treatment.

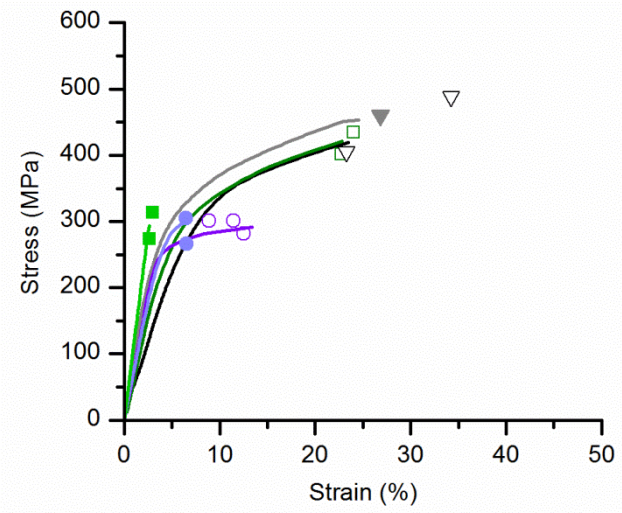

Figure A.6. Stress-strain curves before (darker, open scatter points) and after (lighter, filled scatter points) 120 °C annealing for naturally spun (black/grey), postdrawn (x1.16 fast; greens) and non-postdrawn (purples)). Scatter points give the break points of repeats of the same silk types. Stress, rather than strain-control is used in these experiments, performed in the DMTA. This explains differences to Figure 4.11.

Table 13. Number of specimens measured at different reeling speeds for paralysed and unparalysed worms. The data from unparalysed worms are used in Figure 4.7, and the data for unparalysed worms without the break specimens included are used in Figure A.4. Both are used in Figure A.3. Star denotes that speeds before or after a break was present in this data set, which was excluded in the next column.

Reeling speed (mm s^{-1})	**Paralysed (n=4 worms)**	**Unparalysed (n=6 worms)**	**Unparalysed without specimens before and after a break (n=6 worms)**
6	19	26	26
10	18	28*	11
15	22	12*	0
20	23	14*	9
25	25	15	15
30	25	18	18

A.3.2 Supplementary discussion

Figure A.5a gives the temperature scans of non-annealed, postdrawn and non-postdrawn forced reeled silk, with a reference naturally spun silk. Recent research by Guan and collaborators has shown that each loss peak is caused by the glass transition of a specific silk structure. Each structure contains different numbers and combinations of hydrogen bonds between the different chemical groups[179]. The main non-natural loss peak is at 175 °C (Figure 4.8b and Figure A.5). This is assigned to the characteristic glass transition temperature of the highly disordered structure of reconstituted silk fibroin[179, 209]. This structure has two hydrogen bonds per peptide segment in a random disordered configuration[179]. The strong loss peak seen at 120 °C has not previously been observed during DMTA analysis of silk fibres. This peak is not due to water, as the TGA profile did not show weight loss at this temperature (Figure 4.10). Calculations using the Guan model[179] suggest that the number of hydrogen bonds for this peak is reduced to one per segment within the disordered structure.

Annealing removed small loss peaks associated with water below 100 °C and most of the peaks below 180 °C, leaving a higher temperature peak comparable to non-annealed naturally spun silkworm silk (Figure A.5b). Annealing creates stronger bonding as disordered structures are irreversibly stretched under slight mechanical load[179]. Over the temperature range for the annealing scan, this eventually would lead to the formation of the most strongly bonded disordered structure possible in a particular specimen.

For non-annealed silk, there are peaks between -60 and +60 °C that suggest that there is more water present and so they will have higher disorder (Figure 4.13). These peaks were highest for non-postdrawn, lower for postdrawn silks and lowest for naturally spun silks (no RSF was measured in annealing mode; Figure 4.13a). Annealing to 120 °C removed the loss peaks under 100 °C by removing the water from the silk specimens (Figure 4.13a). Similar annealing effects have been observed and explained likewise in soy protein[230].

Following 120 °C annealing, the most disordered *Bombyx*-derived protein was RSF (Figure 4.13b). The large RSF loss peak at 175 °C has been assigned to highly disordered macromolecular structure, which shows the largest area under the loss peak due to the high contribution of disordered structure[179]. These structures are caused by the formation of solid silk from solutions made by the chaotropic medium of aqueous concentrated lithium bromide solution[209]. The non-postdrawn silk loss peak was the least ordered of the forced reeled silks and was most similar to the RSF, suggesting that the non-crystalline fraction is likely to be highly disordered with a structure analogous to RSF.

A.4 Chapter 6

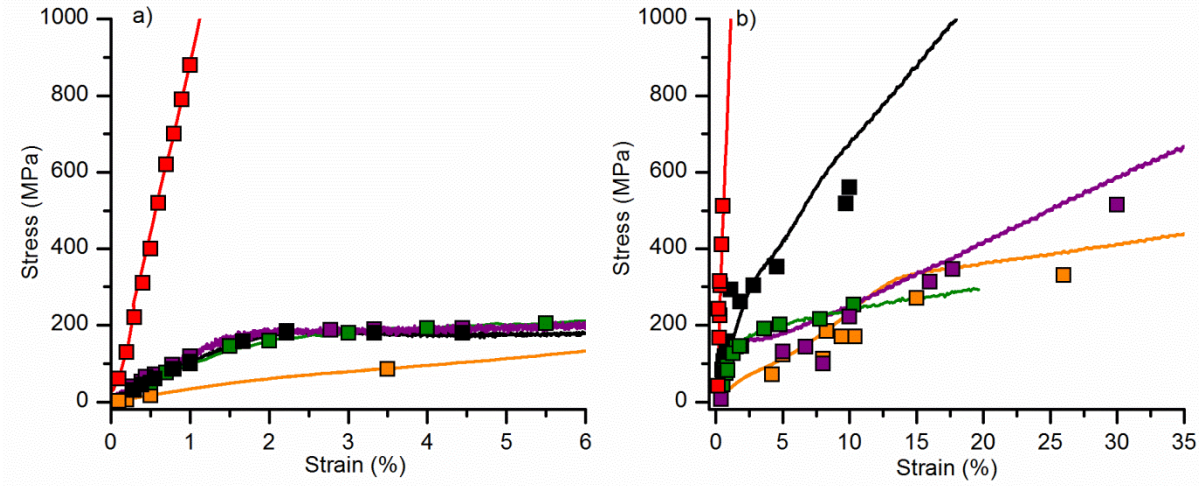

Figure A.7. Vibrometry data stress-strain scatter points with a reference quasi-static stress-strain curve for **a)** longitudinal specimens (over 140 mm) and **b)** transverse 12.5 mm specimens. Materials: metal wire (red), silkworm cocoon silk (dark green), nylon (orange), *Nephila* major ampullate spider silk (black) and *Nephila* minor ampullate spider silk (purple).

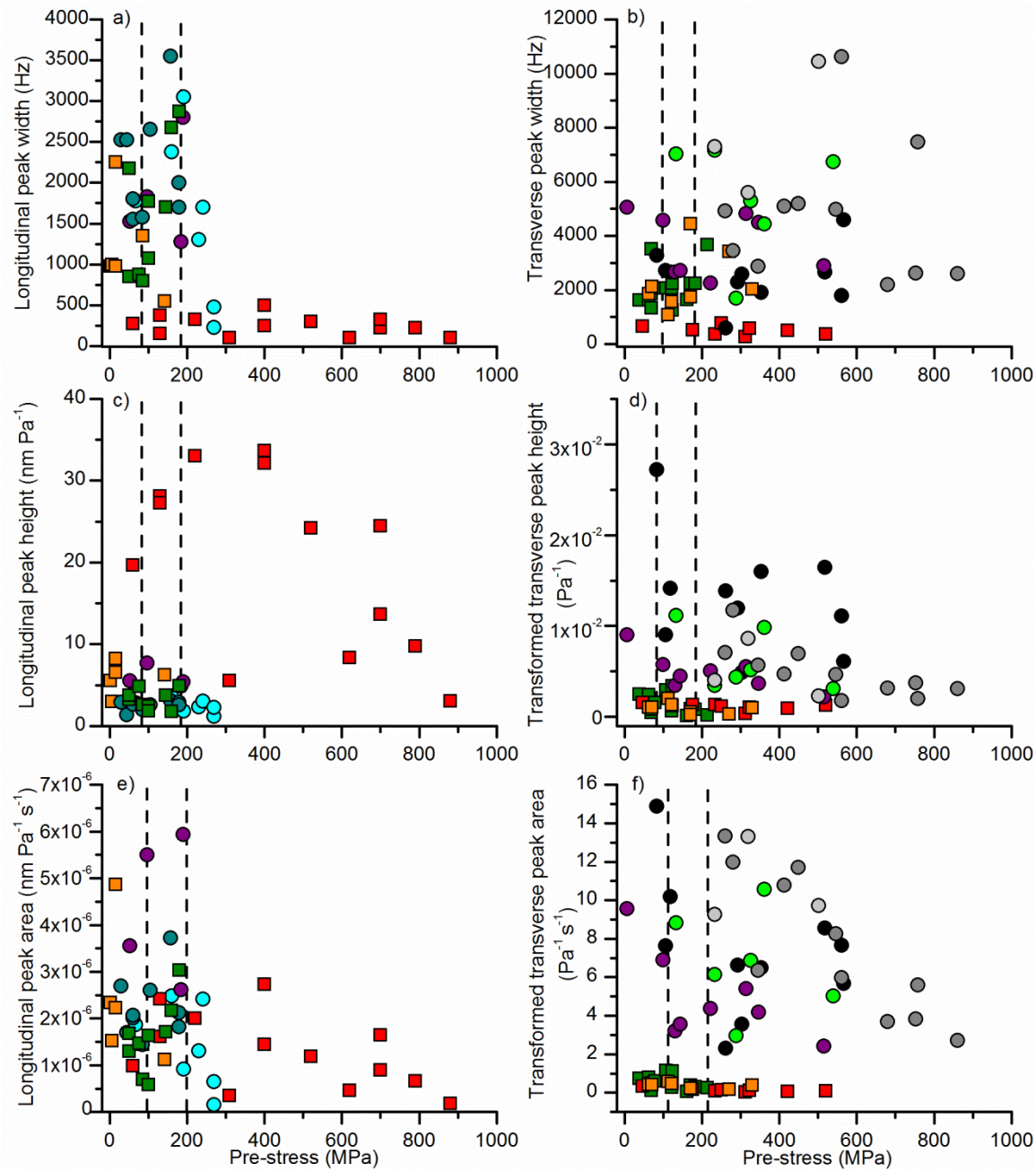

Figure A.8: Resonant peak shapes versus pre-stress. Width data for **a)** longitudinal waves and **b)** transverse waves, height data for **c)** longitudinal waves, and **d)** transverse waves, and area data for **e)** longitudinal waves and **f)** transverse waves. Height and area outputs are transformed for transverse waves. Materials: metal wire (red), nylon (orange) and silkworm cocoon silk (dark green) are given by squares; spider silks are given by circles: *Nephila* major ampullate (MA) spider silk (big size, black; medium size, dark cyan; small size, dark grey), *Nephila* minor ampullate (MiA) spider silk (purple), mixture of *Nephila* silks (medium size 2 MA, 2 MiA, cyan; small size 1 MA, 2 MiA, light grey), and *Araneus* spider bundle (2 MA, 2 MiA, green). Dashed lines give the approximate end of the elastic region ~100 MPa and the approximate end of yield ~200 MPa for the polymers.

A.5 Chapter 7

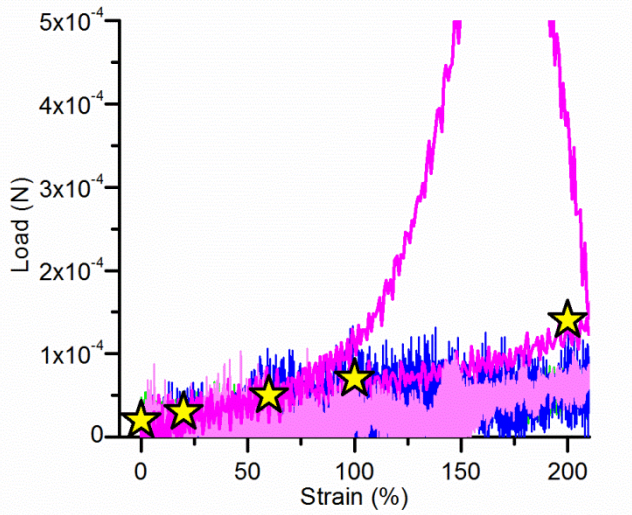

Figure A.9. Load-extension curves of *Nephila* capture spiral silk from webs from different individuals (pink, blue and green). Pink silks are measured at different rates, dark pink is 5 mm s^{-1} and light pink is 0.25 mm s^{-1}. Stars give the load-strain relationship used to work out the vibrational properties of capture spiral silks.

Appendix B Chapter 5 Appendix

B.1 List of terms

C_w observed transverse wavespeed (m s^{-1})

C_t true transverse wavespeed (m s^{-1})

V velocity of projectile (m s^{-1})

W particle velocity (m s^{-1})

T_0 pre-tension (N)

μ mass per unit length (kg m^{-1})

C_l longitudinal wavespeed (m s^{-1})

ρ density (kg m^{-3})

t one time point during impact (s)

E modulus (Pa, often converted to MPa or GPa)

ε_0 pre-strain, ε_1 high-rate strain (unitless, often converted to percentage)

σ_0 pre-stress, σ_1 high-rate stress (Pa, often converted to MPa or GPa)

B.2 Methods

B.2.1 Experimental set-up

Experiments were performed in the Department of Engineering Science using an apparatus designed by D. R. Drodge and C. R. Siviour. An overview of the method was given in Chapter 5 and more specific details are given here. The gas gun had a barrel of 12.7 mm diameter and was

instrumented with two light gates to measure projectile speed and to trigger the flashes and cameras. The light gates were 50 mm apart, positioned approximately 22 cm from the fibre.

Two high-speed cameras were used, a framing camera that takes video over an area, and a streak camera, which takes video over a single vertical line (these cameras are commonly used for photo finishes in races). Images of the propagating wave were taken as close to the time and point of impact as possible, because viscoelastic processes and air resistance will affect the fibre to greater extents as the deformation progresses. Framing images were taken using a Phantom 7.1 high-speed video, with an inter-frame time of 20.75 μs, and exposure time of 2 μs. Streak images were generated using a Lightning Digistreak camera, recording at 1.8 μs per line, with 1024 pixels on each line, which therefore offers finer velocity resolution than framing images. All experiments were illuminated using a pair of Bowens 500C flash lamps. As the deflection was symmetric about the point of impact, the thread was only imaged above the point of impact. The streak data were stacked together into a streak image, in which the horizontal axis gives time and the vertical axis gives position (Figure B.1). Therefore, the angle of the streak line gives the speed of silk deformation, or the observed transverse wavespeed, C_w. Pictures were analysed by D. R. Drodge to measure the projectile velocity (V) and the observed transverse wavespeed (C_w).

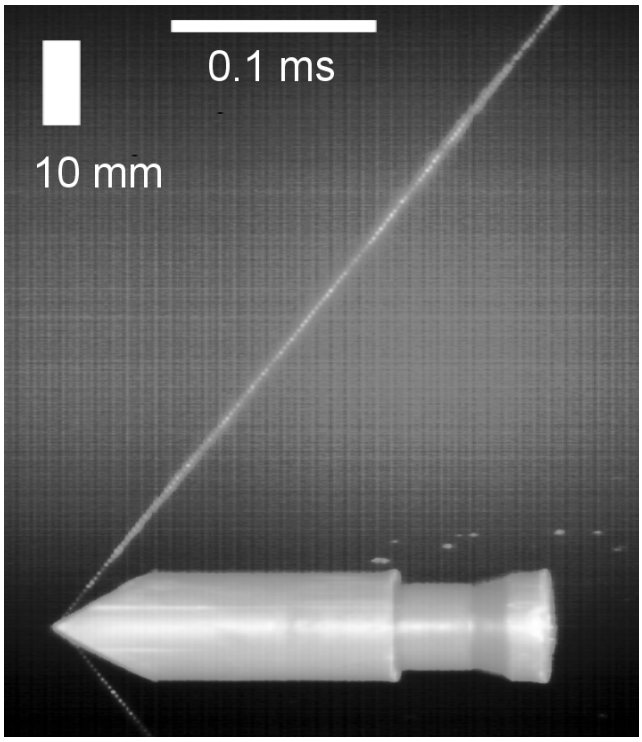

Figure B.1. Example streak image. Streak camera line positioned 3 mm from the stationary fibre. Vertical (position) and horizontal (time) scale bars are shown. Time increases to the right.

B.2.2 Numerical analysis

The following numerical analysis was developed by D. R. Drodge and C. R. Siviour and will be referred to as Analysis 1.

Figure B.2 describes the physical situation during impact of a heavy projectile on a light thread, which causes a velocity *V* to be imposed at point X. A longitudinal tensile wave travels outward from X, the point of impact, at velocity C_l. It extends the thread as it passes, causing material to flow inward, towards the impact point, with particle velocity *W*. The transverse wave follows at velocity C_w, giving the material a velocity *V* in the direction of the impact, causing it to displace in that direction and take up the slack released by the extension. The passage of the transverse wave does not change the strain in the extended part of the thread (whilst initially assumed to be the case, this has since been shown mathematically[238]).

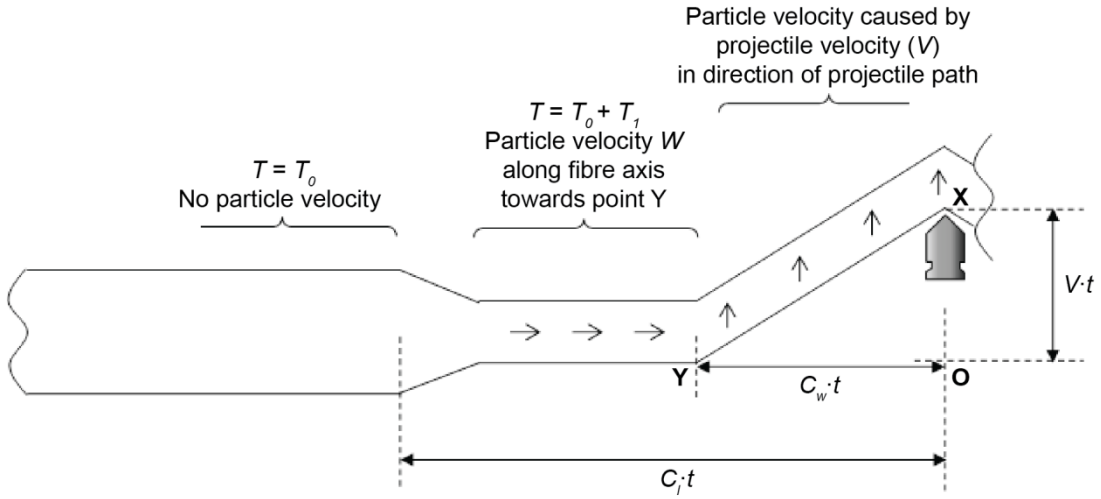

Figure B.2. Adapted from Drodge *et al.* (2012)[132] and Roylance *et al.* (1973)[309]. A tensile wave, travelling at velocity C_l, causes material to flow at velocity W towards the point of impact (towards Y), increasing the strain and tension of the thread. A transverse wave, travelling at a slower velocity of C_W, causes material to move at velocity V in the direction of impact.

The observed (and measured) transverse wave, C_w, is not the same as the true transverse wave, C_t, as it is slowed down by the particle velocity, W, in the opposite direction. To convert to the true transverse wave C_t, the extension of the fibre and the particle velocity must be accounted for (Equation 5):

$$C_t = \frac{(C_w + W)}{(1+\varepsilon)} \qquad \text{Equation (5)}$$

The true transverse wave velocity, C_t, is given by Equation 6 (also given in Chapter 6)[310]:

$$C_t^{\,2} = \frac{T}{\mu(1+\varepsilon)} \qquad \text{Equation (6)}$$

Here, T is the total tension in the thread and μ is the mass per unit length. This will be due to both the static load prior to impact, T_0, and the additional tension T_1 induced by the tensile wave (Equation 7):

$$T = T_0 + T_1 \qquad \text{Equation (7)}$$

In Figure B.2, a triangle XOY is formed by the projectile tip, the position of the transverse wavefront, and the point of impact on the undisturbed fibre. The vertical and horizontal sides

have length $V \cdot t$ and $C_W \cdot t$ respectively. Compatibility of displacements requires that the diagonal, i.e. the length of thread over which the transverse wave has passed, be $(1+\varepsilon)C_W \cdot t$.

The relationship between the unknown W, and the measurable V and C_W is given by Equation 8:

$$V^2 = (C_w + W)^2 - {C_w}^2 \qquad \text{Equation (8)}$$

The analysis proceeds by relating the particle velocity W, and the wave tension T_1, to the longitudinal wavespeed. For a general constitutive model $\sigma(\varepsilon)$, the particle velocity resulting from the passage of a longitudinal wave of strain amplitude ε is given by Equation 9[311]:

$$W = \int_0^{\varepsilon} \sqrt{\frac{1}{\rho}\frac{d\sigma}{d\varepsilon}}\, d\varepsilon = \int_0^{\varepsilon} C(\varepsilon) d\varepsilon \qquad \text{Equation (9)}$$

As $C(\varepsilon)$ is determined by the local gradient of the stress-strain curve, the full treatment requires *a priori* knowledge of a high-rate constitutive model and the application of Equation 5 above. By assuming that material response is elastic, however, C can be estimated using the approach used by Prevorsek *et al.* for various materials struck under a range of static tensions[312]. This technique is of great interest when studying rubber-like disordered fibres, as a static stress will induce polymer chain alignment. Such a response is relevant on both a physical level, as it relates impact response to molecular configuration; and on a practical level, as the performance of a fibre-based armour may be altered by accidental or deliberate pre-tensioning prior to impact.

Assuming an elastic response allows for the calculation of the increase in strain and tension due to the passage of the longitudinal wave using the following equations:

$$W = C\varepsilon \qquad \text{Equation (10)}$$

$$T_1 = \mu C W \qquad \text{Equation (11)}$$

In the manner of Prevorsek *et al.*, these relations can be applied to Smith's result (Equation 8) to arrive at a quadratic in *C*:

$$C^2 + \left(\frac{{C_w}^2}{W} + 2C_w - \frac{T_0}{\mu W}\right) C + \frac{T_0}{\mu} = 0 \qquad \text{Equation (12)}$$

This is solved for *C*, and the Young's modulus *E* is thus obtained (equivalent equation also given in Chapter 6):

$$E = \rho C^2 \qquad \text{Equation (13)}$$

This approach assumes a simple elastic step from the pre-stress to impact-stress state, whereas a thorough analysis would take account of the dependence of particle velocity on the stress-strain curve via Equation 9. However, this would require prior knowledge of the stress path not only under dynamic load but also given an initial pre-stress. This assumption provides a much more accessible first approach to obtaining an impact-rate stress-strain curve.

The equations presented here are subject to the assumption that the constitutive relation for the material is not shock-forming in the region of interest – i.e. the jump in strain caused by the passage of the longitudinal wave does not pass through a region in which the gradient of $C(\varepsilon)$ increases[313]. For a given point on the stress-strain curve, this is satisfied if the gradient is greater than that of a line drawn from ε = -1 on the stress axis, to said point. This must be true for all points up to the highest stress-state reached during the impact, which is true for the data obtained here.

B.2.3 Alternative analyses

There are two alternative analyses to calculate the high-rate stress-strain co-ordinates for the vary speed method. These analyses are compared to the method described above in Figure B.3.

The first analysis method, Analysis 2, is developed by David Porter (unpublished) in which it is assumed that $C_w \approx C_t$, i.e. it is assumed that the particle velocity due to the longitudinal wave is small compared to the speed of the transverse wave. This means that the stress and strain caused by passage of the longitudinal wave and its associated particle motion, *W*, is ignored during analysis. Using this method, the high-rate stress (σ_1) is worked out directly from C_t (Equation 14, rearrangement of Equation 6):

$$\sigma_1 = C_t{}^2 \rho \qquad \text{Equation (14)}$$

The high-rate strain (ε_1) is worked out from the right-angled triangle XOY (Figure B.2), giving Equation 15, which is solved for ε:

$$[(1+\varepsilon)C_w \cdot t]^2 = (V \cdot t)^2 + (C_w \cdot t)^2 \qquad \text{Equation (15)}$$

The second alternative analysis, Analysis 3, is developed by Drodge *et al.*, published in their 2012 paper[132]. This approach is based on research by Smith *et al.* (1963)[314], where the stress-strain curve is built in small increments of strain, starting with the lowest speed data point, and building up to the highest speed data point. Given a proposed dynamic material response, $\sigma(\varepsilon)$, the Equations 1 – 5 can predict a curve relating C_W to *V*. This can be compared to the curve formed by the experimentally measured (C_W, *V*) points. In the model, the corresponding stress is varied until the predicted C_W versus *V* curve matches the experimental trend. This approach works out longitudinal wavespeed and modulus in a completely different way to the previous analyses, so is a somewhat complementary analysis technique.

B.3 Results

Figure B.3 compares the three analysis methods for the 'vary speed' data for Nylon and *Bombyx* naturally spun silk: 1) Analysis 1, used in Chapter 5, detailed above in Section B.2.2 (squares); 2) Analysis 2 by Porter, using equations assuming C_w=C_t detailed in B.2.3 (triangles); and 3) Analysis

3 by Drodge *et al.* (2012) using the modelling approach, detailed in B.2.3 (circles). The figure also plots a quasi-static stress-strain curve and the 'vary static load' data (stars), analysed using Analysis 1.

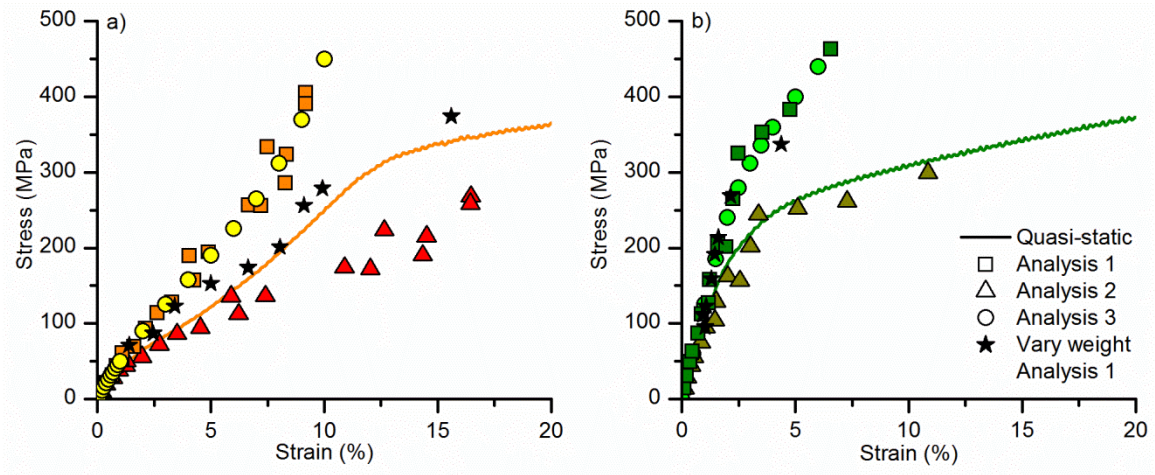

Figure B.3. Comparison of high-rate stress-strain co-ordinates for: **a)** nylon and **b)** *Bombyx* naturally spun silk under different analyses. Vary speed data: squares use Analysis 1, outlined in Section B.2.2 (this analysis method is used for the data in Chapter 5), triangles give Analysis 2 by Porter, outlined in Section B.2.3 and circles give Analysis 3, the modelling approach used in Drodge *et al.* (2012), outlined in Section B.2.3. The line gives a quasi-static stress-strain curve. Stars give the vary static load data, analysed using Analysis 1 (same analysis used for squares).

For both nylon and *Bombyx* silk, the modelling and numerical analyses presented in Drodge *et al.* (2012) agree for the vary speed data. Whether these analyses are valid and the reason for their divergence from the numerical analysis of Porter is currently under investigation. The numerical analysis of *Drodge et al.* (2012) was chosen for Chapter 5 due to the agreement of these methods, and prior publication.

Secondly, the vary static load methods show interesting divergences between nylon and *Bombyx* silk. The former follows the high-rate stress-strain response of the vary speed data up until c. 150 MPa, and then follows a more quasi-static-like response. For *Bombyx* silk, both the vary static load and vary speed data agree. This means that these two materials have a different path dependence – they vary their high-rate stress-strain response based on whether the stress is wholly dynamic (vary speed) or both static and dynamic (vary static load; see Figure 5.2 in Chapter 5). This may be due to differences in the structures of the polymers, where silks have

nano-sized order-disorder domains that allow energy to stored and dissipated at faster rates than nylons[56, 132]. It may also be explained by the effect of yield, as nylons are more yielded than *Bombyx* silks in the vary static load data, which affects the validity of the analysis methods.

Appendix C References

1. Dawkins, R., *The extended phenotype*. 1982, Oxford: O.U.P.
2. Vollrath, F. and Knight, D.P., *Liquid crystalline spinning of spider silk.* Nature, 2001. **410**(6828): p. 541-548.
3. Hayashi, C.Y., *Convergent evolution of sequence elements in spider and insect silk proteins.* Am. Zool., 2001. **41**(6): p. 1468-1468.
4. Vollrath, F. and Selden, P., *The role of behavior in the evolution of spiders, silks, and webs.* Annu. Rev. Ecol. Evol. Syst., 2007. **38**: p. 819-846.
5. Porter, D. and Vollrath, F., *Silk as a biomimetic ideal for structural polymers.* Adv. Mater., 2009. **21**(4): p. 487-492.
6. Sponner, A., Schlott, B., Vollrath, F., Unger, E., Grosse, F. and Weisshart, K., *Characterization of the protein components of Nephila clavipes dragline silk.* Biochemistry, 2005. **44**(12): p. 4727-4736.
7. Davies, G.J.G., Knight, D.P. and Vollrath, F., *Structure and function of the major ampullate spinning duct of the golden orb weaver, Nephila edulis.* Tissue Cell, 2013. **45**(5): p. 306-311.
8. Knight, D.P. and Vollrath, F., *Liquid crystals and flow elongation in a spider's silk production line.* Proc. R. Soc. Lond. Ser. B-Biol. Sci., 1999. **266**(1418): p. 519-523.
9. Knight, D.P. and Vollrath, F., *Changes in element composition along the spinning duct in a Nephila spider.* Naturwissenschaften, 2001. **88**(4): p. 179-182.
10. Boulet-Audet, M., Terry, A., Vollrath, F. and Holland, C., *Silk protein aggregation kinetics revealed by rheo-ir.* Acta Biomater., 2014. **10**(2): p. 776-784.
11. Holland, C., Urbach, J.S. and Blair, D.L., *Direct visualization of shear dependent silk fibrillogenesis.* Soft Matter, 2012. **8**(9): p. 2590-2594.
12. Holland, C., Terry, A.E., Porter, D. and Vollrath, F., *Comparing the rheology of native spider and silkworm spinning dope.* Nat. Mater., 2006. **5**(11): p. 870-874.
13. Xia, X.X., Qian, Z.G., Ki, C.S., Park, Y.H., Kaplan, D.L. and Lee, S.Y., *Native-sized recombinant spider silk protein produced in metabolically engineered Escherichia coli results in a strong fiber.* Proc. Natl. Acad. Sci. U. S. A., 2010. **107**(32): p. 14059-14063.
14. Jones, J., Rothfuss, H., Steinkraus, H. and Lewis, R., *Transgenic goats producing spider silk protein in their milk; behavior, protein purification and obstacles.* Transgenic Res., 2010. **19**(1): p. 135-135.
15. Vollrath, F., Porter, D. and Holland, C., *There are many more lessons still to be learned from spider silks.* Soft Matter, 2011. **7**(20): p. 9595-9600.
16. Knight, D. and Vollrath, F., *Hexagonal columnar liquid crystal in the cells secreting spider silk.* Tissue Cell, 1999. **31**(6): p. 617-620.
17. Gronau, G., Qin, Z. and Buehler, M.J., *Effect of sodium chloride on the structure and stability of spider silk's N-terminal protein domain.* Biomater. Sci., 2013. **1**: p. 276-284.
18. Gaines, W.A., Sehorn, M.G. and Marcotte, W.R., Jr., *Spidroin N-terminal domain promotes a pH-dependent association of silk proteins during self-assembly.* J. Biol. Chem., 2010. **285**(52): p. 40745-40753.
19. Vollrath, F., Porter, D. and Holland, C., *The science of silks.* MRS Bull., 2013. **38**(01): p. 73-80.
20. Craig, C., *Evolution of arthropod silks.* Ann. Rev. Entomol., 1997. **42**: p. 231-267.
21. Sutherland, T., Young, J. and Weisman, S., *Insect silk: One name, many materials.* Ann. Rev. Entomol., 2009. **55**: p. 171-188.
22. Kronenberger, K., Dicko, C. and Vollrath, F., *A novel marine silk.* Naturwissenschaften, 2012. **99**(1): p. 3-10.

23. Coddington, J.A. and Levi, H.W., *Systematics and evolution of spiders (Araneae).* Annu. Rev. Ecol. Syst., 1991. **22**: p. 565-592.
24. Haupt, J. and Kovoor, J., *Silk-gland system and silk production in Mesothelae (Araneae).* Ann. Sci. Nat. Bot. Zool., 1993. **14**(2): p. 35-48.
25. Palmer, J., *The silk and silk production system of the funnel-web mygalomorph spider Euagrus (Araneae, Dipluidae).* J. Morphol., 1985. **186**: p. 195-207.
26. Brunetta, L. and Craig, C.L., *Spider silk*. 2010, New Haven: Yale University Press.
27. Swanson, B.O., Anderson, S.P., Digiovine, C., Ross, R.N. and Dorsey, J.P. *The evolution of complex biomaterial performance: The case of spider silk*. Integr. Comp. Biol., 2009. **49**: p. 21-31.
28. Naftilan, S.A., *Transmission of vibrations in funnel and sheet spider webs.* Int. J. Biol. Macromol., 1999. **24**(2-3): p. 289-293.
29. Costa, F.G. and Perez-Miles, F., *Behavior, life cycle and webs of Mecicobothrium thorelli (Araneae, Mygalomorphae, Mecicobothriidae).* J. Arachnol., 1998. **26**(3): p. 317-329.
30. Singer, F., Riechert, S.E., Xu, H.F., Morris, A.W., Becker, E., Hale, J.A. and Noureddine, M.A., *Analysis of courtship success in the funnel-web spider Agelenopsis aperta.* Behaviour, 2000. **137**: p. 93-117.
31. Gatesy, J., Hayashi, C., Motriuk, D., Woods, J. and Lewis, R., *Extreme diversity, conservation, and convergence of spider silk fibroin sequences.* Science, 2001. **291**(5513): p. 2603-2605.
32. Garb, J.E., Dimauro, T., Lewis, R.V. and Hayashi, C.Y., *Expansion and intragenic homogenization of spider silk genes since the triassic: Evidence from Mygalomorphae (tarantulas and their kin) spidroins.* Mol. Biol. Evol., 2007. **24**(11): p. 2454-2464.
33. Tian, M.Z., Liu, C.Z. and Lewis, R., *Analysis of major ampullate silk cdnas from two non-orb-weaving spiders.* Biomacromolecules, 2004. **5**(3): p. 657-660.
34. Xu, M. and Lewis, R.V., *Structure of a protein superfiber - spider dragline silk.* Proc. Natl. Acad. Sci. U. S. A., 1990. **87**(18): p. 7120-7124.
35. Hinman, M.B. and Lewis, R.V., *Isolation of a clone encoding a 2nd dragline silk fibroin – Nephila clavipes dragline silk is a 2-protein fiber.* J. Biol. Chem., 1992. **267**(27): p. 19320-19324.
36. Colgin, M.A. and Lewis, R.V., *Spider minor ampullate silk proteins contain new repetitive sequences and highly conserved non silk-like "Spacer regions".* Protein Sci., 1998. **7**: p. 667-672.
37. Hayashi, C.Y. and Lewis, R.V., *Spider flagelliform silk: Lessons in protein design, gene structure, and molecular evolution.* Bioessays, 2001. **23**(8): p. 750-756.
38. Garb, J.E. and Hayashi, C.Y., *Modular evolution of egg case silk genes across orb-weaving spider superfamilies.* Proc. Natl. Acad. Sci. U. S. A., 2005. **102**(32): p. 11379-11384.
39. Rousseau, M.E., Lefevre, T. and Pezolet, M., *Conformation and orientation of proteins in various types of silk fibers produced by Nephila clavipes spiders.* Biomacromolecules, 2009. **10**(10): p. 2945-2953.
40. Hayashi, C.Y., Blackledge, T.A. and Lewis, R.V., *Molecular and mechanical characterization of aciniform silk: Uniformity of iterated sequence modules in a novel member of the spider silk fibroin gene family.* Mol. Biol. Evol., 2004. **21**(10): p. 1950-1959.
41. Hayashi, C.Y., Swanson, B.O., Blackledge, T.A. and Summers, A.P., *Evolution of the material properties of spider dragline silk.* Integr. Comp. Biol., 2005. **45**(6): p. 1009-1009.
42. Boutry, C., Rezac, M. and Blackledge, T.A., *Plasticity in major ampullate silk production in relation to spider phylogeny and ecology.* Plos One, 2011. **6**(7).
43. Guerette, P.A., Ginzinger, D.G., Weber, B.H.F. and Gosline, J.M., *Silk properties determined by gland-specific expression of a spider fibroin gene family.* Science, 1996. **272**(5258): p. 112-115.
44. Vollrath, F. and Porter, D., *Spider silk as an archetypal protein elastomer.* Soft Matter, 2006. **2**: p. 377-385.

45. Blackledge, T.A. and Hayashi, C.Y., *Silken toolkits: Biomechanics of silk fibers spun by the orb web spider Argiope argentata (Fabricius 1775).* J. Exp. Biol., 2006. **209**(13): p. 2452-2461.
46. Vollrath, F. and Edmonds, D.T., *Modulation of the mechanical-properties of spider silk by coating with water.* Nature, 1989. **340**(6231): p. 305-307.
47. Gosline, J.M., Guerette, P.A., Ortlepp, C.S. and Savage, K.N., *The mechanical design of spider silks: From fibroin sequence to mechanical function.* J. Exp. Biol., 1999. **202**(23): p. 3295-3303.
48. Swanson, B.O., Blackledge, T.A. and Hayashi, C.Y., *Spider capture silk: Performance implications of variation in an exceptional biomaterial.* J. Exp. Zool., 2007. **307A**(11): p. 654-666.
49. Van Nimmen, E., Gellynck, K., Gheysens, T., Van Langenhove, L. and Mertens, J., *Modeling of the stress-strain behavior of egg sac silk of the spider Araneus diadematus.* J. Arachnol., 2005. **33**(2): p. 629-639.
50. Perry, D.J., Bittencourt, D., Siltberg-Liberles, J., Rech, E.L. and Lewis, R.V., *Piriform spider silk sequences reveal unique repetitive elements.* Biomacromolecules, 2010. **11**(11): p. 3000-3006.
51. Wynne, A., *Textiles*. The motivate series. 1997, Oxford, UK: Macmillan Education.
52. Van Nimmen, E., Gellynck, K., Gheysens, T., Van Langenhove, L. and Mertens, J., *Modelling of the stress-stain behavior of egg sac silk of the spider Araneus diadematus.* J. Arachnol., 2005. **33**(2): p. 629-639.
53. Simmons, A.H., Michal, C.A. and Jelinski, L.W., *Molecular orientation and two-component nature of the crystalline fraction of spider dragline silk.* Science, 1996. **271**(5245): p. 84-87.
54. Liivak, O., Flores, A., Lewis, R. and Jelinski, L.W., *Conformation of the polyalanine repeats in minor ampullate gland silk of the spider Nephila clavipes.* Macromolecules, 1997. **30**(23): p. 7127-7130.
55. Hayashi, C.Y., Shipley, N.H. and Lewis, R.V., *Hypotheses that correlate the sequence, structure, and mechanical properties of spider silk proteins.* Int. J. Biol. Macromol., 1999. **24**(2,3): p. 271-275.
56. Porter, D. and Vollrath, F., *Nanoscale toughness of spider silk.* Nano Today, 2007. **2**(3): p. 6.
57. Hayashi, C.Y. and Lewis, R.V., *Molecular architecture and evolution of a modular spider silk protein gene.* Science, 2000. **287**(5457): p. 1477-1479.
58. Dicko, C., Porter, D., Bond, J., Kenney, J.M. and Vollratht, F., *Structural disorder in silk proteins reveals the emergence of elastomericity.* Biomacromolecules, 2008. **9**(1): p. 216-221.
59. Knight, D.P. and Vollrath, F., *Liquid crystal spinning in nature.* Comp. Biochem. Phys. B, 2000. **126B**(Suppl. 1): p. S56.
60. Rudall, K.M., *Silk and other cocoon proteins*, in *Comparative biochemistry*, M. Florkin and H.S. Mason, Editors. 1962, Academic Press: New York. p. 397-433.
61. Sturm, H., *Mating-behavior and sexual dimorphism in Promesomachilis hispanica silvestri, 1923 (Machilidae, Archaeognatha, Insecta).* Zool. Anz., 1992. **228**(1-2): p. 60-73.
62. New, T.R., *Biology of the Psocoptera.* Orient. Insects, 1987. **21**: p. 1-109.
63. Okada, S., Weisman, S., Trueman, H.E., Mudie, S.T., Haritos, V.S. and Sutherland, T.D., *An australian webspinner species makes the finest known insect silk fibers.* Int. J. Biol. Macromol., 2008. **43**(3): p. 271-275.
64. Matthews, R.W. and Starr, C.K., *Microstigmus-comes wasps have a method of nest construction unique among social insects.* Biotropica, 1984. **16**(1): p. 55-58.
65. Case, S.T., Powers, J., Hamilton, R. and Burton, M.J., *Silk and silk proteins from two aquatic insects*, in *Silk polymers: Materials science and biotechnology*, D. Kaplan, et al., Editors. 1994, American Chemical Society: Washington. p. 80-90.

66. Izzo, T.J., Pinent, S.M.J. and Mound, L.A., *Aulacothrips dictyotus (Heterothripidae), the first ectoparasitic thrips (Thysanoptera).* Fla. Entomol., 2002. **85**(1): p. 281-283.
67. Bauer, F., Bertinetti, L., Masic, A. and Scheibel, T., *Dependence of mechanical properties of lacewing egg stalks on relative humidity.* Biomacromolecules, 2012. **13**(11): p. 3730-3735.
68. Zhang, K., Si, F.W., Duan, H.L. and Wang, J., *Microstructures and mechanical properties of silks of silkworm and honeybee.* Acta Biomater., 2010. **6**(6): p. 2165-2171.
69. Collin, M.A., Swanson, B.O. and Hayashi, C.Y., *Mechanical properties of Embioptera silk.* Integr. Comp. Biol., 2005. **45**(6): p. 980-980.
70. Crewe, R.M. and Thompson, P.R., *Oecophylla silk - functional adaptation in a biopolymer.* Naturwissenschaften, 1979. **66**(1): p. 57-58.
71. Hepburn, H.R., Chandler, H.D. and Davidoff, M.R., *Extensometric properties of insect fibroins - green lacewing cross-beta, honeybee alpha-helical and greater waxmoth parallel-beta conformations.* Insect Biochem., 1979. **9**(1): p. 69-77.
72. Sutherland, T.D., Weisman, S., Walker, A.A. and Mudie, S.T., *Invited review the coiled coil silk of bees, ants, and hornets.* Biopolymers, 2012. **97**(6): p. 446-454.
73. Chen, F.J., Porter, D. and Vollrath, F., *Morphology and structure of silkworm cocoons.* Mater. Sci. Eng. C- Mater. Biol. Applic., 2012. **32**(4): p. 772-778.
74. Chen, F., Porter, D. and Vollrath, F., *Structure and physical properties of silkworm cocoons.* J. R. Soc. Interface, 2012. **9**(74): p. 2299-2308.
75. Chen, F.J., Hesselberg, T., Porter, D. and Vollrath, F., *The impact behaviour of silk cocoons.* J. Exp. Biol., 2013. **216**(14): p. 2648-2657.
76. Gheysens, T., *Small molecules in silk.* D. Phil Thesis, University of Oxford, 2011.
77. Boulet-Audet, M., Terry, A., Holland, C. and Vollrath, F., *The chemical diversity of silk revealed by infrared spectroscopy.* D. Phil Thesis, University of Oxford, 2013.
78. Chen, F., *Silk cocoons as composites.* D. Phil Thesis, University of Oxford, 2011.
79. Kluge, J.A., Rabotyagova, O., Leisk, G.G. and Kaplan, D.L., *Spider silks and their applications.* Trends Biotechnol., 2008. **26**(5): p. 244-251.
80. Ortlepp, C. and Gosline, J.M., *The scaling of safety factor in spider draglines.* J. Exp. Biol., 2008. **211**(17): p. 2832-2840.
81. Sensenig, A.T., Lorentz, K.A., Kelly, S.P. and Blackledge, T.A., *Spider orb webs rely on radial threads to absorb prey kinetic energy.* J. R. Soc. Interface, 2012. **9**(73): p. 1880-1891.
82. Agnarsson, I., Kuntner, M. and Blackledge, T.A., *Bioprospecting finds the toughest biological material: Extraordinary silk from a giant riverine orb spider.* Plos One, 2010. **5**(9): p. e11234.
83. Porter, D., Guan, J. and Vollrath, F., *Spider silk: Super material or thin fibre?* Adv. Mater., 2013. **25**(9): p. 1275-1279.
84. Teule, F., Miao, Y.G., Sohn, B.H., Kim, Y.S., Hull, J.J., Fraser, M.J., Lewis, R.V. and Jarvis, D.L., *Silkworms transformed with chimeric silkworm/spider silk genes spin composite silk fibers with improved mechanical properties.* Proc. Natl. Acad. Sci. U. S. A., 2012. **109**(3): p. 923-928.
85. Craig, C.L., *Orb-web visibility: The influence of insect flight behaviour and visual physiology on the evolution of web designs within the Araneoidea.* Anim. Behav., 1986. **34**: p. 54-68.
86. Foelix, R.F., *Biology of spiders*. 3rd ed. 2010, Oxford, N.Y: Oxford University Press.
87. Liu, Y., Shao, Z.Z. and Vollrath, F., *Relationships between supercontraction and mechanical properties of spider silk.* Nat. Mater., 2005. **4**(12): p. 901-905.
88. Vollrath, F., Madsen, B. and Shao, Z.Z., *The effect of spinning conditions on the mechanics of a spider's dragline silk.* Proc. R. Soc. Lond. Ser. B-Biol. Sci., 2001. **268**(1483): p. 2339-2346.
89. Vollrath, F., *Biology of spider silk.* Int. J. Biol. Macromol., 1999. **24**(2-3): p. 81-88.
90. Boutry, C. and Blackledge, T.A., *Evolution of supercontraction in spider silk: Structure-function relationship from tarantulas to orb-weavers.* J. Exp. Biol., 2010. **213**(20): p. 3505-3514.

91. Liu, Y., Sponner, A., Porter, D. and Vollrath, F., *Proline and processing of spider silks.* Biomacromolecules, 2008. **9**(1): p. 116-121.
92. Guinea, G.V., Elices, M., Plaza, G.R., Perea, G.B., Daza, R., Riekel, C., Agullo-Rueda, F., Hayashi, C., Zhao, Y. and Perez-Rigueiro, J., *Minor ampullate silks from Nephila and Argiope spiders: Tensile properties and microstructural characterization.* Biomacromolecules, 2012. **13**(7): p. 2087-2098.
93. Hesselberg, T. and Vollrath, F., *The mechanical properties of the non-sticky spiral in Nephila orb webs (Araneae, Nephilidae).* J. Exp. Biol., 2012. **215**(19): p. 3362-3369.
94. Garb, J.E., Dimauro, T., Vo, V. and Hayashi, C.Y., *Evidence from silk proteins for the single origin of spider orb-webs by the early cretaceous.* Integr. Comp. Biol., 2006. **46**: p. E46-E46.
95. Blackledge, T.A., Scharff, N., Coddington, J.A., Szuts, T., Wenzel, J.W., Hayashi, C.Y. and Agnarsson, I., *Reconstructing web evolution and spider diversification in the molecular era.* Proc. Natl. Acad. Sci. U. S. A., 2009. **106**(13): p. 5229-5234.
96. Masters, W.M. and Markl, H., *Vibration signal transmission in spider orb webs.* Science, 1981. **213**(4505): p. 363-365.
97. Denny, M., *The physical properties of spider's silk and their role in design of orb-webs.* J. Exp. Biol., 1976. **65**(2): p. 483-506.
98. Venner, S. and Casas, J., *Spider webs designed for rare but life-saving catches.* Proc. R. Soc. Lond. Ser. B-Biol. Sci., 2005. **272**(1572): p. 1587 - 1592.
99. Blackledge, T.A., *Prey capture in orb weaving spiders: Are we using the best metric?* J. Arachnol., 2011. **39**(2): p. 205-210.
100. Blackledge, T.A., Kuntner, M. and Agnarsson, I., *The form and function of spider orb webs: Evolution from silk to ecosystems*, in *Advances in insect physiology, vol 41: Spider physiology and behaviour - behaviour*, J. Casas, Editor. 2011, Elsevier Science Ltd: London. p. 175-262.
101. Craig, C.L., *The ecological and evolutionary interdependence between web architecture and web silk spun by orb web weaving spiders.* Biol. J. Linnean Soc., 1987. **30**: p. 135-162.
102. Hesselberg, T., *Ontogenetic changes in web design in two orb-web spiders.* Ethology, 2010. **116**(6): p. 535-545.
103. Schneider, J.M. and Vollrath, F., *The effect of prey type on the geometry of the capture web of Araneus diadematus.* Naturwissenschaften, 1998. **85**(8): p. 391-394.
104. Tso, I.M., Chiang, S.Y. and Blackledge, T.A., *Does the giant wood spider Nephila pilipes respond to prey variation by altering web or silk properties?* Ethology, 2007. **113**(4): p. 324-333.
105. Krink, T. and Vollrath, F., *Optimal area use in orb webs of the spider Araneus diadematus.* Naturwissenschaften, 2000. **87**(2): p. 90-93.
106. Nyffeler, M. and Knoernschild, M., *Bat predation by spiders.* Plos One, 2013. **8**(3): p. 1-15.
107. Blackledge, T.A. and Wenzel, J.W., *Do stabilimenta in orb webs attract prey or defend spiders?* Behav. Ecol., 1999. **10**(4): p. 372-376.
108. Tso, I.M., *Stabilimentum of the garden spider Argiope trifasciata: A possible prey attractant.* Anim. Behav., 1996. **52**: p. 183-191.
109. Lin, L.H., Edmonds, D.T. and Vollrath, F., *Structural engineering of an orb-spider's web.* Nature, 1995. **373**(6510): p. 146-148.
110. Sensenig, A.T., Kelly, S.P., Lorentz, K.A., Lesher, B. and Blackledge, T.A., *Mechanical performance of spider orb webs is tuned for high-speed prey.* J. Exp. Biol., 2013. **216**(18): p. 3388-3394.
111. Kelly, S.P., Sensenig, A., Lorentz, K.A. and Blackledge, T.A., *Damping capacity is evolutionarily conserved in the radial silk of orb-weaving spiders.* Zoology, 2011. **114**(4): p. 233-238.
112. Vollrath, F., Downes, M. and Krackow, S., *Design variability in web geometry of an orb-weaving spider.* Physiol. Behav., 1997. **62**(4): p. 735-743.

113. Blackledge, T.A. and Zevenbergen, J.M., *Mesh width influences prey retention in spider orb webs.* Ethology, 2006. **112**(12): p. 1194-1201.
114. Vollrath, F. and Edmonds, D., *Consequences of electrical conductivity in an orb spider's capture web.* Naturwissenschaften, 2013. **100**(12): p. 1163-1169.
115. Vollrath, F., Fairbrother, W.J., Williams, R.J.P., Tillinghast, E.K., Bernstein, D.T., Gallagher, K.S. and Townley, M.A., *Compounds in the droplets of the orb spiders viscid spiral.* Nature, 1990. **345**(6275): p. 526-528.
116. Edmonds, D.T. and Vollrath, F., *The contribution of atmospheric water vapor to the formation and efficiency of a spider's capture web.* Proc. R. Soc. Lond. Ser. B-Biol. Sci., 1992. **248**(1322): p. 145-8.
117. Boutry, C. and Blackledge, T.A., *Wet webs work better: Humidity, supercontraction and the performance of spider orb webs.* J. Exp. Biol., 2013. **216**(19): p. 3606-3610.
118. Swanson, B.O., Blackledge, T.A., Summers, A.P. and Hayashi, C.Y., *Spider dragline silk: Correlated and mosaic evolution in high-performance biological materials.* Evolution, 2006. **60**(12): p. 2539-51.
119. Klarner, D. and Barth, F.G., *Vibratory signals and prey capture in orb-weaving spiders (Zygiella x-notata, Nephila clavipes, Araneidae).* J. Comp. Physiol., 1982. **148**(4): p. 445-455.
120. Landolfa, M.A. and Barth, F.G., *Vibrations in the orb web of the spider Nephila clavipes: Cues for discrimination and orientation.* J. Comp. Physiol. A, 1996. **179**(4): p. 493-508.
121. Masters, W.M., *Vibrations in the orbwebs of Nuctenea sclopetaria (Araneidae). 1. Transmission through the web.* Behav. Ecol. Sociobiol., 1984. **15**(3): p. 207-215.
122. Gheysens, T., Collins, A., Raina, S., Vollrath, F. and Knight, D.P., *Demineralization enables reeling of wild silkmoth cocoons.* Biomacromolecules, 2011. **12**(6): p. 2257-2266.
123. Holland, C., Porter, D. and Vollrath, F., *Comparing the rheology of mulberry and "wild" silkworm spinning dopes.* Biopolymers, 2012. **97**(6): p. 362-367.
124. Chen, F.J., Porter, D. and Vollrath, F., *Silk cocoon (Bombyx mori): Multi-layer structure and mechanical properties.* Acta Biomater., 2012. **8**(7): p. 2620-2627.
125. Perez-Rigueiro, J., Elices, M., Llorca, J. and Viney, C., *Effect of degumming on the tensile properties of silkworm (Bombyx mori) silk fiber.* J. Appl. Polym. Sci., 2002. **84**(7): p. 1431-1437.
126. Blossman-Myer, B.L. and Burggren, W.W., *Metabolic allometry during development and metamorphosis of the silkworm Bombyx mori: Analyses, patterns, and mechanisms.* Physiol. Biochem. Zool., 2010. **83**(2): p. 215-231.
127. Shao, Z.Z. and Vollrath, F., *Surprising strength of silkworm silk.* Nature, 2002. **418**(6899): p. 741-741.
128. Asakura, T., Umemura, K., Nakazawa, Y., Hirose, H., Higham, J. and Knight, D., *Some observations on the structure and function of the spinning apparatus in the silkworm Bombyx mori.* Biomacromolecules, 2007. **8**(1): p. 175-181.
129. Chen, F., Porter, D. and Vollrath, F., *Silkworm cocoons inspire models for random fiber and particulate composites.* Phys. Rev. E, 2010. **82**(4).
130. Ferry, J.D., *Viscoelastic properties of polymers*. 3rd ed. 1980, New York: Wiley VCH.
131. Field, J.E., Walley, S.M., Proud, W.G., Goldrein, H.T. and Siviour, C.R., *Review of experimental techniques for high rate deformation and shock studies.* Int. J. Impact Eng., 2004. **30**(7): p. 725-775.
132. Drodge, D.R., Mortimer, B., Holland, C. and Siviour, C.R., *Ballistic impact to access the high-rate behaviour of individual silk fibres.* J. Mech. Phys. Solids, 2012. **60**(10): p. 1710-1721.
133. Hudspeth, M., Nie, X., Chen, W.N. and Lewis, R., *Effect of loading rate on mechanical properties and fracture morphology of spider silk.* Biomacromolecules, 2012. **13**(8): p. 2240-2246.
134. Cunniff, P.M., Fossey, S.A., Auerbach, M.A., Song, J.W., Kaplan, D.L., Adams, W.W., Eby, R.K., Mahoney, D. and Vezie, D.L., *Mechanical and thermal properties of dragline silk from the spider Nephila clavipes.* Polym. Advan. Technol., 1994. **5**(8): p. 401-410.

135. Guan, J., Vollrath, F. and Porter, D., *Two mechanisms for supercontraction in Nephila spider dragline silk.* Biomacromolecules, 2011. **12**(11): p. 4030-4035.
136. Perez-Rigueiro, J., Elices, M. and Guinea, G., *Controlled supercontraction tailors the tensile behaviour of spider silk.* Polymer, 2003. **44**(13): p. 3733 - 3736.
137. Mortimer, B., Holland, C. and Vollrath, F., *Forced reeling of Bombyx mori silk: Separating behaviour and processing conditions.* Biomacromolecules, 2013. **14**(10): p. 3653-3659.
138. Reed, E.J., Bianchini, L.L. and Viney, C., *Sample selection, preparation methods, and the apparent tensile properties of silkworm (B. mori) cocoon silk.* Biopolymers, 2012. **97**(6): p. 397-407.
139. Ganga, G., *Comprehensive sericulture, volume 2.* Science Publishers, USA., 2003.
140. Madsen, B. and Vollrath, F., *Mechanics and morphology of silk drawn from anesthetized spiders.* Naturwissenschaften, 2000. **87**(3): p. 148-153.
141. Starkweather, H.W. and Brooks, R.E., *Effect of spherulites on the mechanical properties of nylon 66.* J. Appl. Polym. Sci., 1959. **1**(2): p. 236-239.
142. Guan, J., *Investigations on natural silks using dynamic mechanical thermal analysis*, in *Zoology Department*. 2013, D. Phil Thesis, University of Oxford.
143. Siegel, S., *Nonparametric statistics.* Am. Stat., 1957. **11**(3): p. 13-19.
144. Mortimer, B., Drodge, D.R., Dragnevski, K.I., Siviour, C.R. and Holland, C., *In situ tensile tests of single silk fibres in an environmental scanning electron microscope.* J. Mater. Sci., 2013. **48**(14): p. 5055-5062.
145. Offord, C., Vollrath, F. and Holland, C., *Environmental effects on the construction and physical properties of Bombyx mori cocoons.* In prep., 2014.
146. Horrocks, N.P.C., Vollrath, F. and Dicko, C., *The silkmoth cocoon as humidity trap and waterproof barrier.* Comp. Bioc. A., 2013. **164**(4): p. 645-652.
147. Blossman-Myer, B. and Burggren, W.W., *The silk cocoon of the silkworm, Bombyx mori: Macro structure and its influence on transmural diffusion of oxygen and water vapor.* Comp. Bioc. A., 2010. **155**(2): p. 259-263.
148. Fu, C.J., Porter, D. and Shao, Z.Z., *Moisture effects on Antheraea pernyi silk's mechanical property.* Macromolecules, 2009. **42**(20): p. 7877-7880.
149. Seydel, T., Knoll, W., Greving, I., Dicko, C., Koza, M.M., Krasnov, I. and Mueller, M., *Increased molecular mobility in humid silk fibers under tensile stress.* Phys. Rev. E, 2011. **83**(1).
150. Hu, X., Kaplan, D. and Cebe, P., *Dynamic protein-water relationships during beta-sheet formation.* Macromolecules, 2008. **41**(11): p. 3939-3948.
151. Kirk, S., Skepper, J. and Donald, A.M., *Application of environmental scanning electron microscopy to determine biological surface structure.* J. Microsc.-Oxf., 2009. **233**(2): p. 205-224.
152. Stokes, D.J., *Characterisation of soft condensed matter and delicate materials using environmental scanning electron microscopy (ESEM).* Adv. Eng. Mater., 2001. **3**(3): p. 126-130.
153. Donald, A.M., *The use of environmental scanning electron microscopy for imaging wet and insulating materials.* Nat. Mater., 2003. **2**(8): p. 511-516.
154. Danilatos, G.D., *Review and outline of environmental SEM at present.* J. Microsc.-Oxf., 1991. **162**: p. 391-402.
155. Doucet, F.J., Lead, J.R., Maguire, L., Achterberg, E.P. and Millward, G.E., *Visualisation of natural aquatic colloids and particles - a comparison of conventional high vacuum and environmental scanning electron microscopy.* J. Environ. Monitor., 2005. **7**(2): p. 115-121.
156. Mestres, P., Puetz, N., Gomez De Las Heras, S.G., Garcia Poblete, E., Morguet, A. and Laue, M., *The surface topography of the choroid plexus. Environmental, low and high vacuum scanning electron microscopy.* Ann. Anat., 2011. **193**(3): p. 197-204.
157. Misirli, Z., Oener, E.T. and Kirdar, B., *Real imaging and size values of Saccharomyces cerevisiae cells with comparable contrast tuning to two environmental scanning electron microscopy modes.* Scanning, 2007. **29**(1): p. 11-19.

158. Jing, X., Shuling, G. and Ying, L., *Environmental scanning electron microscopy observation of the ultrastructure of demodex.* Microsc. Res. Techniq., 2005. **68**(5): p. 284-9.
159. Mcgregor, J.E. and Donald, A.M., *Esem imaging of dynamic biological processes: The closure of stomatal pores.* J. Microsc., 2010. **239**(2): p. 135-141.
160. Eder, M., Stanzl-Tschegg, S. and Burgert, I., *The fracture behaviour of single wood fibres is governed by geometrical constraints: In situ ESEM studies on three fibre types.* Wood Sci. Technol., 2008. **42**(8): p. 679-689.
161. Mott, L., Shaler, S.M. and Groom, L.H., *A technique to measure strain distributions in single wood pulp fibers.* Wood Fiber Sci., 1996. **28**(4): p. 429-437.
162. Thiel, B.L. and Donald, A.M., *In situ mechanical testing of fully hydrated carrots (Daucus carota) in the environmental SEM.* Ann. Bot., 1998. **82**(6): p. 727-733.
163. Donald, A.M., Baker, F.S., Smith, A.C. and Waldron, K.W., *Fracture of plant tissues and walls as visualized by environmental scanning electron microscopy.* Ann. Bot., 2003. **92**(1): p. 73-77.
164. Stabentheiner, E., Zankel, A. and Polt, P., *Environmental scanning electron microscopy (ESEM)-a versatile tool in studying plants.* Protoplasma, 2010. **246**(1-4): p. 89-99.
165. Franbourg, A., Hallegot, P., Baltenneck, F., Toutain, C. and Leroy, F., *Current research on ethnic hair.* J. Am. Acad. Dermatol., 2003. **48**(6): p. S115-S119.
166. Bos, H.L. and Donald, A.M., *In situ ESEM study of the deformation of elementary flax fibres.* J. Mater. Sci., 1999. **34**(13): p. 3029-3034.
167. Stokes, D.J. and Donald, A.M., *In situ mechanical testing of dry and hydrated breadcrumb in the environmental scanning electron microscope (ESEM).* J. Mater. Sci., 2000. **35**(3): p. 599-607.
168. Rizzieri, R., Baker, F.S. and Donald, A.M., *A study of the large strain deformation and failure behaviour of mixed biopolymer gels via in situ ESEM.* Polymer, 2003. **44**(19): p. 5927-5935.
169. Taylor, J.E., Laity, P.R., Wong, S.S., Norris, K., Khunkamchoo, P., Cable, M., Andrews, G., Johnson, A.F. and Cameron, R.E., *Examination of hard segment and soft segment phase separation in polyurethane medical materials by electron microscopy techniques.* Microsc. Microanal., 2006. **12**(2): p. 151-5.
170. Rizzieri, R., Mahadevan, L., Vaziri, A. and Donald, A., *Superficial wrinkles in stretched, drying gelatin films.* Langmuir, 2006. **22**(8): p. 3622-3626.
171. Ahmad, M.R., Nakajima, M., Kojima, S., Homma, M. and Fukuda, T., *Buckling nanoneedle for characterizing single cells mechanics inside environmental SEM.* IEEE T. Nanotechnol., 2011. **10**(2): p. 226-236.
172. Jauzein, V. and Bunsell, A., *Bio-composite aspects of silk: The sericin sheath acting as a matrix.* J. Mater. Sci., 2012. **47**(7): p. 3082-3088.
173. Bogner, A., Thollet, G., Basset, D., Jouneau, P.H. and Gauthier, C., *Wet stem: A new development in environmental SEM for imaging nano-objects included in a liquid phase.* Ultramicroscopy, 2005. **104**(3-4): p. 290-301.
174. Coetzee, S.H., Jordaan, A. and Mpuchane, S.F., *Low pressure mode combined with OSO_4 vapor fixation and sputter-coating for the preservation of delicate aerial hyphae and conidia in the ESEM.* Microsc. Res. Techniq., 2005. **67**(5): p. 265-270.
175. Stokes, D.J., *Recent advances in electron imaging, image interpretation and applications: Environmental scanning electron microscopy.* Philos. T. R. Soc. Lond. Ser. A, 2003. **361**(1813): p. 2771-2787.
176. Yang, Y., Chen, X., Shao, Z.Z., Zhou, P., Porter, D., Knight, D.P. and Vollrath, F., *Toughness of spider silk at high and low temperatures.* Adv. Mater., 2005. **17**(1): p. 84-88.
177. Guan, J., Porter, D. and Vollrath, F., *Silks cope with stress by tuning their mechanical properties under load.* Polymer, 2012. **53**(13): p. 2717-2726.

178. Cameron, R.E. and Donald, A.M., *Minimizing sample evaporation in the environmental scanning electron-microscope.* J. Microsc.-Oxf., 1994. **173**: p. 227-237.
179. Guan, J., Porter, D. and Vollrath, F., *Thermally induced changes in dynamic mechanical properties of native silks.* Biomacromolecules, 2013. **14**(3): p. 930-937.
180. Brunet, P.C.J. and Coles, B.C., *Tanned silks.* Proc. R. Soc. Lond. Ser. B-Biol. Sci., 1974. **187**(1087): p. 133 - 170.
181. Perez-Rigueiro, J., Elices, M., Llorca, J. and Viney, C., *Tensile properties of silkworm silk obtained by forced silking.* J. Appl. Polym. Sci., 2001. **82**(8): p. 1928-1935.
182. Work, R.W. and Emerson, P.D., *An apparatus and technique for the forcible silking of spiders.* J. Arachnol., 1982. **10**(1): p. 1-10.
183. Liu, Y., Shao, Z.Z. and Vollrath, F., *Extended wet-spinning can modify spider silk properties.* Chem. Commun., 2005. **19**: p. 2489-2491.
184. Madsen, B., Shao, Z.Z. and Vollrath, F., *Variability in the mechanical properties of spider silks on three levels: Interspecific, intraspecific and intraindividual.* Int. J. Biol. Macromol., 1999. **24**(2-3): p. 301-306.
185. Perez-Rigueiro, J., Elices, M., Plaza, G., Real, J.I. and Guinea, G.V., *The effect of spinning forces on spider silk properties.* J. Exp. Biol., 2005. **208**(14): p. 2633-2639.
186. Jin, H.J. and Kaplan, D.L., *Mechanism of silk processing in insects and spiders.* Nature, 2003. **424**(6952): p. 1057-1061.
187. Holland, C., Terry, A.E., Porter, D. and Vollrath, F., *Natural and unnatural silks.* Polymer, 2007. **48**: p. 3388-3392.
188. Zhu, J.X., Zhang, Y.P., Shao, H.L. and Hu, X.C., *Electrospinning and rheology of regenerated Bombyx mori silk fibroin aqueous solutions: The effects of pH and concentration.* Polymer, 2008. **49**(12): p. 2880-2885.
189. Tao, H., Kaplan, D.L. and Omenetto, F.G., *Silk materials - a road to sustainable high technology.* Adv. Mater., 2012. **24**(21): p. 2824-2837.
190. Yin, J., Chen, E., Porter, D. and Shao, Z., *Enhancing the toughness of regenerated silk fibroin film through uniaxial extension.* Biomacromolecules, 2010. **11**(11): p. 2890-2895.
191. Altman, G.H., Diaz, F., Jakuba, C., Calabro, T., Horan, R.L., Chen, J.S., Lu, H., Richmond, J. and Kaplan, D.L., *Silk-based biomaterials.* Biomaterials, 2003. **24**(3): p. 401-416.
192. Fu, C., Shao, Z. and Fritz, V., *Animal silks: Their structures, properties and artificial production.* Chem. Commun., 2009(43): p. 6515-6529.
193. Elices, M., Guinea, G.V., Plaza, G.R., Real, J.I. and Perez-Rigueiro, J., *Example of microprocessing in a natural polymeric fiber: Role of reeling stress in spider silk.* J. Mater. Res., 2006. **21**(8): p. 1931-1938.
194. Sugiura, S. and Yamazaki, K., *The role of silk threads as lifelines for caterpillars: Pattern and significance of lifeline-climbing behaviour.* Ecol. Entomol., 2006. **31**(1): p. 52-57.
195. Brackenbury, J., *Novel locomotory mechanisms in caterpillars: Life-line climbing in Epinotia abbreviana (Tortricidae) and Yponomeuta padella (Yponomeutidae).* Physiol. Entomol., 1996. **21**(1): p. 7-14.
196. Fu, C., Porter, D., Chen, X., Vollrath, F. and Shao, Z., *Understanding the mechanical properties of Antheraea pernyi silk-from primary structure to condensed structure of the protein.* Adv. Funct. Mater., 2011. **21**(4): p. 729-737.
197. Woo, W.C., Kuan, C.H. and Luh, C.J., *The morphology of the head of the lepidopterous larvae as discussed with the silkworm (Bombyx mori.L.).* Acta Entomol. Sinica, 1950. **1**(2): p. 152-163.
198. Moriya, M., Ohgo, K., Masubuchi, Y., Knight, D.P. and Asakura, T., *Micro-computerized tomographic observation of the spinning apparatus in Bombyx mori silkworms.* Polymer, 2008. **49**(26): p. 5665-5669.
199. Vollrath, F. and Woods, A., *Paralysation of silkworm larvae*, U.F.B.O.O.X.T.F. Nefila Ltd, Editor. 2012.

200. Ha, S.D., Nagata, S., Suzuki, A. and Kataoka, H., *Isolation and structure determination of a paralytic peptide from the hemolymph of the silkworm, Bombyx mori.* Peptides, 1999. **20**(5): p. 561-568.
201. Kamimura, M., Nakahara, Y., Kanamori, Y., Tsuzuki, S., Hayakawa, Y. and Kiuchi, M., *Molecular cloning of silkworm paralytic peptide and its developmental regulation.* Biochem. Biophys. Res. Commun., 2001. **286**(1): p. 67-73.
202. Hu, Z.-G., Chen, K.-P., Qin, Y., Gao, G.-T., Xu, J.-P. and Chen, H.-Q., *Cloning and characterization of Bombyx mori pp-bp, a gene induced by viral infection.* Acta Genet. Sinica, 2006. **33**(11): p. 975-983.
203. Khan, M., Morikawa, H., Gotoh, Y., Miura, M., Ming, Z., Sato, Y. and Iwasa, M., *Structural characteristics and properties of Bombyx mori silk fiber obtained by different artificial forcibly silking speeds.* Int. J. Biol. Macromol., 2008. **42**(3): p. 264-270.
204. Knight, D.P., Knight, M.M. and Vollrath, F., *Beta transition and stress-induced phase separation in the spinning of spider dragline silk.* Int. J. Biol. Macromol., 2000. **27**(3): p. 205-210.
205. Choi, K.J., Spruiell, J.E. and White, J.L., *Structure development in biaxially stretched polystyrene film. I. Property-orientation correlation.* Polym. Eng. Sci., 1989. **29**(21): p. 1516-1523.
206. Tanabe, Y. and Kanetsuna, H., *Structure of oriented polystyrene monofilaments and its relationship to brittle-to-ductile transition.* J. Appl. Polym. Sci., 1978. **22**(6): p. 1619-1630.
207. Tanabe, Y. and Kanetsuna, H., *Brittle-to-ductile transition based upon amorphous orientation of polystyrene monofilaments.* J. Appl. Polym. Sci., 1978. **22**(9): p. 2707-2711.
208. Zhang, X.M. and Ajji, A., *Biaxial orientation behavior of polystyrene: Orientation and properties.* J. Appl. Polym. Sci., 2003. **89**(2): p. 487-496.
209. Yuan, Q.Q., Yao, J.R., Huang, L., Chen, X. and Shao, Z.Z., *Correlation between structural and dynamic mechanical transitions of regenerated silk fibroin.* Polymer, 2010. **51**(26): p. 6278-6283.
210. Motta, A., Fambri, L. and Migliaresi, C., *Regenerated silk fibroin films: Thermal and dynamic mechanical analysis.* Macromol. Chem. Phys., 2002. **203**(10/11): p. 1658-1665.
211. Magoshi, J. and Magoshi, Y., *Physical-properties and structure of silk 2. Dynamic mechanical and dielectric properties of silk fibroin.* J. Polym. Sci., Part B: Polym. Phys., 1975. **13**(7): p. 1347-1351.
212. Tsukada, M., Freddi, G., Kasai, N. and Monti, P., *Structure and molecular conformation of tussah silk fibroin films treated with water-methanol solutions: Dynamic mechanical and thermomechanical behavior.* J. Polym. Sci., Part B: Polym. Phys., 1998. **36**(15): p. 2717-2724.
213. Kweon, H.Y., Um, I.C. and Park, Y.H., *Thermal behavior of regenerated Antheraea pernyi silk fibroin film treated with aqueous methanol.* Polymer, 2000. **41**(20): p. 7361-7367.
214. Magoshi, J. and Nakamura, S., *Studies on physical-properties and structure of silk - glass-transition and crystallization of silk fibroin.* J. Appl. Polym. Sci., 1975. **19**(4): p. 1013-1015.
215. Magoshi, J., Magoshi, Y. and Nakamura, S., *Physical properties and structure of silk 3. Glass-transition and conformational-changes of tussah silk fibroin.* J. Appl. Polym. Sci., 1977. **21**(9): p. 2405-2407.
216. Nakamura, S., Saegusa, Y., Yamaguchi, Y., Magoshi, J. and Kamiyama, S., *Physical-properties and structure of silk .11. Glass-transition temperature of wild silk fibroins.* J. Appl. Polym. Sci., 1986. **31**(3): p. 355-356.
217. Hu, X., Kaplan, D. and Cebe, P., *Determining beta-sheet crystallinity in fibrous proteins by thermal analysis and infrared spectroscopy.* Macromolecules, 2006. **39**(18): p. 6161-6170.
218. Um, I.C., Kweon, H.Y., Park, Y.H. and Hudson, S., *Structural characteristics and properties of the regenerated silk fibroin prepared from formic acid.* Int. J. Biol. Macromol., 2001. **29**(2): p. 91-97.

219. Jeong, L., Lee, K.Y., Liu, J.W. and Park, W.H., *Time-resolved structural investigation of regenerated silk fibroin nanofibers treated with solvent vapor.* Int. J. Biol. Macromol., 2006. **38**(2): p. 140-144.
220. Zhou, L., Chen, X., Shao, Z.Z., Huang, Y.F. and Knight, D.P., *Effect of metallic ions on silk formation the mulberry silkworm, Bombyx mori.* J. Phys. Chem. B, 2005. **109**(35): p. 16937-16945.
221. Lu, Q., Zhu, H.S., Zhang, C.C., Zhang, F., Zhang, B. and Kaplan, D.L., *Silk self-assembly mechanisms and control from thermodynamics to kinetics.* Biomacromolecules, 2012. **13**(3): p. 826-832.
222. Jiang, C.Y., Wang, X.Y., Gunawidjaja, R., Lin, Y.H., Gupta, M.K., Kaplan, D.L., Naik, R.R. and Tsukruk, V.V., *Mechanical properties of robust ultrathin silk fibroin films.* Adv. Funct. Mater., 2007. **17**(13): p. 2229-2237.
223. Zhou, G.Q., Shao, Z.Z., Knight, D.P., Yan, J.P. and Chen, X., *Silk fibers extruded artificially from aqueous solutions of regenerated Bombyx mori silk fibroin are tougher than their natural counterparts.* Adv. Mater., 2009. **21**(3): p. 366-370.
224. Wang, Y., Porter, D. and Shao, Z.Z., *Using solvents with different molecular sizes to investigate the structure of Antheraea pernyi silk.* Biomacromolecules, 2013. **14**(11): p. 3936-3942.
225. Ortlepp, C.S. and Gosline, J.M., *Consequences of forced silking.* Biomacromolecules, 2004. **5**(3): p. 727-731.
226. Greving, I., Dicko, C., Terry, A., Callow, P. and Vollrath, F., *Small angle neutron scattering of native and reconstituted silk fibroin.* Soft Matter, 2010. **6**(18): p. 4389-4395.
227. Wang, Q., Yang, Y.H., Chen, X. and Shao, Z.Z., *Investigation of rheological properties and conformation of silk fibroin in the solution of amimcl.* Biomacromolecules, 2012. **13**(6): p. 1875-1881.
228. Yan, J.P., Zhou, G.Q., Knight, D.P., Shao, Z.Z. and Chen, X., *Wet-spinning of regenerated silk fiber from aqueous silk fibroin solution: Discussion of spinning parameters.* Biomacromolecules, 2010. **11**(1): p. 1-5.
229. Van Griethuijsen, L.I. and Trimmer, B.A., *Locomotion in caterpillars.* Biol. Rev. Camb. Philos. Soc., 2014. Online advance.
230. Tian, K., Porter, D., Yao, J.R., Shao, Z.Z. and Chen, X., *Kinetics of thermally-induced conformational transitions in soybean protein films.* Polymer, 2010. **51**(11): p. 2410-2416.
231. Elices, M., Perez-Rigueiro, J., Plaza, G.R. and Guinea, G.V., *Finding inspiration in Argiope trifasciata spider silk fibers.* JOM, 2005. **57**(2): p. 60-66.
232. Thistlethwaite, T., Jakeways, R. and Ward, I.M., *The crystal modulus and structure of oriented poly(ethylene terephthalate).* Polymer, 1988. **29**: p. 61-69.
233. Dicko, C., Vollrath, F. and Kenney, J.M., *Spider silk protein refolding is controlled by changing pH.* Biomacromolecules, 2004. **5**(3): p. 704-710.
234. Zhou, L., Terry, A.E., Huang, Y.F., Shao, Z.Z. and Chen, X., *Metal element contents in silk gland and silk fiber of Bombyx mori silkworm.* Acta Chim. Sinica, 2005. **63**(15): p. 1379-1382.
235. Zhou, L., Chen, X., Shao, Z., Zhou, P., Knight, D.P. and Vollrath, F., *Copper in the silk formation process of Bombyx mori silkworm.* FEBS Lett., 2003. **554**(3): p. 337-41.
236. Peng, X., Shao, Z., Chen, X., Knight, D.P., Wu, P. and Vollrath, F., *Further investigation on potassium-induced conformation transition of Nephila spidroin film with two-dimensional infrared correlation spectroscopy.* Biomacromolecules, 2005. **6**(1): p. 302-308.
237. Foo, C.W.P., Bini, E., Hensman, J., Knight, D.P., Lewis, R.V. and Kaplan, D.L., *Role of pH and charge on silk protein assembly in insects and spiders.* Appl. Phys. A: Mater., 2006. **82**(2): p. 223-233.
238. Walker, J.D. and Chocron, S., *Why impacted yarns break at lower speed than classical theory predicts.* J. Appl. Mech.-Trans. ASME, 2011. **78**(5).

239. Schultz, A.B., *Material behavior in wires of 1100 aluminum subjected to transverse impact.* J. Appl. Mech., 1968. **35**(2): p. 342-348.
240. Faber, T.E., *Fluid dynamics for physicists*. 1st ed. 1995, Cambridge: Cambridge University Press.
241. Hinman, M.B. and Lewis, R.V., *Isolation of a clone encoding a second dragline silk fibroin. Nephila clavipes dragline silk is a two-protein fiber.* J. Biol. Chem., 1992. **267**(27): p. 19320-4.
242. Wirth, E. and Barth, F.G., *Forces in the spider orb web.* J. Comp. Physiol. A, 1992. **171**: p. 359-371.
243. Cranford, S.W., Tarakanova, A., Pugno, N.M. and Buehler, M.J., *Nonlinear material behaviour of spider silk yields robust webs.* Nature, 2012. **482**(7383): p. 72-U91.
244. Le Clerc, C., Bunsell, A.R., Piant, A. and Monasse, B., *Role of skin/core structure and inclusions in the fatigue crack initiation and propagation in organic fibres.* J. Mater. Sci., 2006. **41**(20): p. 6830-6842.
245. Vollrath, F., Porter, D. and Dicko, C., *The structure of silk*, in *Handbook of textile fibre structure*, S.J. Eichhorn, et al., Editors. 2009, Woodhead Publishing: Cambridge.
246. Craig, C., *Evolution of arthropod silks.* Ann. Rev. Entomol., 1997. **42**: p. 231-267.
247. Barth, F.G., *Spider senses - technical perfection and biology.* Zoology, 2002. **105**(4): p. 271-285.
248. Soley, F.G. and Taylor, P.W., *Ploys and counterploys of assassin bugs and their dangerous spider prey.* Behaviour, 2013. **150**: p. 397-425.
249. Maklakov, A.A., Bilde, T. and Lubin, Y., *Vibratory courtship in a web-building spider: Signalling quality or stimulating the female?* Anim. Behav., 2003. **66**: p. 623-630.
250. Tarsitano, M., Jackson, R.R. and Kirchner, W.H., *Signals and signal choices made by the araneophagic jumping spider Portia fimbriata while hunting the orb-weaving web spiders Zygiella x-notata and Zosis geniculatus.* Ethology, 2000. **106**(7): p. 595-615.
251. Hieber, C.S., Wilcox, R.S., Boyle, J. and Uetz, G.W., *The spider and fly revisited: Ploy-counterploy behavior in a unique predator-prey system.* Behav. Ecol. Sociobiol., 2002. **53**(1): p. 51-60.
252. Walcott, C., *Effect of web on vibration sensitivity in spider, Achaearanea tepidariorum (koch).* J. Exp. Biol., 1963. **40**(4): p. 595-611.
253. Burgess, J.W., *Web-signal processing for tolerance and group predation in the social spider Mallos gregalis simon.* Anim. Behav., 1979. **27**(1): p. 157-164.
254. Bukowski, T.C. and Christenson, T.E., *Natural history and copulatory behavior of the spiny orbweaving spider Micrathena gracilis (Araneae, Araneidae).* J. Arachnol., 1997. **25**(3): p. 307-320.
255. Szlep, R., *Change in the response of spiders to repeated web vibrations.* Behaviour, 1964. **23**: p. 203-239.
256. Hoffmaster, D.K., *Responses of the spider Argiope aurantia to low frequency phasic and continuous vibrations.* Anim. Behav., 1982. **30**(1): p. 123-127.
257. Vollrath, F., *Vibrations - their signal function for a spider kleptoparasite.* Science, 1979. **205**(4411): p. 1149-1151.
258. Briceno, R.D. and Eberhard, W.G., *The hub as a launching platform: Rapid movements of the spider Leucauge mariana (Araneae: Tetragnathidae) as it turns to attack prey.* J. Arachnol., 2011. **39**(1): p. 102-112.
259. Boys, C.V., *The influence of a tuning-fork on the garden spider.* Nature, 1880. **23**: p. 149-150.
260. Foelix, R.F., *Biology of spiders*. 2nd ed. 1996, Oxford, N.Y: Oxford University Press.
261. Robinson, M.H. and Robinson, B., *The ecology and behavior of Nephila maculata: A supplement.* Smithson. Contrib. Zool., 1976(218): p. 1-22.
262. Buskirk, R.E., *Aggressive display and orb defence in a colonial spider, Metabus gravidus.* Anim. Behav., 1975. **23**: p. 560-567.

263. Suter, R.B., *Cyclosa turbinata (Araneae, Araneidae) - prey discrimination via web-boune vibrations.* Behav. Ecol. Sociobiol., 1978. **3**(3): p. 283-296.
264. Robinson, M.H. and Mirick, H., *The predatory behavior of the golden-web spider Nephila clavipes Araneae Araneidae.* Psyche, 1971. **78**(3): p. 123-139.
265. Schaber, C.F., Gorb, S.N. and Barth, F.G., *Force transformation in spider strain sensors: White light interferometry.* J. R. Soc. Interface, 2012. **9**(71): p. 1254-1264.
266. Barth, F.G., *A spider's world: Senses and behavior*. 1st ed. 2002, Berlin: Springer-Verlag.
267. Barth, F.G. and Geethabali, *Spider vibration receptors - threshold curves of individual slits in the metatarsal lyriform organ.* J. Comp. Physiol., 1982. **148**(2): p. 175-185.
268. Main, I.G., *Vibrations and waves in physics*. 3rd ed. 1993, Cambridge: Cambridge University Press.
269. Frohlich, C. and Buskirk, R.E., *Transmission and attenuation of vibration in orb spider webs.* J. Theo. Biol., 1982. **95**(1): p. 13-36.
270. Masters, W.M., *Vibrations in the orbwebs of Nuctenea sclopetaria (Araneidae). 2. Prey and wind signals and the spiders response threshold.* Behav. Ecol. Sociobiol., 1984. **15**(3): p. 217-223.
271. Liesenfeld, F.J., *Untersuchungen am netz und uber den erschutterungssinn von Zygiella x-notata (cl) (Araneidae).* Z. Vergl. Physiol., 1956. **38**(6): p. 563-592.
272. Koski, K.J., Akhenblit, P., Mckiernan, K. and Yarger, J.L., *Non-invasive determination of the complete elastic moduli of spider silks.* Nat. Mater., 2013. **12**: p. 262-267.
273. Alam, M.S., Wahab, M.A. and Jenkins, C.H., *Mechanics in naturally compliant structures.* Mech. Mater., 2007. **39**(2): p. 145-160.
274. Qin, Z. and Buehler, M.J., *Spider silk webs measure up.* Nat. Mater., 2013. **12**(3): p. 185-187.
275. Köhler, T. and Vollrath, F., *Thread biomechanics in the two orb weaving spiders Araneus diadematus (Araneae, Araneidae) and Uloborus walckenaerius (Araneae, Uloboridae).* J. Exp. Zool., 1995. **271**(1): p. 1-17.
276. Basu, S., Hay, J.L., Swindeman, J.E. and Oliver, W.C., *Continuous dynamic analysis: Evolution of elastic properties with strain.* MRS Communications, 2014. **4**(1): p. 25-29.
277. Casas, J., Magal, C. and Sueur, J., *Dispersive and non-dispersive waves through plants: Implications for arthropod vibratory communication.* Proc. R. Soc. B-Biol. Sci., 2007. **274**(1613): p. 1087-1092.
278. Guess, K.B. and Viney, C., *Thermal analysis of major ampullate (drag line) spider silk: The effect of spinning rate on tensile modulus.* Thermochim. Acta, 1998. **315**(1): p. 61-66.
279. Riekel, C., Muller, M. and Vollrath, F., *In situ x-ray diffraction during forced silking of spider silk.* Macromolecules, 1999. **32**(13): p. 4464-4466.
280. Liesenfeld, F.J., *Uber leistung und sitz des erschut-terangssinnes von netzspinnen.* Biol. Zbl., 1961. **80**: p. 465-475.
281. Walcott, C., *Behavior and vibration sensitivity in the spider.* Anat. Rec., 1959. **134**(3): p. 650-651.
282. Ashby, M.F., *On the engineering properties of materials.* Acta Metall., 1989. **37**(5): p. 1273-1293.
283. Guinea, G.V., Elices, M., Perez-Rigueiro, J. and Plaza, G.R., *Stretching of supercontracted fibers: A link between spinning and the variability of spider silk.* J. Exp. Biol., 2005. **208**(1): p. 25-30.
284. Stuart, M.A.C., Huck, W.T.S., Genzer, J., Muller, M., Ober, C., Stamm, M., Sukhorukov, G.B., Szleifer, I., Tsukruk, V.V., Urban, M., Winnik, F., Zauscher, S., Luzinov, I. and Minko, S., *Emerging applications of stimuli-responsive polymer materials.* Nat. Mater., 2010. **9**(2): p. 101-113.
285. Pasparakis, G. and Vamvakaki, M., *Multiresponsive polymers: Nano-sized assemblies, stimuli-sensitive gels and smart surfaces.* Polym. Chem., 2011. **2**(6): p. 1234-1248.

286. Agnarsson, I. and Blackledge, T.A., *Can a spider web be too sticky? Tensile mechanics constrains the evolution of capture spiral stickiness in orb-weaving spiders.* J. Zool., 2009. **278**(2): p. 134-140.
287. Sensenig, A.T., Agnarsson, I. and Blackledge, T.A., *Adult spiders use tougher silk: Ontogenetic changes in web architecture and silk biomechanics in the orb-weaver spider.* J. Zool., 2011. **285**(1): p. 28-38.
288. Peters, H.M., *On the structure and glandular origin of bridging lines used by spiders for moving to distant places.* Acta Zool. Fenn., 1990. **190**: p. 309-314.
289. Peters, H.M., *Functional organization of the spinning apparatus of Cyrtophora citricola with regard to the evolution of the web (Araneae, Araneidae).* Zoomorph., 1993. **113**: p. 153-163.
290. Languerand, D.L., Zhang, H., Murthy, N.S., Ramesh, K.T. and Sansoz, F., *Inelastic behavior and fracture of high modulus polymeric fiber bundles at high strain-rates.* Mater. Sci. Eng. A-Struct. Mater. Prop. Microstruct. Process., 2009. **500**(1-2): p. 216-224.
291. Zschokke, S. and Vollrath, F., *Web construction patterns in a range of orb-weaving spiders (Araneae).* E. J. Entomol., 1995. **92**(3): p. 523-541.
292. Pasquet, A., Cardot, J. and Leborgne, R., *Wasp attacks and spider defence in the orb weaving species Zygiella x-notata.* J. Insect. Behav., 2007. **20**(6): p. 553-564.
293. Pasquet, A., Ridwan, A. and Leborgne, R., *Presence of potential prey affects web-building in an orb-weaving spider Zygiella-x-notata.* Anim. Behav., 1994. **47**(2): p. 477-480.
294. Venner, S., Pasquet, A. and Leborgne, R., *Web-building behaviour in the orb-weaving spider Zygiella x-notata: Influence of experience.* Anim. Behav., 2000. **59**: p. 603-611.
295. Venner, S., Bel-Venner, M.C., Pasquet, A. and Leborgne, R., *Body-mass-dependent cost of web-building behavior in an orb weaving spider, Zygiella x-notata.* Naturwissenschaften, 2003. **90**(6): p. 269-272.
296. Harris, B., *Engineering composite materials*. 1999, London: The Institute of Materials.
297. Madsen, B., Hoffmeyer, P., Thomsen, A.B. and Lilholt, H., *Hemp yarn reinforced composites - i. Yarn characteristics.* Compos. Pt. A-Appl. Sci. Manuf., 2007. **38**(10): p. 2194-2203.
298. Porter, D. and Vollrath, F., *The role of kinetics of water and amide bonding in protein stability.* Soft Matter, 2008. **4**(2): p. 328-336.
299. Porter, D., *Group interaction modelling of polymer properties*. 1st ed. 1995, New York: Marcel Dekker.
300. Cao, Y. and Wang, B.C., *Biodegradation of silk biomaterials.* Int. J. Mol. Sci., 2009. **10**(4): p. 1514-1524.
301. Holland, C., Vollrath, F., Ryan, A.J. and Mykhaylyk, O.O., *Silk and synthetic polymers: Reconciling 100 degrees of separation.* Adv. Mater., 2012. **24**(1): p. 105-+.
302. Bunning, T.J., Jiang, H., Adams, W.W., Crane, R.L., Farmer, B. and Kaplan, D., *Applications of silk,* in *Silk Polymers*, D. Kaplan, et al., Editors. 1994, ACS Symposium Series, p. 353-358.
303. Schiffman, J.D. and Schauer, C.L., *A review: Electrospinning of biopolymer nanofibers and their applications.* Polym. Rev., 2008. **48**(2): p. 317-352.
304. Hormiga, G., Eberhard, W.G. and Coddington, J.A., *Web-construction behavior in australian Phonognatha and the phylogeny of nephiline and tetragnathid spiders (Araneae, Tetragnathidae).* Aust. J. Zool., 1995. **43**(4): p. 313-364.
305. Zschokke, S. and Vollrath, F., *Unfreezing the behaviour of two orb spiders.* Phys. Behav., 1995. **58**(6): p. 1167-1173.
306. Hill, P.S.M., *How do animals use substrate-borne vibrations as an information source?* Naturwissenschaften, 2009. **96**(12): p. 1355-1371.
307. Gagliano, M., Mancuso, S. and Robert, D., *Towards understanding plant bioacoustics.* Trends Plant Sci., 2012. **17**(6): p. 323-325.

308. Zemlin, J.C., *A study of the mechanical behavior of spider silks*. 1st ed. 1968, Natick: U.S. Army Natick Report AD-684 333.
309. Roylance, D., *Wave propagation in a viscoelastic fiber subjected to transverse impact.* Trans. ASME, E, J. Appl. Mech., 1973. **40**(1): p. 143-148148.
310. Craggs, J.W., *Wave motion in plastic-elastic strings.* J. Mech. Phys. Solids, 1954. **2**(4): p. 286-295.
311. Von Karman, T. and Duwez, P., *The propagation of plastic deformation in solids.* J. Appl. Phys., 1950. **21**(10): p. 987.
312. Prevorsek, D.C., Chin, H.B., Kwon, Y.D. and Field, J.E., *Strain rate effects in ultrastrong polyethylene fibers and composites.* J. Appl. Polym. Sci., 1991. **47**: p. 45-66.
313. Smith, J.C., Mccrackin, F.L. and Schiefer, H.F., *Stress-strain relationships in yarns subjected to rapid impact loading .5. Wave propagation in long textile yarns impacted transversely.* Tex. Res. J., 1958. **28**(4): p. 288-302.
314. Smith, J.C., Fenstermaker, C.A. and Shouse, P.J., *Stress-strain relationships in yarns subjected to rapid impact loading .10. Stress-strain curves obtained by impacts with rifle bullets.* Tex. Res. J., 1963. **33**: p. 919, 934.